Caracterización funcional de la interacción de la proteïna p53 con la ubiquitina ligasa HERC2

Mónica Cubillos Rojas

Universitat de Barcelona

Caracterización funcional de la interacción de la proteína p53 con la ubiquitina ligasa HERC2

Mónica Cubillos Rojas

Tesis Doctoral

2014

Publicaciones

Monica Cubillos-Rojas
Fabiola Amair-Pinedo
Irantzu Tato
Ramon Bartrons
Francesc Ventura
Jose Luis Rosa

Departament de Ciències Fisiològiques II, IDIBELL, Campus de Bellvitge, Universitat de Barcelona, Barcelona, Spain

Received July 16, 2009
Revised December 23, 2009
Accepted January 11, 2010

Short Communication

Simultaneous electrophoretic analysis of proteins of very high and low molecular mass using Tris-acetate polyacrylamide gels

To separate and analyze giant and small proteins in the same electrophoresis gel, we have used a 3–15% polyacrylamide gradient gel containing 2.6% of the crosslinker bisacrylamide and 0.2 M of Tris-acetate buffer (pH 7.0). Samples were prepared in a sample buffer containing lithium dodecyl sulphate and were run in the gel described above using Tris-Tricine-SDS-sodium bisulfite buffer, pH 8.2, as electrophoresis buffer. Here, we show that this system can be successfully used for general applications of SDS-PAGE such as CBB staining and immunoblot. Thus, by using Tris-acetate 3–15% polyacrylamide gels, it is possible to simultaneously analyze proteins, in the mass range of 10–500 kDa, such as HERC1 (532 kDa), HERC2 (528 kDa), mTOR (289 kDa), Clathrin heavy chain (192 kDa), RSK (90 kDa), S6K (70 kDa), β-actin (42 kDa), Ran (24 kDa) and LC3 (18 kDa). This system is highly sensitive since it allows detection from as low as 10 μg of total protein *per* lane. Moreover, it has a good resolution, low cost, high reproducibility and allows for analysis of proteins in a wide range of weights within a short period of time. All these features together with the use of a standard electrophoresis apparatus make the Tris-acetate-PAGE system a very helpful tool for protein analysis.

Keywords:
Giant proteins / Gradient gel / PAGE / Tris-acetate

DOI 10.1002/elps.200900657

PAGE is one of the most powerful tools used for protein analysis. Several variants of PAGE provide different types of information (mass, charge, purity, *etc.*) from the analyzed proteins. Among these variants, Glycine-SDS-PAGE (also known as Laemmli-SDS-PAGE) and Tricine-SDS-PAGE, which are based on Glycine-Tris and Tricine-Tris buffer systems, respectively, are the most commonly used SDS electrophoretic techniques for separating proteins according to their size [1, 2]. Polyacrylamide gels are composed of acrylamide and the crosslinker bisacrylamide. By using different concentrations of these molecules – generally indicated by their total percentage and the percentage of the crosslinker with respect to the total polyacrylamide – and one of the above buffers to make a gel, it is possible to separate proteins in the range of 1–500 kDa [2–3]. For separation of proteins <30 kDa, it has been recommended to use a Tricine-SDS-PAGE gel and for proteins >30 kDa, the Glycine-SDS-PAGE system can be used [2]. If we aim to separate proteins of very different masses, an option is to use a gel with a gradient of acrylamide concentration (high percentage at the bottom and a lower percentage at the top). However, these gradient gels usually fail to resolve giant proteins (>300 kDa), which are too big to even enter the gel, and small proteins (<20 kDa) at the same PAGE. To solve these problems, a combination of low-percentage acrylamide and gradient SDS-PAGE gels (LAG gel) has been proposed [3].

In the last years, several companies have commercialized electrophoresis systems based on Tris-acetate gels to separate proteins of different mass range. The composition of these gels is not publicly available and, for this reason, the researcher is given no choice but to buy the precast gels and their optimized buffers. These electrophoresis systems use a discontinuous buffer system that results in a neutral pH environment during electrophoresis, stabilizing both proteins and gel matrix and providing a better band resolution.

To assess whether Tris-acetate gels can be made easily in a biochemistry/biology laboratory, we used glass plates from a Mini-PROTEAN II electrophoresis system (Bio-Rad) to make mini-gels (gel size: 8 cm × 8 cm; spacers: 1.5 mm) with different concentrations of acrylamide:bisacrylamide (80:1, 40:1) and Tris-acetate buffer (1–0.15 M) (pH 7.0). We started with the concentration 1 M of Tris-acetate because

Correspondence: Dr. Jose Luis Rosa, Departament de Ciències Fisiològiques II, IDIBELL, Campus de Bellvitge, Universitat de Barcelona, E-08907, L'Hospitalet de Llobregat, Barcelona, Spain
E-mail: joseluisrosa@ub.edu
Fax: +34-934024268

Abbreviations: CHC, clathrin heavy chain**; HEK,** human embryonic kidney**; LAG,** low-percentage acrylamide gel and a gradient SDS-PAGE gel

this concentration was used for Tricine-SDS-PAGE [2]. This gel was very dense in our conditions and therefore we started to decrease the concentration down to 0.15 M. After running all these combinations (see below), we obtained the best results using a standard acrylamide:bisacrylamide solution (40:1) containing a 2.6% concentration of bisacrylamide (from Bio-Rad or AppliChem) and a final concentration of 0.2 M Tris-acetate buffer in the gel. Using these reagents in the presence of 0.042% w/v ammonium peroxodisulfate (from Merck) and 0.12% v/v TEMED (from Bio-Rad), we made polyacrylamide gels of 4, 8, 10 and 12%. These gels were used to separate protein standards (from Bio-Rad and/or Fermentas) with very good resolution (not shown). We used an electrophoresis buffer (50 mM Tricine, 50 mM Tris, 0.1% SDS, 1.3 mM sodium bisulfite, pH 8.2) similar to the one used for Tricine-SDS-PAGE [2] but adding the anti-oxidant sodium bisulfite in order to maintain the proteins in a reduced state during the run. Next, we analyzed whether it was possible to use these mini-gels to separate proteins of high and low molecular mass in the same electrophoresis. To this end, we checked different combinations of gradient gels of polyacrylamide (3–8%, 3–10%, 3–15%) that we made with a gradient maker (Hoefer) in Tris-acetate buffer (Fig. 1A and data not shown). We also used a new protein standard (HiMark from Invitrogen) with a protein mass range of 31–460 kDa. Samples of human embryonic kidney (HEK) 293 were tested in these different gradient gels. Samples were prepared in lysis buffer (10 mM Tris-HCl, pH 7.5, 100 mM NaCl, 0.3% CHAPS, 50 mM NaF, 0.5 mM EDTA, 1 mM sodium vanadate, 1 mM phenylmethylsulfonyl fluoride, 5 μg/mL leupeptin, 5 μg/mL aprotinin, 1 μg/mL pepstatin A, 50 mM β-glycerophosphate, 100 μg/mL benzamidine, 1 μM E-64). After rocking during 20 min at 4°C, lysates were centrifuged (15 000 × *g* for 15 min at 4°C) and concentrated sample buffer was added to the supernatants. The final concentration of the sample buffer was 250 mM Tris-HCl, pH 8.5, 2% w/v lithium dodecyl sulphate, 100 mM DTT, 0.4 mM EDTA, 10% v/v glycerol, 0.2 mM phenol red, 0.2 mM Brilliant Blue G. We used this sample buffer because complete reduction of disulfides of the proteins is obtained under mild heating conditions (10 min at 70°C). Besides, cleavage of Asp-Pro bonds is avoided, since this occurs when the sample is heated at 100°C in Laemmli sample buffer [4]. After mild heating, the sample was loaded and then it was run (ΔV = 130 V, 1 h 15 min at room temperature) in a Tris-acetate polyacrylamide gel. The best resolution and separation were obtained with the 3–15% gradient gel as shown with CBB staining (Fig. 1B).

To test the possible applications of this system and its detection sensitivity for large and small proteins, an immunoblot analysis was performed. Different amounts of protein (10–100 μg) from HEK 293 samples were prepared as described above and loaded in a Tris-acetate 3–15% polyacrylamide mini-gel previously made in glass plates. After running it, the gel was consistent and easy to manipulate. Proteins were transferred to a PVDF membrane

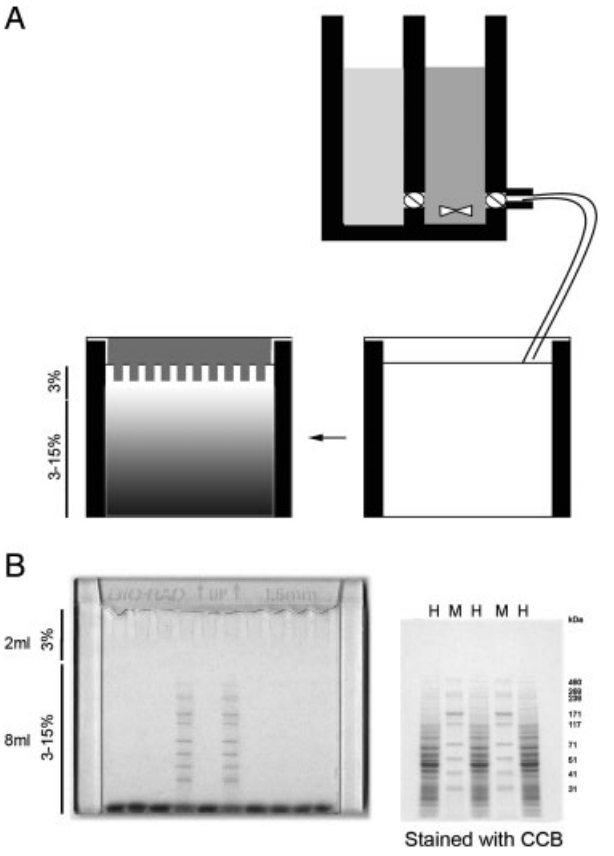

Figure 1. The Tris-acetate polyacrylamide gel. (A) Schematic representation of how to make a 3–15% gradient gel with a gradient maker. The 3 and 15% polyacrylamide solutions (from a 40% acrylamide:bisacrylamide stock with 2.6% of bisacrylamide) are poured in each compartment of the gradient maker at the same time. Immediately after the gradient is made, a 3% solution is added before letting the gradient gel solidify between glass plates from a slab apparatus. (B) Example of Tris-acetate polyacrylamide gel. Gel was made in glass plates from Bio-Rad (Miniprotean system II) with 1.5-mm spacers. Volumes used are indicated (left side). Pre-stained protein standards (31, 41, 51, 71, 117, 171, 238, 268 and 460 kDa from Invitrogen) and 50 μg of protein from a lysate of HEK 293 cells were separated in a 3–15% polyacrylamide gradient gel (left side) and visualized by CCB staining (right side). Standards and lysate are indicated as M and H, respectively.

using a standard wet apparatus (Bio-Rad) for 2 h (I = 200 mA) or overnight (ΔV = 20 V). The transfer buffer contained 20% methanol, 25 mM Bicine, 25 mM Bis-Tris, 1 mM EDTA, 1.3 mM sodium bisulfite, pH 7.2. Under these conditions, commercial protein markers (31–460 kDa) were completely transferred (Fig. 2). By following the previous indications, proteins of all sizes could be simultaneously analyzed by immunoblot. Using specific antibodies, we could detect the following human proteins: HECT (homologous to the E6-AP carboxyl terminus) domain and RCC1 (regulator of chromosome condensation 1)-like domain-containing protein 1 (HERC1, 532 kDa), HECT domain and RCC1-like domain-containing protein 2 (HERC2, 528 kDa), mammalian target of rapamycin (mTOR, 289 kDa), clathrin

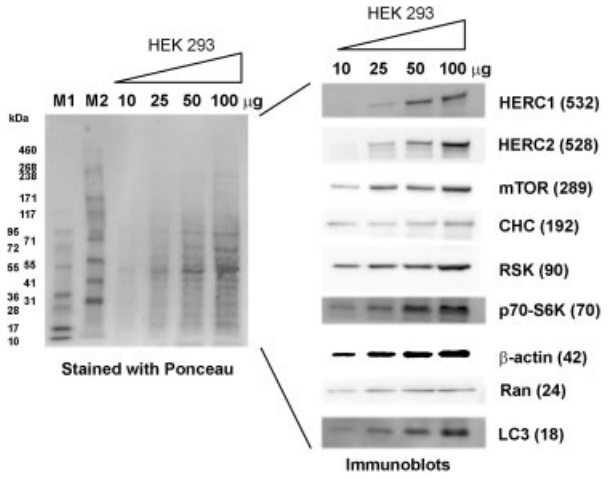

Figure 2. Immunoblot analysis of proteins in the mass range of 10–500 kDa using Tris-acetate polyacrylamide gels to demonstrate the system sensitivity. Lysates from HEK 293 cells were loaded and then they were run in a 3–15% polyacrylamide gradient gel, stained with S-Ponceau (left side), transferred to a PVDF membrane and analyzed by immunoblot (right side) with specific antibodies against the following proteins: HERC1 (532 kDa), HERC2 (528 kDa), mTOR (289 kDa), CHC (192 kDa), RSK (90 kDa), p70-S6K (70 kDa), β-actin (42 kDa), Ran (24 kDa) and LC3 (18 kDa). To check the system sensitivity, 10–100 µg of protein were analyzed. Two different pre-stained protein standards, M1 (10, 17, 28, 36, 55, 72 and 95 kDa from Fermentas) and M2 (31, 41, 51, 71, 117, 171, 238, 268 and 460 kDa from Invitrogen), were used (left side).

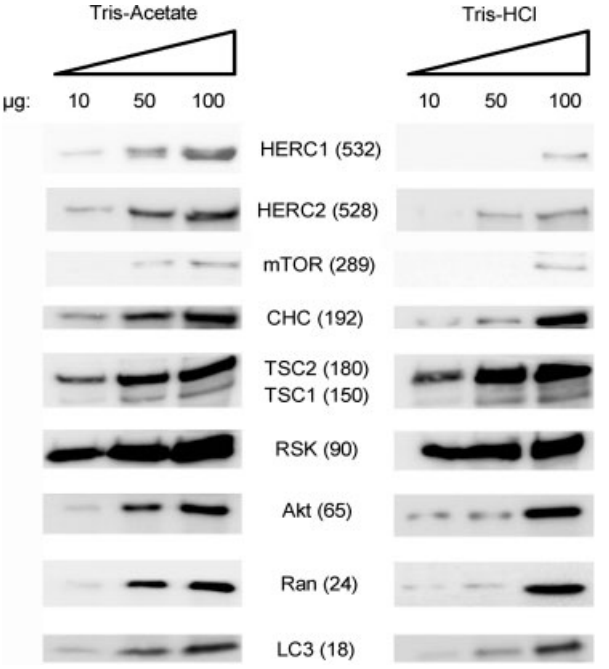

Figure 3. Comparison of Tris-acetate and Tris-HCl PAGE systems. Immunoblot analysis of proteins (mass range of 10–500 kDa) using Tris-acetate and Tris-HCl buffers. Lysates (10, 50 and 100 µg of protein) from HEK 293 cells were loaded and then they were run in a 3–15% polyacrylamide gradient gel, transferred to a PVDF membrane and analyzed by immunoblot with specific antibodies against the following proteins: HERC1 (532 kDa), HERC2 (528 kDa), mTOR (289 kDa), CHC (192 kDa), TSC2 (180 kDa), TSC1 (150 kDa), RSK (90 kDa), Akt (65 kDa), Ran (24 kDa) and LC3 (18 kDa).

heavy chain (CHC, 192 kDa), ribosomal S6 kinase (RSK, 90 kDa), ribosomal protein S6 kinase 1 (p70-S6K, 70 kDa), β-actin (42 kDa), ras-related nuclear protein (Ran, 24 kDa) and microtubule-associated protein 1 light chain 3 (LC3, 18 kDa) (Fig. 2). We have reproduced this separation/detection more than 30 times with similar results, indicating the high reproducibility of this methodology. These data clearly demonstrate that this system is useful to separate and analyze simultaneously proteins in the mass range of 10–500 kDa. Furthermore, the system showed to be very sensitive as it was able to detect even 10 µg of protein of almost all the analyzed proteins from a lysate of human cells (Fig. 2; longer exposures are not shown).

To show the importance of Tris-acetate buffer for the separation of proteins in a wide mass range, we compared Tris-acetate (0.2 M, pH = 7.0) buffer with the classical Tris-HCl (0.375 M, pH = 8.8) buffer of SDS-PAGE. We observed that with similar gradient gels (3–15%) and under similar running/transferring/immunoblotting conditions, the Tris-acetate buffer gave better results. In Fig. 3, we could observe that the Tris-acetate PAGE system was more sensitive in detecting proteins in the 18–532 kDa range by Western blot, particularly small (LC3, Ran) and giant (HERC2, HERC1) proteins.

We have previously reported the LAG system as a helpful tool to analyze simultaneously large and small proteins by electrophoresis [3]. In a comparison between the LAG system and the Tris-acetate PAGE system, we found advantages in using the latter. For example, we need more amount of protein with the LAG system (100–200 µg) than with the Tris-acetate system (10 µg is enough for many detections) in detecting the same proteins by immunoblot. Because of this, we used large gels (16 cm × 18 cm) with the LAG system. The Tris-acetate system uses small gels (8 cm × 8 cm), which are easier to manipulate and cheaper to fabricate due to the reduced reagent volume requirements as compared to larger gels. Moreover, we spent less time running and transferring these gels. For all these reasons, we conclude that the Tris-acetate system is more sensitive, efficient, cheaper and easier to handle than the LAG system. We observed that the major differences between the two systems were the buffers and the gel composition. In Fig. 3, using similar gradient gels, we showed the importance to use Tris-acetate buffer (0.2 M, pH = 7.0) for the separation of proteins in a wide mass range. The effect of gel pH could explain some of these differences. Hachmann and Amshey showed the importance of the environment to which proteins are exposed in Tris-glycine gels [5]. At basic pH, the possibility of protein modification, specially by alkylation of cysteine sulfhydryls, is very high because the pKa of cysteine ranges from 8–9 and because the reducing agent present in

the loading buffer does not co-migrate with the proteins. The use of near-neutral pH gel formulations, electrophoresis buffers at a pH below the pKa of cysteine and reducing agents (*e.g.* sodium bisulfite) that move into the gel ahead of the proteins to maintain a reducing environment reduces significantly this risk [5–7].

In conclusion, we show that Tris-acetate polyacrylamide gels make it possible to simultaneously separate and analyze proteins in the mass range of 10–500 kDa with a high resolution and sensitivity, extending the utility of the PAGE system.

We thank O. Suescún and O. Hadjebi for their comments. This study was supported by grants from Spain (BFU-2008-02084/BMC), European Union (FEDER), ISCIII (RETIC RD06/0020) and Generalitat de Catalunya (2009SGR1059). F. A. P. and I. T. are supported by a doctoral fellowship from Generalitat de Catalunya and by the Juan de la Cierva program, respectively.

The authors have declared no conflict of interest.

References

[1] Maizel, J. V., *Trends Biochem. Sci.* 2000, *25*, 590–592.

[2] Schägger, H., *Nat Protoc.* 2006, *1*, 16–22.

[3] Casas-Terradellas, E., Garcia-Gonzalo, F. R., Hadjebi, O., Bartrons, R., Ventura, F., Rosa, J. L., *Electrophoresis* 2006, *27*, 3935–3938.

[4] Kubo, K., *Anal. Biochem.* 1995, *225*, 351–353.

[5] Hachmann, J. P., Amshey, J. W., *Anal. Biochem.* 2005, *342*, 237–245.

[6] Schägger, H., von Jagow, G., *Anal. Biochem.* 1987, *166*, 368–379.

[7] Wiltfang, J., Arold, N., Neuhoff, V., *Electrophoresis* 1991, *12*, 352–366.

Chapter 17

Tris–Acetate Polyacrylamide Gradient Gels for the Simultaneous Electrophoretic Analysis of Proteins of Very High and Low Molecular Mass

Monica Cubillos-Rojas, Fabiola Amair-Pinedo, Irantzu Tato, Ramon Bartrons, Francesc Ventura, and Jose Luis Rosa

Abstract

Polyacrylamide gel electrophoresis (PAGE) is one of the most powerful tools used for protein analysis. We describe the use of Tris–acetate buffer and 3–15% polyacrylamide gradient gels to simultaneously separate proteins in the mass range of 10–500 kDa. We show that this system is highly sensitive, it has good resolution and high reproducibility, and that it can be used for general applications of PAGE such as Coomassie Brilliant Blue staining and immunoblotting. Moreover, we describe how to generate mini Tris–acetate polyacrylamide gels to use them in miniprotein electrophoresis systems. These economical gels are easy to generate and to manipulate and allow a rapid analysis of proteins. All these features make the Tris–acetate–PAGE system a very helpful tool for protein analysis.

Key words: Electrophoresis, Giant proteins, Gradient gel, PAGE, Protein separation, Tris–acetate

1. Introduction

The sodium dodecyl sulfate polyacrylamide gel electrophoresis (SDS-PAGE) is a tool frequently used for protein analysis. Glycine–SDS-PAGE (also known as Laemmli–SDS-PAGE) and tricine–SDS-PAGE, which are based on Tris–glycine and Tris–tricine buffer systems, respectively, are the most commonly used variants to separate proteins by their size (1, 2). Polyacrylamide gels are composed of acrylamide and the cross-linker bisacrylamide. Variations in the concentrations of acrylamide and bisacrylamide into Laemmli–SDS-PAGE and tricine–SDS-PAGE allow separating proteins in the range of 1–500 kDa. Proteins smaller than 30 kDa are well resolved using tricine–SDS-PAGE. Glycine–SDS-PAGE

Biji T. Kurien and R. Hal Scofield (eds.), *Protein Electrophoresis: Methods and Protocols*, Methods in Molecular Biology, vol. 869, DOI 10.1007/978-1-61779-821-4_17,

system is recommended for proteins larger than 30 kDa (2, 3). The different separation characteristics of these systems are related to the *p*Ka values of glycine and tricine that permit different electrophoretic mobilities and increasing the resolution of proteins of a specific mass range. Thus, to separate proteins in a wide mass range, it would be necessary to use both electrophoresis systems (2). Alternatively, it is also recommended to use a gradient gel with high percentage of acrylamide at the bottom and a lower percentage at the top to resolve giant and small proteins in the same PAGE (3).

In this chapter, we describe an electrophoresis system based on Tris–acetate gels to separate proteins in the mass range of 10–500 kDa (4). In the last few years, several companies have commercialized Tris–acetate gels to separate proteins of different mass range. The composition of these gels is not available for customers and, for this reason, the researcher has no choice but to purchase precast gels and their optimized buffers. These electrophoresis systems are based on a discontinuous buffer system that results in a neutral pH environment during electrophoresis, stabilizing both proteins and gel matrix and providing a better band resolution. The relevance of the environment to which proteins are exposed was previously showed by Hachmann and Amshey using Tris–glycine gels (5). At basic pH, there is a high possibility of protein modification, especially by alkylation of cysteine sulfhydryls, due to the cysteine pKa that ranges from 8 to 9 and because the reducing agent contained in the loading buffer does not co-migrate with the proteins. The use of near-neutral pH gel formulations, electrophoresis buffers at a pH lower than the cysteine pKa, and reducing agents (e.g., sodium bisulfite) that move into the gel ahead of the proteins to maintain a reducing environment reduces this risk significantly (5–7). We have assessed several combinations of these parameters (concentrations, pH, acrylamide:bisacrylamide ratios, gradients) obtaining the best results using a 3–15% polyacrylamide gradient gel made with 0.2 M Tris–acetate (pH 7.0) buffer and a standard acrylamide:bisacrylamide solution (40:1), containing a 2.6% concentration of bisacrylamide, 0.042% ammonium persulfate (APS), and 0.12% *N*,*N*,*N*′,*N*′-tetramethylethylenediamine (TEMED) (4).

The composition of the running buffer (50 mM tricine, 50 mM Tris, 0.1% SDS, 1.3 mM sodium bisulfite, pH 8.2) is similar to the buffer used for tricine–SDS-PAGE (2), but the antioxidant sodium bisulfite is added in order to maintain the proteins in a reduced state during the run. The sample of proteins is prepared in a sample buffer that contains lithium dodecyl sulfate (LDS): 250 mM Tris–HCl pH 8.5, 2% (w/v) LDS, 100 mM DTT, 0.4 mM EDTA, 10% (v/v) glycerol, 0.2 mM phenol red, and 0.2 mM Coomassie Brilliant Blue (CBB) G. This sample buffer allows the reduction of disulfides of the proteins under mild heating conditions (10 min at 70°C) avoiding the cleavage of Asp-Pro bonds that occurs when

the sample is heated at 100°C in Laemmli sample buffer (8). After the run, proteins in the gel can be stained (e.g., CBB) or transferred to a membrane (e.g., nitrocellulose or polyvinylidene fluoride (PVDF)). To transfer the run to a PVDF membrane, we have used a transfer buffer containing 20% methanol, 25 mM bicine, 25 mM Bis–Tris, 1 mM EDTA, and 1.3 mM sodium bisulfite, pH 7.2. Under these conditions, it is possible to separate and simultaneously analyze proteins in the mass range of 10–500 kDa in a single PAGE. This system also provides high sensibility in detecting small amounts of protein: it is possible to analyze by immunoblotting proteins around 500 kDa, running samples containing only 10 μg of total protein. Interestingly, we have optimized this Tris–acetate system to use small gels (8 cm × 8 cm) in miniprotein electrophoresis systems, which are easier to manipulate and cheaper to fabricate due to reduced reagent volume requirements. Moreover, the time required to run and transfer these gels is also reduced.

2. Materials

Prepare all solutions using ultrapure water (Milli-Q quality) and analytical grade reagents.

2.1. Tris–Acetate Polyacrylamide Gradient Gel Components

1. 3 M Tris–acetate pH 7.0 gel buffer (15×): Dissolve 36.33 g Tris base in 90 mL water. Mix and adjust pH with acetic acid. Make up to 100 mL with water. Store at 4°C.
2. LDS sample buffer (4×): 4 mL of 2.5 M Tris–HCl pH 8.5, 0.8 g LDS (Sigma, St Louis, MO, USA), 0.006 g EDTA, 5 mL glycerol (Roche, Indianapolis, IN, USA) 80%, 0.75 mL of 1% CBB G solution, and 0.25 mL of 1% phenol red solution. Mix well and store at room temperature.
3. 40% Acrylamide solution: 37.5:1 (acrylamide/bisacrylamide mix). Store at 4°C.
4. APS: 10% solution in water.
5. TEMED. Store at 4°C.
6. DTT (1,4-dithiothreitol): 1 M solution in water. Aliquot and store at –20°C. We recommend not to freeze samples again for further uses.
7. Running buffer (1×): Dissolve 8.95 g tricine, 6.06 g Tris base, 1 g dodecyl sulfate sodium salt (SDS), and 0.25 g sodium bisulfite in 1 L water. Mix and store at 4°C. The pH of this solution is 8.24. It is not necessary to adjust it.
8. Gradient Maker (Hoefer Instruments, San Francisco, CA).
9. Stir bar and agitator.

10. Mini-PROTEAN II electrophoresis system (Bio-Rad, Hercules, CA, USA).
11. Bicinchoninic acid (BCA) assay kit (Thermo Scientific, Rockford, Ill, USA).

2.2. Immunoblotting Components

1. PVDF membranes (Millipore, Bedford, MA, USA).
2. Transfer buffer (20×): Dissolve 40.8 g Bicine, 52.4 g Bis–Tris, and 3 g EDTA in 500 mL water. Store at 4°C. For western, dilute this buffer to 1× in water with 20% methanol (e.g., for 1 L, 50 mL of 20× transfer buffer/750 mL of water/200 mL methanol and add 0.25 g of the antioxidant sodium bisulfite). The pH of this solution is 7.2. pH adjustment is not necessary.
3. Whatman chromatography papers (17 CHR, Whatman).
4. Mini Trans-Blot Electrophoretic Transfer Cell (Bio-Rad).

3. Methods

Carry out all procedures at room temperature unless otherwise specified.

3.1. Casting the Gel

1. We use the gel cassette of Mini-PROTEAN II to cast the gel (see Fig. 1).
2. Select and prepare the appropriate gradient solutions to separate the proteins of interest. The volumes of reagents required for a mini 3–15% polyacrylamide gradient gel (dimensions: 8 cm × 8 cm; spacers: 1.5 mm) are indicated in Table 1 (see Note 1).
3. Mix solutions before pouring into the chambers of the gradient maker. Add 4 mL of the lower polyacrylamide percentage solution (3%) into the non-outlet chamber (reservoir) (left chamber of gradient maker in Fig. 1a) and 4 mL of the higher polyacrylamide percentage solution (15%) into the outlet chamber that must be equipped with a stir bar (right chamber of gradient maker in Fig. 1a). The valves are closed at this moment. Keep the remaining volume (3 mL) of the lower percentage solution to add later (see Note 2).
4. Start pouring the mixture (or mixed solution) into the glass sandwich. Open the outlet valve. Let the higher percentage solution arrive at the bottom of the glass sandwich and open immediately the other valve. This way, solutions are mixed and form the gradient progressively while pouring. The flow must be constant. Fast flow will cause turbulence that disrupts the gradient, and slow flow rates will cause polymerization of the acrylamide before completing the pouring.

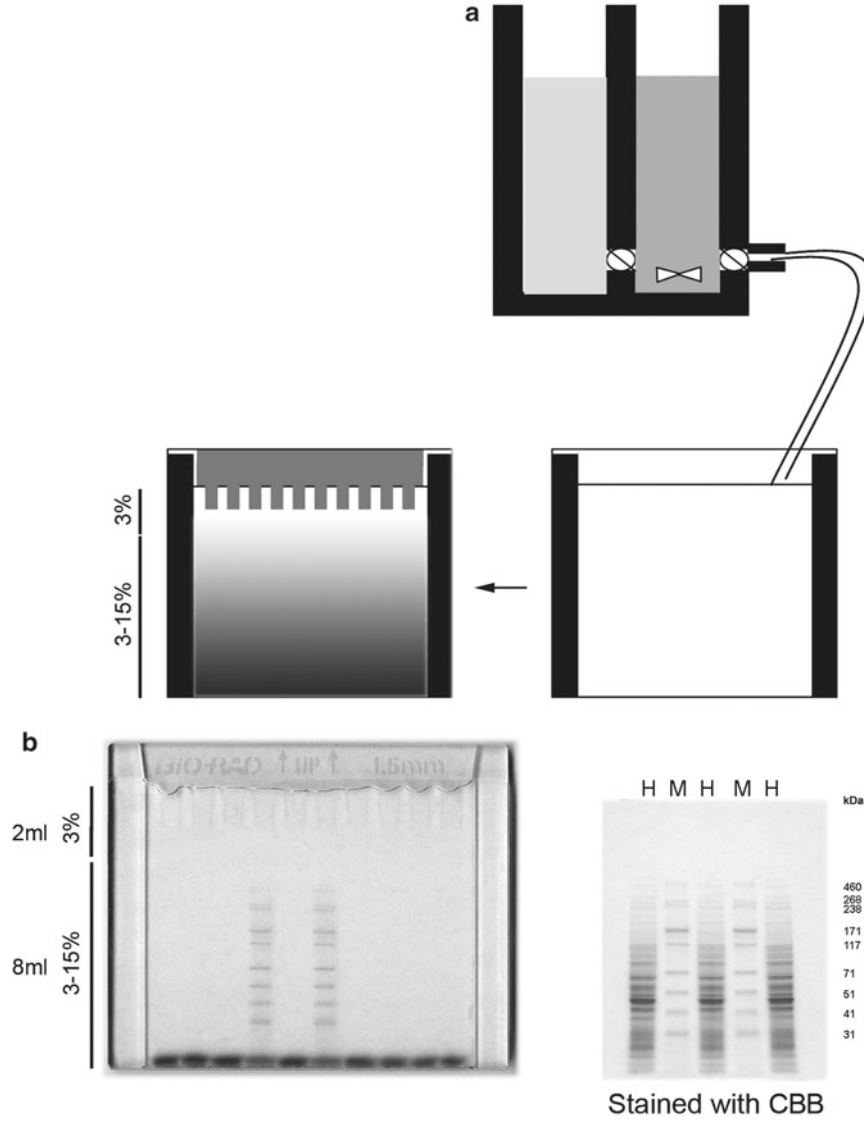

Fig. 1. The Tris–acetate polyacrylamide gel. (**a**) Schematic representation of how to make a 3–15% gradient gel with a gradient maker. The 3 and 15% polyacrylamide solutions [from a 40% acrylamide (37.5:1 acrylamide/bisacrylamide mix) stock solution] are poured in *left* and *right* compartments, respectively, of the gradient maker at the same time. Immediately after the gradient is made, a 3% solution is added before letting the gradient gel solidify between glass plates from a slab apparatus. (**b**) Example of Tris–acetate polyacrylamide gel. Gel was made in glass plates from Bio-Rad (Mini-PROTEAN II system) with 1.5 mm spacers. Volumes used are indicated (left side). Pre-stained protein standards (31, 41, 51, 71, 117, 171, 238, 268, and 460 kDa from Invitrogen) and 50 μg of protein from a lysate of HEK 293 cells were separated in a 3–15% polyacrylamide gradient gel (*left side*) and visualized by CBB staining (*right side*). Standards and lysates are indicated as M and H, respectively. Reproduced from ref. 4 with permission from Elsevier.

5. When solutions inside the chambers are about to consume, add 3 mL of the lower percentage solution into the reservoir chamber and wait until the total pouring of the sandwich is completed. Put the comb. Recover the volume that did not

Table 1
Gel composition to make a 3–15% gradient gel

	3%	15%
3 M Tris–acetate pH 7.0 (15×) (mL)	0.47	0.27
40% Acrylamide solution (mL)	0.53	1.5
Milli-Q water (mL)	6	2.23
Total volume (mL)	7	4
TEMED (μL)	8.75	5
APS 10% (μL)	33.25	19

enter into the sandwich (1 mL approximately) to know when the gel has polymerized.

6. Wash the gradient maker immediately with abundant water to prevent acrylamide polymerization.
7. Leave the gel to polymerize (see Note 3).

3.2. Sample Preparation and Protein Loading

1. Lyse the samples (see Note 4).
2. Centrifuge the samples (e.g., 15,000×*g* for 15 min at 4°C). Collect the supernatant and determine the protein concentration by the BCA assay or a similar method. Add sample buffer 4× without DTT to a final concentration 1×. At this moment, you can use these samples or store them at −20°C.
3. Add DTT (final concentration: 100 mM, e.g., 5 μL of 1 M DTT in 50 μL of total volume) when protein samples are used in PAGE (see Note 5).
4. Heat the samples for 10 min at 70°C and load them into the wells of the gel (see Note 6).

3.3. Electrophoresis Conditions

1. Run at $\Delta V = 130$ V ($I = 115$ mA). The run time estimated for a 3–15% gradient gel is approximately 1 h 15 min. As shown in Fig. 1b and Fig. 2, molecular weight markers ranging from 10 to 460 KDa were separated. These gels can be used for CBB staining (Fig. 1b, right) or to perform immunoblotting (Fig. 2).

3.4. Transfer Conditions

1. Submerge the fiber pads and the Whatman paper in transfer buffer. Place the gel in transfer buffer using a separate tray.
2. Activate the PVDF membrane in methanol for 2 min, wash with deionized water, and submerge in transfer buffer.
3. When the phenol red dye reaches the end of the gel, turn the power supply off. Remove the cast (glasses with the gel).

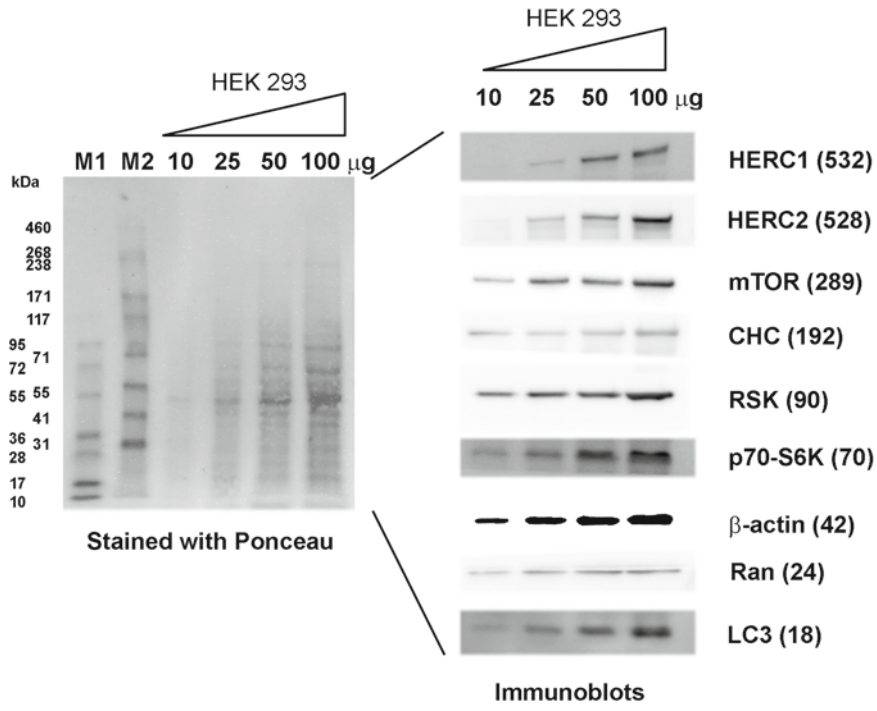

Fig. 2. Applications of the Tris–acetate polyacrylamide gel: analysis by staining and immunoblotting of proteins in the mass range of 10–500 kDa. Lysates from HEK 293 cells were loaded, and then they were run in a 3–15% polyacrylamide gradient gel, stained with S-Ponceau (*left side*), transferred to a PVDF membrane, and analyzed by immunoblot (*right side*) with specific antibodies against the following proteins: HERC1 (532 kDa), HERC2 (528 kDa), mTOR (289 kDa), CHC (192 kDa), RSK (90 kDa), p70-S6K (70 kDa), β-actin (42 kDa), Ran (24 kDa), and LC3 (18 kDa). To check the system sensitivity, 10–100 μg of protein was analyzed. Two different pre-stained protein standards, M1 (10, 17, 28, 36, 55, 72, and 95 kDa from Fermentas) and M2 (31, 41, 51, 71, 117, 171, 238, 268, and 460 kDa from Invitrogen), were used (*left side*). Reproduced from ref. 4 with permission from Elsevier.

Rinse the cast carefully with deionized water and equilibrate it in transfer buffer for few minutes.

4. Separate the thinner glass of the gel carefully with the help of a spatula. Cover the gel with Whatman paper and separate both the gel and the paper from the cast with the help of tweezers or a spatula (see Note 7).
5. Assemble the sandwich as follows (from bottom to top, in the transfer direction): fiber pad, Whatman paper, Whatman paper with the gel, PVDF membrane, two Whatman papers, and fiber pad.
6. Slide the assembled transfer cassette into Mini Trans-Blot Electrophoretic Transfer Cell. Add the transfer buffer and connect the power supply.
7. Perform the transfer for 2 h ($I = 200$ mA) or overnight ($\Delta V = 20$ V).

4. Notes

1. APS and TEMED should be added last, immediately before pouring the gels. The APS solution should be prepared fresh to ensure good resolution of the gel.
2. It is very important to assure that there are no air bubbles between the chambers of the gradient maker before casting the gel. For air bubbles removal, pour 4 mL of the lower percentage solution in the reservoir chamber, open the valve between the chambers, and allow flowing approximately 1 mL of the solution, recovering it and after that pouring the higher percentage solution in the outlet chamber.
3. The gels can be stored at 4°C in running buffer up to 3 days.
4. We have used CHAPS buffer to lyse the cells. This buffer contains 10 mM Tris–HCl pH 7.5, 100 mM NaCl, 0.3% CHAPS, 50 mM NaF, 0.5 mM EDTA, 1 mM sodium vanadate, 1 mM phenylmethylsulfonyl fluoride, 5 μg/mL leupeptin, 5 μg/mL aprotinin, 1 μg/mL pepstatin A, 50 mM β-glycerophosphate, 100 μg/mL benzamidine, and 1 μM E-64. After rocking during 20 min at 4°C, lysates are centrifuged at 15,000 × *g* for 15 min at 4°C. Pellets are discarded and supernatants analyzed.
5. Freeze samples in sample buffer 1×. Do not freeze the samples after thawing. Add fresh DTT just before heating the samples.
6. To eliminate traces of non-polymerized acrylamide, rinse wells with running buffer before applying samples.
7. Because the bottom of the gel is more dense, it is important to start separating the glass from the bottom. Extracting the gel from glasses without the paper implies the risk of distortion of the upper part of the gel; this part is very viscous and must be handled carefully.

Acknowledgments

This study was supported by grants from Spain (BFU2008-02084 and BFU2011-22498), European Union (FEDER), ISCIII (RETICRD06/0020), and Generalitat de Catalunya (2009SGR1059). M.C.R, F. A. P., and I. T. are supported by a doctoral fellowship from IDIBELL, Generalitat de Catalunya, and by the Juan de la Cierva program, respectively.

References

1. Maizel JV (2000) SDS polyacrylamide gel electrophoresis. TIBS 25:590–592
2. Schägger H (2006) Tricine-SDS-PAGE. Nat Protoc 1:16–22
3. Casas-Terradellas E, Garcia-Gonzalo FR, Hadjebi O et al (2006) Simultaneous electrophoretic analysis of proteins of very high and low molecular weights using low-percentage acrylamide gel and a gradient SDS-PAGE gel. Electrophoresis 27:3935–3938
4. Cubillos-Rojas M, Amair-Pinedo F, Tato I et al (2010) Simultaneous electrophoretic analysis of proteins of very high and low molecular mass using Tris-acetate polyacrylamide gels. Electrophoresis 31:1318–1321
5. Hachmann JP, Amshey JW (2005) Models of protein modification in Tris-glycine and neutral pH Bis-Tris gels during electrophoresis: effect of gel pH. Anal Biochem 342:237–245
6. Schägger H, von Jagow G (1987) Tricine-sodium dodecyl sulfate-polyacrylamide gel electrophoresis for the separation of proteins in the range from 1 to 100 kDa. Anal Biochem 166: 368–379
7. Wiltfang J, Arold N, Neuhoff V (1991) A new multiphasic buffer system for sodium dodecyl sulfate-polyacrylamide gel electrophoresis of proteins and peptides with molecular masses 100,000–1000, and their detection with picomolar sensitivity. Electrophoresis 12:352–366
8. Kubo K (1995) Effect of incubation of solutions of proteins containing dodecyl sulfate on the cleavage of peptide bonds by boiling. Anal Biochem 225:351–353

JMG Online First, published on December 14, 2012 as 10.1136/jmedgenet-2012-101367

ORIGINAL ARTICLE

Mutation of HERC2 causes developmental delay with Angelman-like features

Gaurav V Harlalka,[1] Emma L Baple,[1] Harold Cross,[2] Simone Kühnle,[3] Monica Cubillos-Rojas,[4] Konstantin Matentzoglu,[3] Michael A Patton,[1] Karin Wagner,[5] Roselyn Coblentz,[5] Debra L Ford,[6] Deborah J G Mackay,[7] Barry A Chioza,[1] Martin Scheffner,[3] Jose Luis Rosa,[4] Andrew H Crosby[1]

ABSTRACT

Background Deregulation of the activity of the ubiquitin ligase E6AP (UBE3A) is well recognised to contribute to the development of Angelman syndrome (AS). The ubiquitin ligase HERC2, encoded by the *HERC2* gene in patients with Angelman/Prader-Willi syndrome, is thought to be a key regulator of E6AP.

Methods and results Using a combination of autozygosity mapping and linkage analysis, we studied an autosomal-recessive neurodevelopmental disorder with some phenotypic similarities to AS, found among the Old Order Amish. Our molecular investigation identified a mutation in *HERC2* associated with the disease phenotype. We establish that the encoded mutant HERC2 protein has a reduced half-life compared with its wild-type counterpart, which is associated with a significant reduction in HERC2 levels in affected individuals.

Conclusions Our data implicate a model in which disruption of HERC2 function relates to a reduction in E6AP activity resulting in neurodevelopmental delay, suggesting a previously unrecognised role of HERC2 in the pathogenesis of AS.

INTRODUCTION

Angelman syndrome (AS, (MIM 105830)) and Prader–Willi syndrome (PWS, (MIM 176270)) are distinct neurodevelopmental conditions caused by abnormalities at the 15q11–q13 imprinted region. Both conditions present with characteristic developmental, neurological and behavioural phenotypes. Most commonly these disorders result from a 5–7 Mb deletion of the imprinted region, which is either paternal in origin (PWS) or maternal in origin (AS), with clustered breakpoints at either of two centromeric sites and one telomeric site.

Homologous recombination between chromosome-specific low-copy repeats (duplicons) is the mechanism underlying a number of genetic disorders.[1] Sequences homologous to the *HERC2* (*HECT* domain and *RCC1*-like domain 2, MIM 605837, NM 004667.4) gene, encoding a giant 528 kDa protein, form the basis of the low-copy repeats associated with the 15q11–15q13 breakpoints. Evolutionary evidence is suggestive of a *HERC2* duplicon-mediated process leading to an increased tendency for chromosomal rearrangements to occur in this region. Although AS and PWS deletion patients are hemizygous for *HERC2*, to date there has been no evidence that this gene contributes to either phenotype.[2–5]

Patients with classical AS present with severe mental retardation and profound speech impairment with only minimal use of words, although non-verbal and receptive communication skills are higher than expressive language skills. A movement disorder ranging from ataxia to clumsiness or unsteadiness and a characteristic behaviour pattern of hyperactivity, a happy personality and episodes of inappropriate bursts of laughter are typically seen. A wide based gait with pronation at the ankles and arms held at shoulder level and flexed at the elbows are frequent findings. Hypotonia and feeding difficulties are common in infancy with increased tone in the lower limbs and hyperactive reflexes developing later. Seizures are present in over 80% of AS patients and comprise a diversity of types; an EEG pattern of 2–3 Hz large amplitude slow wave bursts is typical and seizures decrease in frequency in adulthood. Brain structure is normal by CT or MRI imaging.

Scoliosis, strabismus and hyperactivity are associated features of the condition. Dysmorphic features are subtle and include microcephaly (by the age of 2 years), prominent chin, macrostomia, hypopigmentation of skin, hair and eyes (deletion patients only). The clinical features of AS have been reviewed previously.[6–9]

Recently we demonstrated physical and functional interactions of HERC2 with E6AP, the primary molecule implicated in the pathogenesis of AS. Most significantly HERC2 was shown to stimulate the E3 ubiquitin-protein ligase activity of E6AP implicating it as a regulator of E6AP and raising the intriguing possibility that HERC2 may play an important role in the AS phenotype.[10] In the current study, we investigated a unique and recognisable inherited neurodevelopmental condition with some phenotypic similarities to AS, present at high frequency among the Ohio Old Order Amish community, which we show to be due to *HERC2* mutation.

METHODS

Subjects

Blood or buccal samples were obtained from affected children, parents and unaffected siblings. DNA and RNA were extracted by standard procedures. A single 0.4 mm diameter skin biopsy was

▸ Additional data are published online only. To view these files please visit the journal online (http://dx.doi.org/10.1136/jmedgenet-2012-101367).

[1]Centre for Human Genetics, St. George's, University of London, London, UK
[2]Department of Ophthalmology and Vision Science, College of Medicine, University of Arizona, Tucson, Arizona, USA
[3]Department of Biology and Konstanz Research School Chemical Biology, University of Konstanz, Konstanz, Germany
[4]Departament de Ciències Fisiològiques II, IDIBELL, Campus de Bellvitge, Universitat de Barcelona, L'Hospitalet del Llobregat, Barcelona, Spain
[5]Windows of Hope Genetic Study, Holmes County, Ohio, USA
[6]Verde Valley Guidance Clinic, Cottonwood, Arizona, USA
[7]Division of Human Genetics, University of Southampton, Southampton, UK

Correspondence to
Dr Andrew H Crosby, Centre for Human Genetics, St George's University of London, Cranmer Terrace, SW17 0RE London, UK;
acrosby@sgul.ac.uk

GVH, ELB, HC, SK, MC-R, BAC, MS and JLR contributed equally.

Received 16 October 2012
Revised 7 November 2012
Accepted 9 November 2012

To cite: Harlalka GV, Baple EL, Cross H, *et al*. *J Med Genet* Published Online First: 13 December 2012 doi:10.1136/jmedgenet-2012-101367

taken from affected individuals XI:2, XI:3, X:I and X:2 and from unaffected individuals. All samples were obtained with approved informed consent (University of Arizona IRB00000291).

Genotyping and linkage analysis

Single-nucleotide polymorphism (SNP) microarray genotyping was performed using Illumina Human CytoSNP-12v2.0 and 2.1 330 K arrays. Marker saturation was carried out using existing and newly generated microsatellite markers (primer sequences available on request). Alleles were size-fractionated using 8% polyacrylamide gels and DNA was visualised by silver staining. Multipoint linkage analysis performed with Simwalk2[11] under a model of autosomal recessive inheritance with full penetrance, using a disease allele frequency estimated at 0.0003. The pedigree was deconstructed to facilitate computational efficiency.

Mutation analysis

Unique intronic primers were designed for 52 HERC2 exons as well as exons of other genes located in the critical interval. The repetitive nature of HERC2 prohibited amplification from genomic DNA; as such the remaining 40 exons were amplified from cDNA using unique exonic primers. Primers were designed using online Primer3 software based on sequences from the online University of California, Santa Cruz (UCSC) Genome Browser database and ordered from Sigma-Aldrich (optimum PCR conditions are available on request). RT-PCR was carried out using PrimeScript One Step RT-PCR Kit V.2, TaKaRa according to the manufacturer's instructions.

Purified PCR amplification products were sequenced using dye-terminator chemistry and electrophoresed on an ABI3130 XLA capillary sequencer (Applied Biosystems). Mutation analysis was carried out using Finch TV 1.4.0 (created by Geospiza Inc.) and Gene Tool 1.0.0.1 (created by Bio Tools Inc). Both strands of each product were sequenced.

Seventy nine anonymised regional control and 169 European control DNA samples were screened by bidirectional sequencing for HERC2 exon 13.

Cell lines, plasmids and transfections

Primary fibroblasts, HEK293T cells and U2OS cells were cultured in DMEM (Sigma Aldrich) with 10% fetal bovine serum (FCS), 2 mM Glutamine (Invitrogen) and 1% penicillin and streptomycin.

Expression constructs (transient transfection experiments) encoding HA-tagged wild-type (wt) E6AP (isoform 1), the HA-tagged catalytically inactive p.Cys820Ala mutant of E6AP, Myc-tagged p.Ile53Ser Ring1B mutant, HA-tagged HERC2 and His-tagged ubiquitin were described previously;[12] Myc-HERC2 (1–1295) was kindly provided by T. Ohta. The cDNAs encoding the p.Pro594Leu HERC2 mutants (full-length or amino acid residues: 1–1295), were generated by a PCR-based approach (further details will be provided upon request) and expressed as N-terminally HA-tagged or Myc-tagged forms from pcDNA3. For transient expression, HEK293T and U2OS cells were transfected with the respective constructs in the presence of a reporter construct encoding β-galactosidase by lipofection (Lipofectamine 2000 or LTX) according to the manufacturer's instructions (Invitrogen). Protein extracts were prepared 24–48 h after transfection as described[13] and transfection efficiency was determined by measuring β-galactosidase activity. Extracts were analysed by Polyacrylamide gel electrophoresis (PAGE) and immunoblotting as previously described.[13] Protein levels were normalised and expressed as percentage of controls. The antibodies used were: anti-HERC2 (BD Biosciences); anti-E6AP (Santa Cruz Biotechnology, Inc); anti-XPA (Kamiya Biomedical Company); anti-Myc (Roche); anti- α tubulin (Calbiochem); anti-Ran; horseradish peroxidase-conjugated secondary antibodies (Invitrogen).

Ubiquitination and degradation assays

For ubiquitination of p.Ile53Ser Ring1B mutant within cells, one 6 cm plate of HEK293T cells was transfected with expression constructs encoding HA-tagged p.Ile53Ser Ring1B mutant (1 μg), E6AP (1.6 μg), His-tagged ubiquitin (1.5 μg) and HERC2 or the p.Pro594Leu HERC2 mutant (3.5 μg, 2.5 μg or 1.5 μg) as indicated (figure 4). Twenty-four hours after transfection, 30% of the cells were lysed under non-denaturing conditions to determine expression levels of E6AP, p.Ile53Ser Ring1B mutant and the two forms of HERC2. The remaining cells were lysed under denaturing conditions, and ubiquitinated proteins were purified. For cycloheximide assays using ectopically expressed HERC2 and p.Pro594Leu HERC2 mutant, 10^7 HEK293T cells were transfected with 10 μg of the HERC2 expression constructs indicated. Twenty-four hours post transfection, cells were trypsinised, pooled and equal aliquots seeded onto 8×6 cm plates. After additional 24 h, cells were treated with 60 μg/ml cycloheximide (dissolved in MeOH) in the absence or presence of 10 μM MG132 (dissolved in Dimethyl sulfoxide (DMSO)) and harvested at the times indicated. Protein extracts were prepared and analysed by SDS-PAGE followed by western blot analysis. Levels of the various HA-tagged proteins (E6AP, p.Cys820Ala E6AP mutant, HERC2 and p.Pro594Leu HERC2 mutant) and Myc-tagged p.Ile53Ser Ring1B mutant were determined by western blot analysis. The antibodies used for detection were the mouse monoclonal HA11 (Hiss Diagnostics, Freiburg, Germany) for HA-tagged proteins and the mouse monoclonal 9E10 (Abcam) for Myc-taggedp.Ile53Ser Ring1B mutant protein.

RESULTS

Fifteen affected individuals, aged between 11 months and 39 years, were identified (figure 1). Cardinal features include global developmental delay, hypotonia, delay in ambulation between ages 3–5 years, an unstable gait frequently with a broad base and arms held upwards and bent at the elbows with brisk walking or running. Failure to acquire normal speech was present in all affected individuals. Those with extreme poverty of speech use gesturing and communication aids effectively and understanding is far greater than language ability. Seizures were reported in 4/15 affected cases. Neuroimaging was only available for 6/15 individuals, in three cases absence of the posterior half of the corpus callosum was reported, the remaining three were said to be unremarkable.

Affected individuals were frequently reported to have poor concentration and hyperactivity. Dysmorphic features are subtle and include plagiocephaly, prognathism, narrow palate, elongated hallux, sandal gap and excessive pronation of the feet occasionally requiring surgery. The clinical features are detailed in tables 1A and 1B.

Interestingly the majority of affected individuals in the Amish community have bright blue eyes due to the coincident close proximity of the causative founder mutation to a SNP rs12913832 in *HERC2* that influences OCA2 expression and is associated with eye colour (data not shown).[14]

Assuming that a founder mutation was responsible we undertook a genome wide microarray scan using Illumina Human CytoSNP-12v2.0 and 2.1 330K arrays using DNA from the

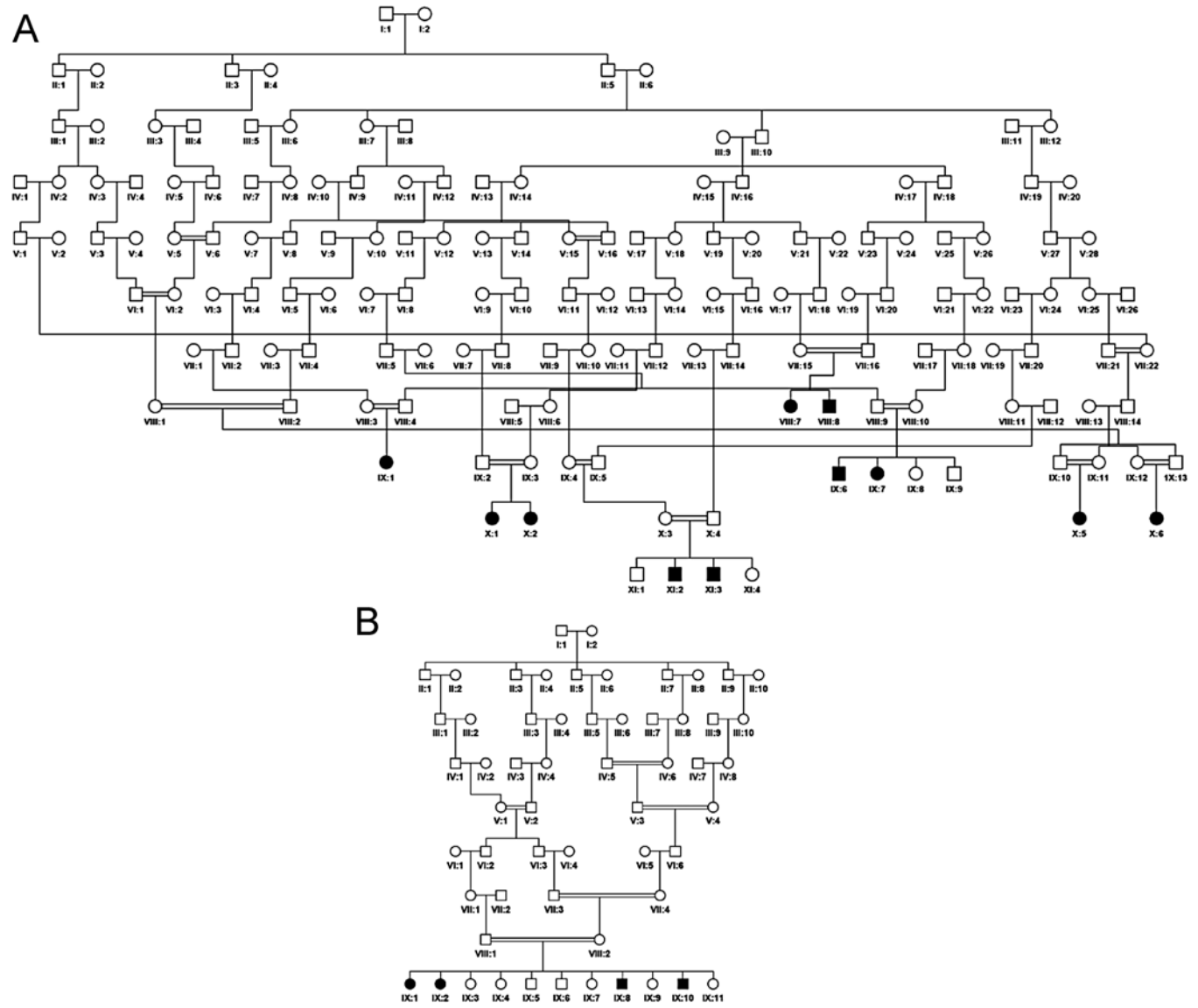

Figure 1 (A) and (B) Pedigree drawings of the two Amish families.

affected individuals initially available (VIII:7, VIII:8, IX:6, IX:7, X:5, X:6). This identified a single notable homozygous region shared by all affected individuals of 1.8Mb on chromosome 15q13.1–q13.3, delimited by markers rs1378094 and rs10162860, likely to correspond to the disease locus. Subsequent microsatellite marker analysis (see online supplementary figure S1) confirmed autozygosity across this region and refined and precisely positioned the disease locus (LODmax 12.5). The putative disease locus is predicted to contain 28 transcript-encoding regions, of which three are hypothetical, two are microRNAs and 17 are pseudogenes. While screening the remaining six genes a non-synonymous base variant was identified in exon 13 of *HERC2* (NM_004667.5:c.1781C>T), predicted to encode a HERC2 protein with substitution of proline by leucine at amino acid position 594 (see online supplementary figure S2). This substitution is not a known SNP and is not present in the 1000 Genomes Project or the Exome Variant Server, NHLBI GO Exome Sequencing Project (6503 subjects). Genotyping of the full family revealed that the sequence variant cosegregated appropriately for a recessive disorder among the entire extended family comprising seven nuclear families, with affected individuals being homozygous, parents being heterozygous carriers and unaffected siblings being either wt or heterozygous carriers of the variant (figure 1A). The c.1781C>T variant was also found to cosegregate in a second Amish family comprising four affected individuals from a distinct Amish deme (figure 1B). Analysis of 158 control chromosomes from unaffected individuals from the same Ohio Amish community identified two heterozygous carriers of the sequence variant. RNA was extracted from the whole blood of two of the affected cases (IX:6 and IX:7) for cDNA synthesis and sequencing, which verified the presence of the variant in the RNA transcript.

Given the proximity of the *HERC2* gene to the AS/PWS imprinting control region, we analysed methylation status at the *SNRPN* imprinted locus by methylation specific PCR; no abnormalities were detected (data not shown).

We next investigated the functional consequences of the *HERC2* mutation. Western blot analysis revealed a profound effect of the mutation on protein levels, with HERC2 protein being almost undetectable in fibroblasts derived from four affected individuals in comparison with three healthy controls.

Table 1A A comparison of the clinical findings of individuals homozygous for *HERC2* c.1781C>T (Pedigree 1A)

	VIII:7	VIII:8	IX:1	IX:6	IX:7	X:1	X:2	X:4	X:5	XI:2	XI:3
Gender	F	M	F	M	F	F	F	F	F	M	M
Age (years)	39	35	24	17	19	13.6	12.6	5.1	6.7	7.8	5.1
Growth Parameters											
Birth weight SDS	N/K	N/K	N/K	1.06	1.43	−1.83	−1.08	−1.22	0.30	0.3	−0.09
OFC SDS	−0.37	0.14	N/K	2.98	N/K	−1.77	N/K	−2.63	−1.23	−1.8	−2.7
Development											
Speech	100 words	<30 Words	SS	SS	SS	<30 words	10 words	–	SS	Limited	20 words
Walked (years)	4.3	4.3	4	4	4	4	4	–	5	3.5	–
Intellectual disability	Moderate	Moderate/severe	Moderate	Moderate	Moderate	Moderate	Moderate	Moderate/severe	Moderate	Mild	Moderate
Neurology											
Childhood hypotonia	+	+	+	+	+	+	+	+	+	+	+
Gait	Arms raised+bent (run)	Arms raised+bent (run)	BB	Arms raised+bent (run)	BB	Arms raised +bent	Arms raised+bent (run)	N/A	Arms raised + bent	Clumsy	N/A
Foot pronation	–	–	N/K	+	+	+	+	N/A	+	+	N/A
Seizures	–	–	–	Absence GM	–	–	–	–	–	–	3xGM
Neuroimaging	CT Normal	N/K	N/K	N/K	CT Normal	CT Normal	N/K	CT Absent post CC	N/K	N/K	MRI Absent post CC
Hyperactivity	+	–	+	+	+	+	+	–	+	+	–
Behavioural characteristics	Affectionate	Aggression Repetitive behaviour		Affectionate Sociable	Affectionate Sociable	Affectionate Sociable	Affectionate Sociable	Interactive Flaps hands	Repetitive behaviour		Irritable Head banging
Physical anomalies											
Strabismus	+	–	–	–	–	–	–	+	+	–	+
High narrow palate	+	N/K	+	+	+	+	+	N/K	+	N/K	N/K
Feet	Small	Small	Elongated hallux SG OT	Elongated hallux	N/K	Elongated hallux SG	N/K	SG OT	SG OT	Elongated hallux SG	Elongated hallux SG
Other physical findings	Scoliosis Freq OM	MVP Basal skin syndactyly all digits	Freq OM					Freq OM NGT fed until 4 years			TGA

BB, broad base; CC, corpus callosum; CT, computerised tomography; Freq, frequent; GM, Grand mal seizures; MRI, magnetic resonance imaging; MVP, mitral valve prolapse; N/K, not known; N/A, not available; OFC, occipital frontal circumference; OT, overlapping toes; OM, otitis media; Post, posterior; SG, sandal gap; SDS, standard deviation scores; SS, short sentences; TGA, transposition of the great arteries.

Table 1B A comparison of the clinical findings of individuals homozygous for *HERC2* c.1781C>T (Pedigree 1B)

	IX:8	IX:10	IX:1	IX:2
Gender	M	M	F	F
Age (years)	17.8	16.8	0.97	2.7
Growth parameters				
Birth weight SDS	N/K	−2.52	−0.27	−0.44
OFC SDS	N/K	N/K	−1.16	−1.64
Development				
Speech	SS	SS	–	<10 words
Walked (years)	4.5	4	–	–
Intellectual disability	Mild/moderate	Mild/moderate	Moderate	Mild/moderate
Neurology				
Childhood hypotonia	N/K	N/K	+	+
Gait	N/K	BB	N/K	N/A
Foot pronation	+	+	N/A	+
Seizures	FC	none	FC	–
Neuroimaging	MRI Absent post CC	N/K	N/K	N/K
Hyperactivity	–	–	N/A	–
Behavioural characteristics			N/A	Sociable
Physical anomalies				
Strabismus	–	–	–	–
High narrow palate	N/K	N/K	N/K	N/K
Feet	N/K	N/K	SG	SG
Other physical findings				

BB, broad base; CC, corpus callosum; Freq, frequent; FC, febrile convulsion; MRI, magnetic resonance imaging; MVP, mitral valve prolapse; N/K, not known; N/A, not available; OFC, occipital frontal circumference; OM, otitis media; OT, overlapping toes; Post, posterior; SDS, SD scores; SS, short sentences; SG, sandal gap; TGA, transposition of the great arteries.

This effect seems specific for HERC2 because protein levels of known HERC2 interacting proteins such as E6AP or XPA, or the unrelated protein α-tubulin were not significantly altered (figure 2A). The dramatic reduction of HERC2 protein levels may relate to reduced expression at the mRNA level associated with reduced transcription rate or mRNA stability, or reduced stability of the translated protein product. We therefore evaluated *HERC2* mRNA levels by quantitative PCR and tested the effect of a proteasome inhibitor cocktail on p.Pro594Leu HERC2 levels in patient primary fibroblasts. This revealed no significant alteration in mRNA levels (data not shown). Evaluation of HERC2 levels in patient fibroblasts following treatment with proteasome inhibitors was suggestive of increased turnover, although this could not be established conclusively due to limited availability of suitable patient cellular material (data not shown). Consequently, we analysed the turnover of the mutant protein by transiently expressing wt HERC2 as well as p.Pro594Leu mutant HERC2 in HEK293T cells. This revealed more rapid degradation of the p.Pro594Leu HERC2 mutant (figure 2B) indicating that the mutant protein has a shorter half-life than wt HERC2.

A possible explanation for the apparent instability of the p.Pro594Leu HERC2 mutant may be provided using structural data from the protein data bank.[15] HERC2 is a member of the RCC1 (Regulator of Chromosome Condensation 1) superfamily, each of which contains at least one RCC1-like domain (RLD). Within its 4834 amino acid sequence, HERC2 contains three RLD domains and a C-terminal HECT domain (homologous to E6AP carboxy terminus) with E3 ligase activity. The p.Pro594Leu amino acid substitution affects a proline residue of the RLD1 domain of HERC2 highly conserved in all species examined (see online supplementary figure S3A,B) and among all human RCC1 superfamily proteins.[16 17] All RLDs are thought to consist of a seven-bladed β-propeller structure similar to RCC1.[18] Although no structural data is available for RLD1 of HERC2, given its similarity to RLD3,[17] it is highly likely to form such a β-propeller structure. In silico superposition of RCC1 and predicted HERC2 RLD3 structures (Jmol/SuperPose/FirstGlance) permitted us to extrapolate the position of P594 in the RLD1 domain of HERC2 to the fourth propeller blade (figure 3). Substitution of the highly conserved Pro594, located within the fourth blade of the propeller, is likely to disrupt the loop between the fourth and the fifth blades and may result in a conformational change affecting protein structural stability and lead to increased turnover rate. To investigate this further, we transfected U2OS cells with wt Myc-HERC2 (residues 1–1249) as well as p.Pro594Leu mutant Myc-HERC2 (residues 1–1249) gene constructs. This confirmed a profound reduction of protein levels associated with substitution of Pro594 (figure 2C), further evidence that protein instability is the likely cause of reduced HERC2 levels in patient fibroblasts. In light of the observation that HERC2 stimulates E6AP, we next examined the effect of the p.Pro594Leu HERC2 substitution on E6AP E3 ligase activity. Given that known substrates of E6AP are either not detectable in primary fibroblasts (activity-regulated cytoskeleton-associated protein (ARC); unpublished data) or particularly short-lived (Ring1B),[19] we studied E6AP-mediated ubiquitination of a Ring1B mutant in transient transfection experiments. This revealed that wt HERC2 as well as p.Pro594Leu HERC2 mutant stimulate E6AP-mediated ubiquitination of Ring1B in a dose-dependent manner (figure 4), however mutant HERC2 was found to be less active than wt HERC2. Similar results were obtained for autoubiquitination of E6AP (data not shown). Although the E6AP activation

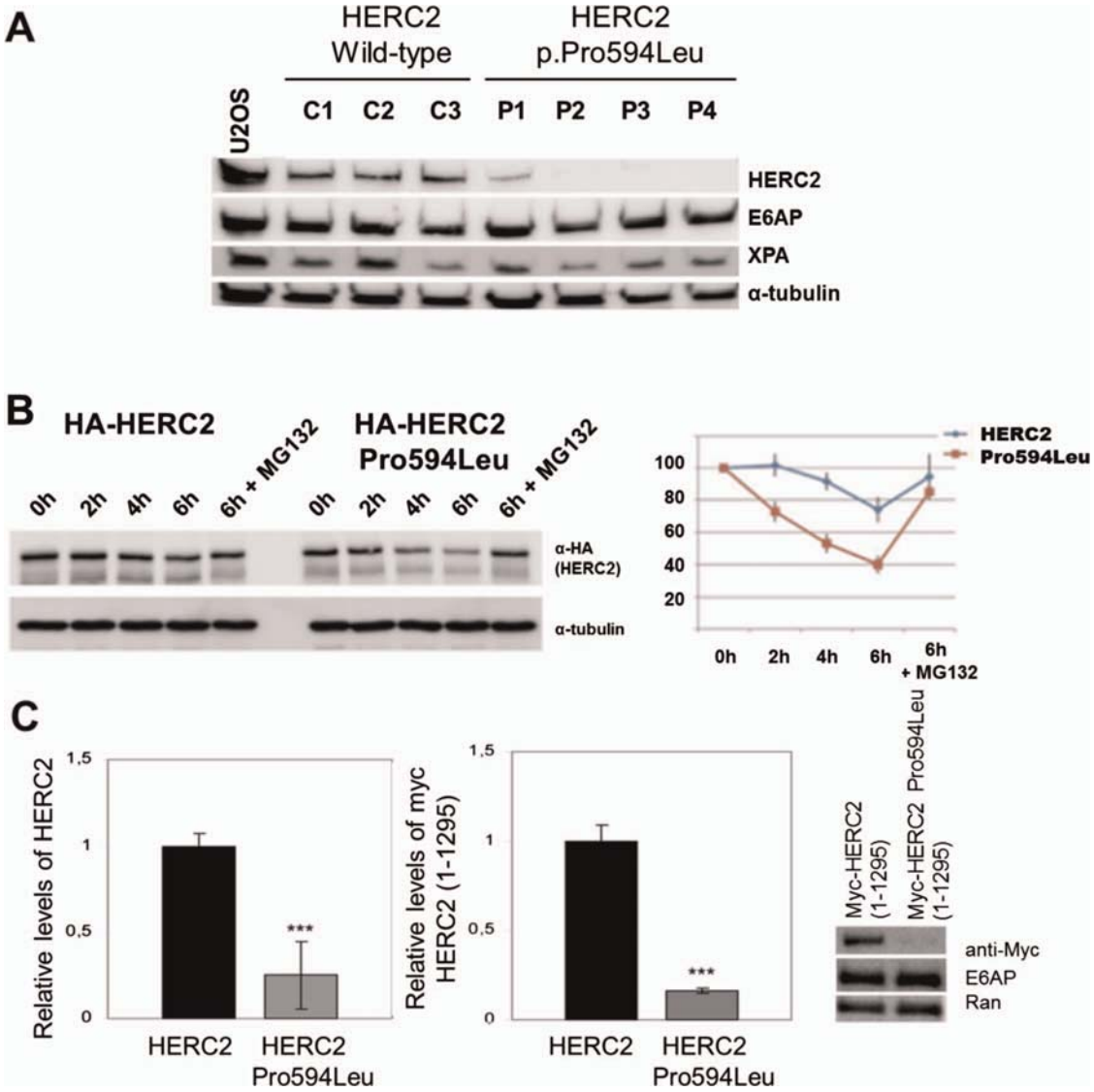

Figure 2 (A) Levels of HERC2 are diminished in fibroblasts from affected individuals. Lysates from fibroblasts of wild-type (wt) controls and affected individuals were analysed by immunoblot with the indicated antibodies. The levels of HERC2 were normalised with respect to α-tubulin as is indicated in the right panel. (B) The p.Pro594Leu HERC2 mutant has a shorter half-life than the wt protein. HEK293T cells with a stable knockdown of endogenous HERC2 expression (unpublished) were transfected with expression constructs encoding HA-tagged forms of wt HERC2 and p.Pro594Leu mutant HERC2. After 48 h, cells were treated with cycloheximide in the absence or presence of 10 μM MG132, harvested at the times indicated, and protein levels analysed by western blot analysis using the antibodies indicated. (C) U2OS cells were transfected with the indicated constructs and analysed by immunoblot. The right panel shows the levels of expression with respect to Ran.

difference detected was moderate, and may not in itself be functionally significant, the dose-dependent nature of HERC2 on E6AP activation is likely to exacerbate effects of the p.Pro594Leu HERC2 mutation.

DISCUSSION

Taken together our genetic and cellular data implicate HERC2 in a human disease phenotype which, although a distinct entity, has some AS-like features.

There are 18 reported members of the human RCC1 protein superfamily, six of these within the HERC subgroup. A number of proteins within this family have been associated with a diverse set of human diseases,[17 20] until now however no HERC subgroup members had been causally linked. Human and mouse HERC2 protein display 95% homology and 99% similarity[5] and HERC2 homozygous and hemizygous mutations have been identified as the cause of the mouse rjs syndrome (runty, jerky, sterile) also known as jdf2 (juvenile development and fertility-2). Affected mice are 20% smaller than their normal counterparts from birth, have abnormal gait and display behavioural abnormalities,[21] reflecting similarities with features seen in our affected subjects. None of the affected individuals that we have seen have shown any significant differences from their healthy siblings in terms of birth weight or subsequent growth, nor have any pubertal abnormalities been reported. We have not observed any reduction in life expectancy; however the oldest affected individual we have seen is 39 years old. There does however appear to be some cognitive and behavioural decline in two of our oldest patients. Currently there is no mouse model of p.Pro594Leu HERC2, and production of such a future model may allow a more direct phenotypic comparison.

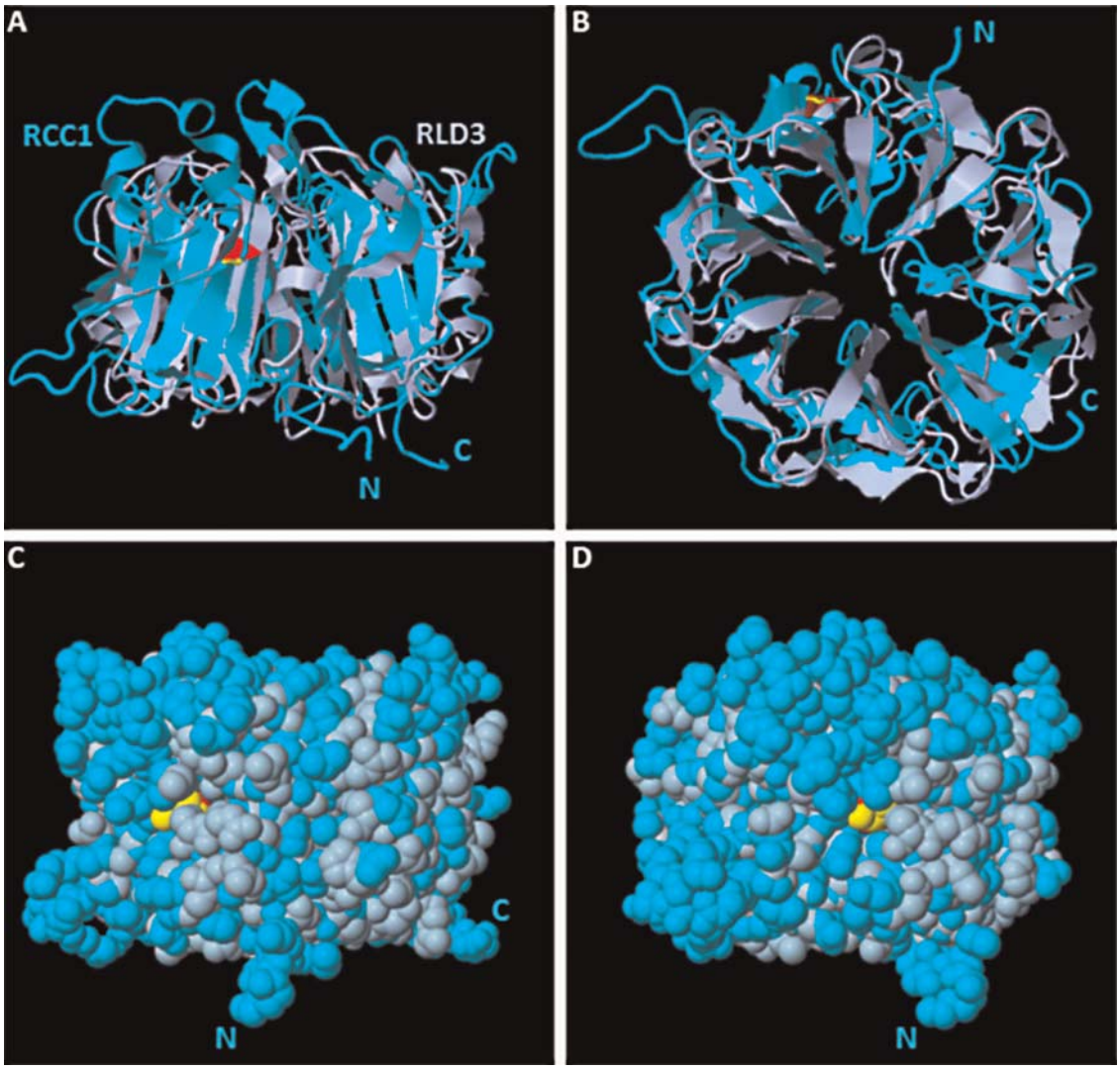

Figure 3 Superposition of Human RCC1 (cyan) and human HERC2 RLD3 (light blue) Lateral (A,C,D) and bottom (B) views of the β-propeller. High conserved proline, equivalent to proline 594 of HERC2, is shown in RCC1 (yellow) and in RLD3 (red). The N-termini and C-termini of RCC1 are indicated. The figure was generated and edited using the SuperPose and FirstGlance in Jmol programmes. Protein Data Bank entries: 1A12 for RCC1 and 3KCI for HERC2 RLD3.

All AS cases associated with *UBE3A* mutations reported to date are predicted to affect the E3 ligase activity of E6AP.[7] The previously reported interaction between HERC2 and E6AP results in stimulation of E6AP E3 ligase activity and involves HERC2 RLD2,[10] whereas the variant reported here affects RLD1. Our data indicate a profound effect of the p.Pro594Leu mutation on HERC2 protein levels, which likely relate to reduced half-life resulting from distortion of the structure of the HERC2 molecule. The modest effect on E6AP stimulation associated with the HERC2 p.Pro594Leu mutation described here may in part explain why the developmental difficulties observed in our subjects are not as profound as those seen in AS patients in whom there is likely a more significant loss of E6AP activity. Seizures are reported in excess of 80% of AS patients. Although seizure activity was only reported in 4/15 subjects, we speculate that this may indicate that a subtle decrease in E6AP activity lowers the threshold for seizure activity. Microcephaly is not a feature of this condition, however this feature of AS is most commonly associated with microdeletions and less so with other molecular mechanisms leading to AS.[9] Notable similarities between AS and the individuals with HERC2 mutation described here include hypotonia in childhood, a similar arms raised posture when walking particularly at speed, excessive pronation of the ankles, clumsiness and poor concentration. AS individuals, most commonly women, frequently develop scoliosis with age. Although we only observed three adult females, it is noteworthy that one had developed severe scoliosis. Strabismus is another feature commonly seen in AS and was reported in 4/15 affected individuals. Importantly a number of significant differences between the two conditions were also apparent. Although the parents of our Amish subjects did not report inappropriate bouts of laughter, many did remark on the sociability and loving nature of their children, however behavioural difficulties, aggression and stereotypies were also reported. Further distinguishing features include lack of the classical AS facial gestalt and no reports of ataxia. It is interesting that in three out of six of our subjects with neuroimaging data there was absence of the posterior part of the corpus callosum, which in association with the other clinical features described may be helpful in terms of reaching a diagnosis in patients with this condition. Finally although both conditions are characterised by significant speech abnormalities, AS individuals rarely

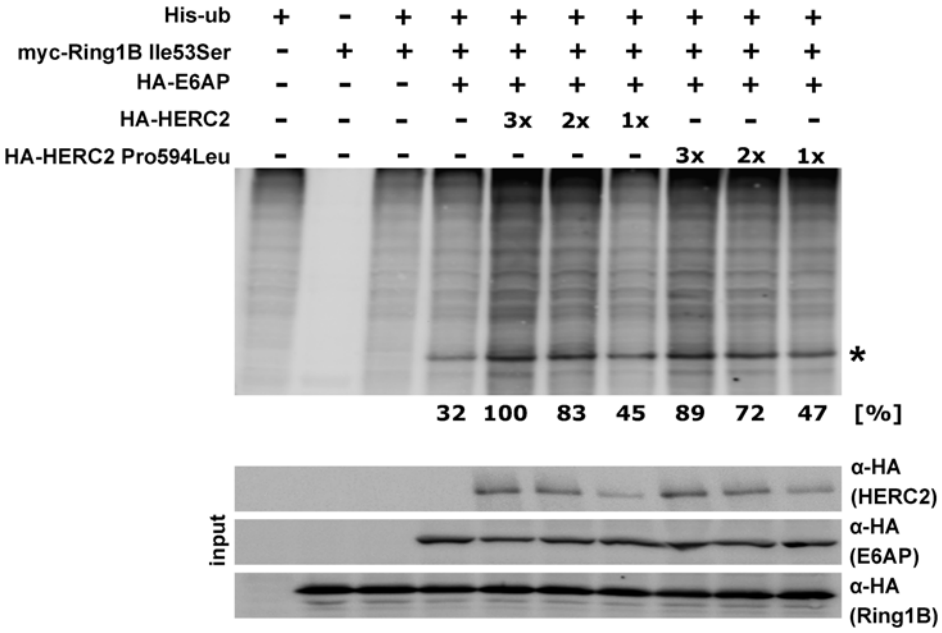

Figure 4 Effect of p.Pro594Leu HERC2 on E6AP-mediated Ring1B ubiquitination. HEK293T cells with a stable knockdown of endogenous HERC2 expression (unpublished) were co-transfected with expression constructs for His-tagged ubiquitin, Myc-tagged p.Ile53Ser Ring1B mutant, HA-tagged E6AP, and HA-tagged full-length versions of HERC2 or p.Pro594Leu mutant HERC2 as indicated. 24 h after transfection, protein extracts were prepared and ubiquitinated proteins were isolated by Ni^{2+}-affinity chromatography. Upon purification, levels of ubiquitinated p.Ile53Ser Ring1B mutant protein were determined by western blot analysis with an anti-Myc antibody (upper panel). Input, corresponds to 20% of the proteins extracts used for affinity purification. *, monoubiquitinated p.Ile53Ser Ring1B mutant protein.

develop any meaningful speech, whereas a number of individuals homozygous for the HERC2 mutation have developed the ability to communicate effectively with language. Good non-verbal communication skills and relatively preserved receptive language ability are features of both conditions. It was notable that those subjects who had received early and intensive speech and language therapy appeared to have made significantly more progress in language attainment.

In the current report, we describe a novel neurodevelopmental syndrome with some features reminiscent of AS arising due to HERC2 mutation. Although AS had not been suspected in any of the patients described here and we recognise that there are important differences between the two conditions, it remains an intriguing possibility that more deleterious mutations in the HERC2 gene may be detected in more severely affected patients who display a more significant phenotypic overlap with AS.

Acknowledgements We are very grateful to the Amish families for partaking in this study, and to the Amish community for their continued support of the Windows of Hope project. We thank G. Pons for his help with protein structure programmes and T. Ohta for the Myc-HERC2 plasmid.

Contributors AHC designed the genetics experiments. GVH, ELB, BAC and DJGM performed the genetics experiments. AHC, JLR, MS and ELB designed the functional cell biology experiments. SK, MCR, KM, JLR and MS performed the cell biology experiments. ELB, HC, DLF, MAP, KW and RC contributed clinical data to the manuscript. AHC, ELB, BAC, JLR and MS wrote the manuscript.

Funding The work was supported by MRC grant (G1002279), Newlife Foundation (AHC, GVH and ELB), MRC Clinical Research Training fellowship (G1001931 to ELB), the Deutsche Forschungsgemeinschaft (SCHE 346/6-1 to MS), and by MICINN (Ministerio de Ciencia e Innovación) grant (BFU2011-22498) to JLR. MCR is supported by a doctoral fellowship from Generalitat de Catalunya.

Competing interests None.

Ethics approval University of Arizona.

Provenance and peer review Not commissioned; externally peer reviewed.

Data sharing statement Any unpublished data from this study is available on request from the corresponding author.

Web references The URLs for data presented herein are as follows: Online Mendelian Inheritance in Man (OMIM), http://www.omim.org/. ClustalW2, http://www.ebi.ac.uk/Tools/msa/clustalw2/. Jalview, http://www.jalview.org. Jmol, http://www.jmol.sourceforge.net. FirstGlance in Jmol, http://www.bioinformatics.org/firstglance/fgij/. SuperPose, http://www.wishart.biology.ualberta.ca/SuperPose/. Primer3, http://www.frodo.wi.mit.edu/. 1000 Genomes Project, http://www.1000genomes.org. Exome Variant Server, NHLBI GO Exome Sequencing Project (ESP), Seattle, WA,: http://evs.gs.washington.edu/EVS/) (accessed, November, 2012).

Accession numbers The databank accession number for *HERC2* reported in this paper is NM_004667.5.

REFERENCES

1 Ji Y, Eichler EE, Schwartz S, Nicholls RD. Structure of chromosomal duplicons and their role in mediating human genomic disorders. *Genome Res* 2000;10:597–610.
2 Amos-Landgraf JM, Ji Y, Gottlieb W, Depinet T, Wandstrat AE, Cassidy SB, Driscoll DJ, Rogan PK, Schwartz S, Nicholls RD. Chromosome breakage in the Prader-Willi and Angelman syndromes involves recombination between large, transcribed repeats at proximal and distal breakpoints. *Am J of Hum Genet* 1999;65:370–86.
3 Chai JH, Locke DP, Greally JM, Knoll JH, Ohta T, Dunai J, Yavor A, Eichler EE, Nicholls RD. Identification of four highly conserved genes between breakpoint hotspots BP1 and BP2 of the Prader-Willi/Angelman syndromes deletion region that have undergone evolutionary transposition mediated by flanking duplicons. *Am J Hum Genet* 2003;73:898–925.
4 Ji Y, Rebert NA, Joslin JM, Higgins MJ, Schultz RA, Nicholls RD. Structure of the highly conserved HERC2 gene and of multiple partially duplicated paralogs in human. *Genome Res* 2000;10:319–29.
5 Ji Y, Walkowicz MJ, Buiting K, Johnson DK, Tarvin RE, Rinchik EM, Horsthemke B, Stubbs L, Nicholls RD. The ancestral gene for transcribed, low-copy repeats in the Prader-Willi/Angelman region encodes a large protein implicated in protein trafficking, which is deficient in mice with neuromuscular and spermiogenic abnormalities. *Hum Mol Genet* 1999;8:533–42.
6 Dagli A, Buiting K, Williams CA. Molecular and clinical aspects of Angelman syndrome. *Mol Syndromol* 2012;2:100–12.
7 Van Buggenhout G, Fryns JP. Angelman syndrome (AS, MIM 105830). *Eur J Hum Genet* 2009;17:1367–73.
8 Williams CA, Beaud AL, Clayton-Smith J, Knoll JH, Kyllerman M, Laan LA, Magenis RE, Moncla A, Schinzel AA, Summers JA, Wagstaff J. Angelman syndrome 2005: updated consensus for diagnostic criteria. *Am J Med Genet A* 2006;140:413–18.
9 Lossie AC, Whitney MM, Amidon D, Dong HJ, Chen P, Theriaque D, Hutson A, Nicholls RD, Zori RT, Williams CA, Driscoll DJ. Distinct phenotypes distinguish the molecular classes of Angelman syndrome. *J Med Genet* 2001;38834–45.
10 Kühnle S, Kogel U, Glockzin S, Marquardt A, Ciechanover A, Matentzoglu K, Scheffner M. Physical and functional interaction of the HECT ubiquitin-protein ligases E6AP and HERC2. *J Biol Chem* 2011;286:19410–6.
11 Sobel E, Lange K. Descent graphs in pedigree analysis: applications to haplotyping, location scores, and marker-sharing statistics. *Am J Hum Genet* 1996;58:1323–37.
12 Wu W, Sato K, Koike A, Nishikawa H, Koizumi H, Venkitaraman AR, Ohta T. HERC2 is an E3 ligase that targets BRCA1 for degradation. *Cancer Res* 2010;70:6384–92.
13 Cubillos-Rojas M, Amair-Pinedo F, Tato I, Bartrons R, Ventura F, Rosa JL. Simultaneous electrophoretic analysis of proteins of very high and low molecular mass using Tris-acetate polyacrylamide gels. *Electrophoresis* 2010;31:1318–21.

14 Eiberg H, Troelsen J, Nielsen M, Mikkelsen A, Mengel-From J, Kjaer KW, Hansen L. Blue eye color in humans may be caused by a perfectly associated founder mutation in a regulatory element located within the HERC2 gene inhibiting OCA2 expression. *Hum Genet* 2008;123:177–87.
15 Berman H, Henrick K, Nakamura H. Announcing the worldwide Protein Data Bank. *Nat Struct Biol* 2003;10:980.
16 Garcia-Gonzalo FR, Rosa JL. The HERC proteins: functional and evolutionary insights. *Cell Mol life Sci* 2005;62:1826–38.
17 Hadjebi O, Casas-Terradellas E, Garcia-Gonzalo FR, Rosa JL. The RCC1 superfamily: from genes, to function, to disease. *Biochim Biophys Acta* 2008;1783:1467–79.
18 Renault L, Nassar N, Vetter I, Becker J, Klebe C, Roth M, Wittinghofer A. The 1.7 A crystal structure of the regulator of chromosome condensation (RCC1) reveals a seven-bladed propeller. *Nature* 1998;392:97–101.
19 Zaaroor-Regev D, de Bie P, Scheffner M, Noy T, Shemer R, Heled M, Stein I, Pikarsky E, Ciechanover A. Regulation of the polycomb protein Ring1B by self-ubiquitination or by E6-AP may have implications to the pathogenesis of Angelman syndrome. *Proc Nat Acad Sci USA* 2010;107:6788–93.
20 Otto EA, Trapp ML, Schultheiss UT, Helou J, Quarmby LM, Hildebrandt F. NEK8 mutations affect ciliary and centrosomal localization and may cause nephronophthisis. *J Am Soc Nephrol* 2008;19:587–92.
21 Lehman AL, Nakatsu Y, Ching A, Bronson RT, Oakey RJ, Keiper-Hrynko N, Finger JN, Durham-Pierre D, Horton DB, Newton JM, Lyon MF, Brilliant MH. A very large protein with diverse functional motifs is deficient in rjs (runty, jerky, sterile) mice. *Proc Nat Acad Sci USA* 1998;95:9436–41.

Mutation of HERC2 causes developmental delay with Angelman-like features

Gaurav V Harlalka, Emma L Baple, Harold Cross, et al.

J Med Genet published online December 14, 2012
doi: 10.1136/jmedgenet-2012-101367

Contribution of S6K1/MAPK Signaling Pathways in the Response to Oxidative Stress: Activation of RSK and MSK by Hydrogen Peroxide

Anna Siebel[1,2☯], Monica Cubillos-Rojas[1☯], Roberto Christ Santos[4☯], Taiane Schneider[1], Carla Denise Bonan[2], Ramon Bartrons[1], Francesc Ventura[1], Jarbas Rodrigues de Oliveira[3], Jose Luis Rosa[1*]

1 Departament de Ciències Fisiològiques II, Campus de Bellvitge, Institut d'Investigació Biomèdica de Bellvitge (IDIBELL), Universitat de Barcelona, L'Hospitalet de Llobregat, Barcelona, Spain, **2** Laboratório de Neuroquímica e Psicofarmacologia, Faculdade de Biociências, Pontifícia Universidade Católica do Rio Grande do Sul, PUCRS, Porto Alegre, Rio Grande do Sul, Brazil, **3** Laboratório de Biofísica Celular e Inflamação, Faculdade de Biociências, Pontifícia Universidade Católica do Rio Grande do Sul, PUCRS, Porto Alegre, Rio Grande do Sul, Brazil, **4** Laboratório de Microbiologia Clínica, Ciências da Saúde, Centro Universitário Franciscano, UNIFRA, Santa María, Rio Grande do Sul, Brazil

Abstract

Cells respond to different kind of stress through the coordinated activation of signaling pathways such as MAPK or p53. To find which molecular mechanisms are involved, we need to understand their cell adaptation. The ribosomal protein, S6 kinase 1 (S6K1), is a common downstream target of signaling by hormonal or nutritional stress. Here, we investigated the initial contribution of S6K1/MAPK signaling pathways in the cell response to oxidative stress produced by hydrogen peroxide (H_2O_2). To analyze S6K1 activation, we used the commercial anti-phospho-Thr389-S6K1 antibody most frequently mentioned in the bibliography. We found that this antibody detected an 80-90 kDa protein that was rapidly phosphorylated in response to H_2O_2 in several human cells. Unexpectedly, this phosphorylation was insensitive to both mTOR and PI3K inhibitors, and knock-down experiments showed that this protein was not S6K1. RSK and MSK proteins were candidate targets of this phosphorylation. We demonstrated that H_2O_2 stimulated phosphorylation of RSK and MSK kinases at residues that are homologous to Thr389 in S6K1. This phosphorylation required the activity of either p38 or ERK MAP kinases. Kinase assays showed activation of RSK and MSK by H_2O_2. Experiments with mouse embryonic fibroblasts from p38 animals' knockout confirmed these observations. Altogether, these findings show that the S6K1 signaling pathway is not activated under these conditions, clarify previous observations probably misinterpreted by non-specific detection of proteins RSK and MSK by the anti-phospho-Thr389-S6K1 antibody, and demonstrate the specific activation of MAPK signaling pathways through ERK/p38/RSK/MSK by H_2O_2.

Citation: Siebel A, Cubillos-Rojas M, Santos RC, Schneider T, Bonan CD, et al. (2013) Contribution of S6K1/MAPK Signaling Pathways in the Response to Oxidative Stress: Activation of RSK and MSK by Hydrogen Peroxide. PLoS ONE 8(9): e75523. doi:10.1371/journal.pone.0075523

Editor: Shou-Jiang Gao, University of Southern California Keck School of Medicine, United States of America

Received May 24, 2013; **Accepted** August 14, 2013; **Published** September 18, 2013

Funding: This research was supported by grants from MICINN (Ministerio de Ciencia e Innovación) (BFU2011-22498 and PHB2008-0080-PC) and ISCIII (Instituto de Salud Carlos III) (RETIC, RD06/0020) in Spain, and from CAPES/DGU (190/09) in Brazil. The funders had no role in study design, data collection and analysis, decision to publish, or preparation of the manuscript.

Competing interests: The authors have declared that no competing interests exist.

* E-mail: joseluisrosa@ub.edu

☯ These authors contributed equally to this work.

Introduction

Reactive oxygen species (ROS) function as important physiological regulators of intracellular signaling pathways [1]. High ROS levels are associated with diseases such as neurodegeneration, atherosclerosis, chronic inflammation, diabetes or cancer [1-4]. An increase in ROS is also observed with age, probably caused by the accumulation over time of free radicals from aerobic metabolism and linked to a decreased antioxidant capacity and/or mitochondrial dysfunction [1,5]. The emerging role of ROS in physiological and pathophysiological processes demonstrates the importance of understanding the cell signaling pathways involved in redox signaling [1,3,6].

The mitogen-activated protein kinase (MAPK) signaling pathways allow cells to interpret a wide range of external signals and respond by generating a plethora of different biological effects. Members of the MAPK family, including extracellular signal-regulated kinases (ERK), c-Jun N-terminal kinases (JNK) and p38, are activated by ROS. The activation of these kinases usually regulates the expression of a variety of

genes involved in survival, proliferation or cell death, depending on the stimulus and the cell-type studied [1,3,7].

The ribosomal protein S6 kinase 1 (S6K1) is a common downstream target of signaling by hormones and nutrients. S6K1 is a substrate of the mammalian target of rapamycin (mTOR) complex 1 (mTORC1). This complex is a Ser/Thr kinase that regulates S6K1 activation through its phosphorylation at Thr389 (T389). Activated S6K1 regulates the phosphorylation of other substrates such as the ribosomal protein S6 to promote protein synthesis, cell growth and cell proliferation [8-10]. In recent years, several studies have also involved S6K1 in the response to oxidative stress. Thus, whereas some authors propose that mTOR inhibition is required for H_2O_2-induced cell death [11], others demonstrate that the mTOR/S6K1 pathway is not responsible for this effect [12]. In some cases, S6K1 phosphorylation was observed [12,13], whereas in others a decrease in this phosphorylation was reported [11,14,15]. These apparently controversial findings have been justified by the complexity of the pathways involved and by the function of these pathways possibly depending on the cell type, H_2O_2 dose and duration of the stress signal [12].

S6K1 activation is measured by the increase of its phosphorylation at T389 and/or by the phosphorylation increase of its substrate, the ribosomal protein S6, at S235/S236. Thus, antibodies against these phosphorylated residues are a valuable tool for analyzing S6K1 activation. The specificity of these antibodies is crucial to interpretation of the data. S6K1 is member of a family of serine /threonine kinases named AGC. Other members of this family, such as the mitogen- and stress-activated kinases (MSK) and the p90 ribosomal S6 kinases (RSK), show a high degree of homology, in particular a serine residue within the hydrophobic motif of the RSK and MSK proteins [16]. Previous studies have shown the cross-reaction of anti-phosphorylated-T389 (P-T389)-S6K1 antibody with phosphorylated RSK and MSK proteins and that activation of these kinases also regulate the phosphorylation of the ribosomal protein S6 at S235/S236 [17].

In response to oxidative stress, MAPK signaling pathways are activated; contradictory data have been reported for the S6K1 signaling pathway. We asked whether under these conditions the anti-P-T389-S6K1 antibody detected RSK and MSK proteins and could be a motif to misinterpret these findings. In the present study, we showed that S6K1 is not involved in the fast response to incubation with H_2O_2 and that the anti-P-T389-S6K1 antibody detected the phosphorylation of RSK and MSK proteins by H_2O_2 in a p38- and ERK-dependent manner.

Materials and Methods

Reagents

Insulin, wortmannin, rapamycin and anti-P-ERK1/2 antibody (Sigma-Aldrich); hydrogen peroxide solution (H_2O_2) (Panreac); U0126 and SB203580 (Calbiochem); anti-mTOR, anti-P-T389-S6K1 (1A5), anti-P-S380-RSK, anti-P-S376-MSK, anti-P-S235/236-S6, anti-S6 (54D2) and anti-PT180/Y182-p38 antibodies (Cell Signaling Technology); anti-MSK, anti-S6K1 (C-18) and anti-RSK1 (C-21) antibodies (Santa Cruz Biotechnology, Inc.); Alexa Fluor 488, Alexa Fluor 546, TO-PRO3 (Molecular Probes); anti-P- H2AX antibody, Immobilon-P PVDF transfer membrane (Millipore Corporation); siRNA used: mTOR (CCCUGCCUUUGUCAUGCCUdTdT), S6K1 (GGGGGCUAUGGAAAGGUUUdTdT), RSK1 (**GCUAUACCGUCGUGA**-GAUCdTdT), RSK2 (GGAGGAGAUUAACCCACAAdTdT), MSK1 (**GGAACUGG**-AGCUUAUGGAAdTdT), MSK2 (UUGCACAUGAUCUCGGCCGdTdT) and non-targeting control (UAGCGACUAAACACAUCAAdTdT).

Cell culture and transfections

WT and p38α-deficient MEFs were a gift from Dr. A. Nebreda (Institute for Research in Biomedicine, Barcelona, Spain) [18]. All cell lines were cultured at 37°C in Dulbecco's Modified Eagle medium (DMEM) (Gibco), containing 10% fetal bovine serum. siRNA transfections were carried out in MCF7 cells with the calcium phosphate transfection system. For experiments with insulin, cells were deprived of serum overnight and then incubated with 200 nM insulin for 30 min. For experiments with H_2O_2, cells were treated with 0.4 mM H_2O_2 for 30 min, without overnight serum deprivation. The specific inhibitors were added 60 min before the treatment with H_2O_2 or insulin at a final concentration of 20 nM rapamycin, 100 nM wortmannin, 5 μM U0126 and 5 μM SB203580.

Cell lysate and immunoblotting

Previously treated cells were lysed in CHAPS lysis buffer (10 mM Tris–HCl, pH 7.5, 100 mM NaCl, 0.3% CHAPS, 50 mM NaF, 1 mM sodium vanadate, 1 mM phenylmethylsulfonyl fluoride, 5 μg/ml leupeptin, 5 μg/ml aprotinin, 1 μg/ml pepstatin A, 50 mM β-glycerophosphate, 100 μg/ml benzamidine) for 1 h at 4°C and equal amounts of proteins were separated by electrophoresis. To analyze simultaneously large and small proteins in the same gel, we used Tris-Acetate PAGE systems [19]. After running the gel, the proteins were transferred to PVDF membranes and viewed by immunoblotting, as described elsewhere [17]. Band intensities were analyzed with a gel documentation system (LAS-3000 Fujifilm). Protein levels were standardized with respect to mTOR or Ran levels and expressed as a percentage of controls.

Confocal microscopy

MCF-7 cells were fixed with 4% paraformaldehyde for 20 min at room temperature (RT). The cells were blocked and permeabilized with 10% fetal bovine serum and 0.1% Triton X-100 in PBS for 2h. The primary antibodies, anti-PT180/Y182-p38 (1:200), anti-P-S380-RSK (1:50), anti-P-ERK1/2 (1:200) and anti-P- H2AX (γH2AX) (1:500), were incubated at 4°C overnight; and the secondary antibodies, at RT for 2h. Nuclei were stained with TO-PRO-3 and the cells were examined by laser confocal microscopy.

Immunoprecipitations and kinase assay

Lysates from MCF7 cells were immunoprecipitated with anti-RSK or anti-MSK antibodies. Lysis and immunoprecipitation

were carried out in a buffer containing 40 mM Hepes, pH 7.5, 120 mM NaCl, 50 mM NaF, 0.3% CHAPS and the above protease inhibitors. Immunoprecipitates were washed three times with lysis buffer and once with kinase buffer (30 mM Tris-HCl, pH 7.5, 10 mM $MgCl_2$, 1 mM DTT). The kinase assay was performed as previously described [17] in kinase buffer using GST-S6 as substrate (3 µg substrate per assay) in the presence or absence of ATP (500 µM), during 30 min at 30°C. Reactions were stopped in ice with sample buffer and analyzed by immunoblot with anti-P-S235/S236-S6 antibody to detect the incorporation of phosphate. Band intensities were analyzed with a gel documentation system (LAS-3000 Fujifilm).

Statistical analysis

The results are expressed as mean ± SEM. Data were analyzed by one-way ANOVA followed by Dunn's post-hoc test.

Results

Phosphorylation of p85 and S6 ribosomal proteins in response to H_2O_2

To study S6K1 regulation in response to oxidative stress, we analyzed by Western blot the phosphorylation of endogenous S6K1 by H_2O_2, using a commercial monoclonal anti-P-T389-S6K1 antibody (1A5, Cell Signaling Technology). MCF7 cells were incubated with H_2O_2 for 30 min. We used these human cells because they have been extensively used to study the response to oxidative stress. As a positive control of S6K1 activation, MCF7 cells were stimulated with insulin after overnight serum deprivation. As shown in Figure 1A, phosphorylation of endogenous S6K1 p70 isoform was detected by Western blot with anti-P-T389-S6K1 antibody after 30 min of treatment with insulin. No variation in p85 isoform phosphorylation was detected in this cell line with insulin treatment. Unexpectedly, after treatment with H_2O_2, we detected an increase in a band with similar mobility to S6K1 p85 isoform that we named p85 protein. No increase was seen in p70 isoform phosphorylation. With both treatments, an increase in the phosphorylation of the ribosomal S6 protein was observed. These treatments did not modify endogenous levels of S6K1 or S6 proteins (Figure 1A). Levels of other proteins involved in the S6K1 signaling pathway such as mTOR were also unaltered (Figure 1A). These results were confirmed in other human cell types such as U2OS or H1299 (Figure 1B), indicating that the response to H_2O_2 is not restricted to one cell type.

Experiments of time and dose course confirmed the previous data. Thus, rapid (5 min) and specific phosphorylation of endogenous p85 protein was seen on incubation with various concentrations of H_2O_2 (Figure 1C/1D). Maximum effects were observed after 15-30 min incubation.

The mTOR/S6K1 signaling pathway is not activated in response to the oxidative stress produced by H_2O_2

To analyze the phosphorylation regulation of p85 protein, we performed experiments with H_2O_2 in the presence of known inhibitors of S6K1 activation (Figure 2). We observed that the phosphorylation of p85 protein was not significantly modified by rapamycin or wortmannin, inhibitors of mTORC1 and PI3K and mTOR kinases, respectively. S6 phosphorylation correlated with the increase in p85 phosphorylation and was not significantly modified by rapamycin and wortmannin. As control, in parallel experiments, cell stimulation with insulin confirmed the previously reported inhibition of S6K1 phosphorylation and S6 phosphorylation by rapamycin and wortmannin (Figure 2).

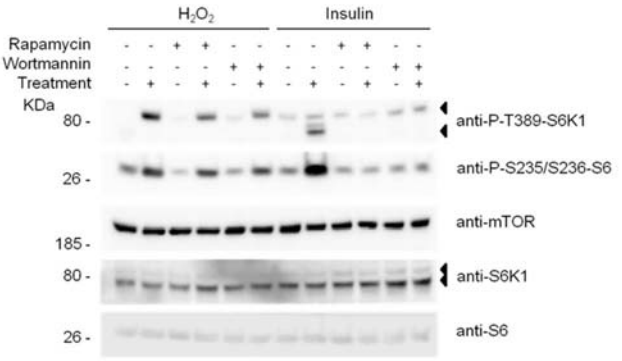

Figure 2

Figure 2. Effect of rapamycin and wortmannin on phosphorylation of p85 protein by H_2O_2. MCF7 cells were treated with 0.4 mM H_2O_2 for 30 min. Where indicated, MCF7 cells were pre-incubated with 100 nM wortmannin or 20 nM rapamycin for 60 min before treatment with H_2O_2. Cell lysates were analyzed by Western blot with the indicated antibodies. Molecular weight markers are indicated on the left.
doi: 10.1371/journal.pone.0075523.g002

It was shown that rapamycin inhibits the phosphorylation of S6K1 isoforms by mTORC1 [10]. The above data seem to indicate that, in response to H_2O_2, this phosphorylation is not regulated by rapamycin (Figure 2) and suggest that another kinase might be involved in this regulation. To discard a role of mTOR protein, knockdown experiments were performed. As shown in Figure 3, in response to H_2O_2, the phosphorylation of endogenous p85 protein was not altered by the absence of mTOR, indicating that p85 protein is not a substrate of mTOR complexes.

We had previously reported that, in response to amino acids, anti-P-T389-S6K1 antibody recognized a phosphorylated p85 protein that was not S6K1 [17]. The similarity of these results with what we obtained with H_2O_2 led us to analyze whether the phosphorylated p85 protein was S6K1. To this end, knockdown experiments of S6K1 were performed. As shown in Figure 3, the phosphorylation of endogenous p85 protein was not altered by the absence of S6K1, indicating that the phosphorylated protein detected by the anti-P-T389-S6K1 antibody is not S6K1.

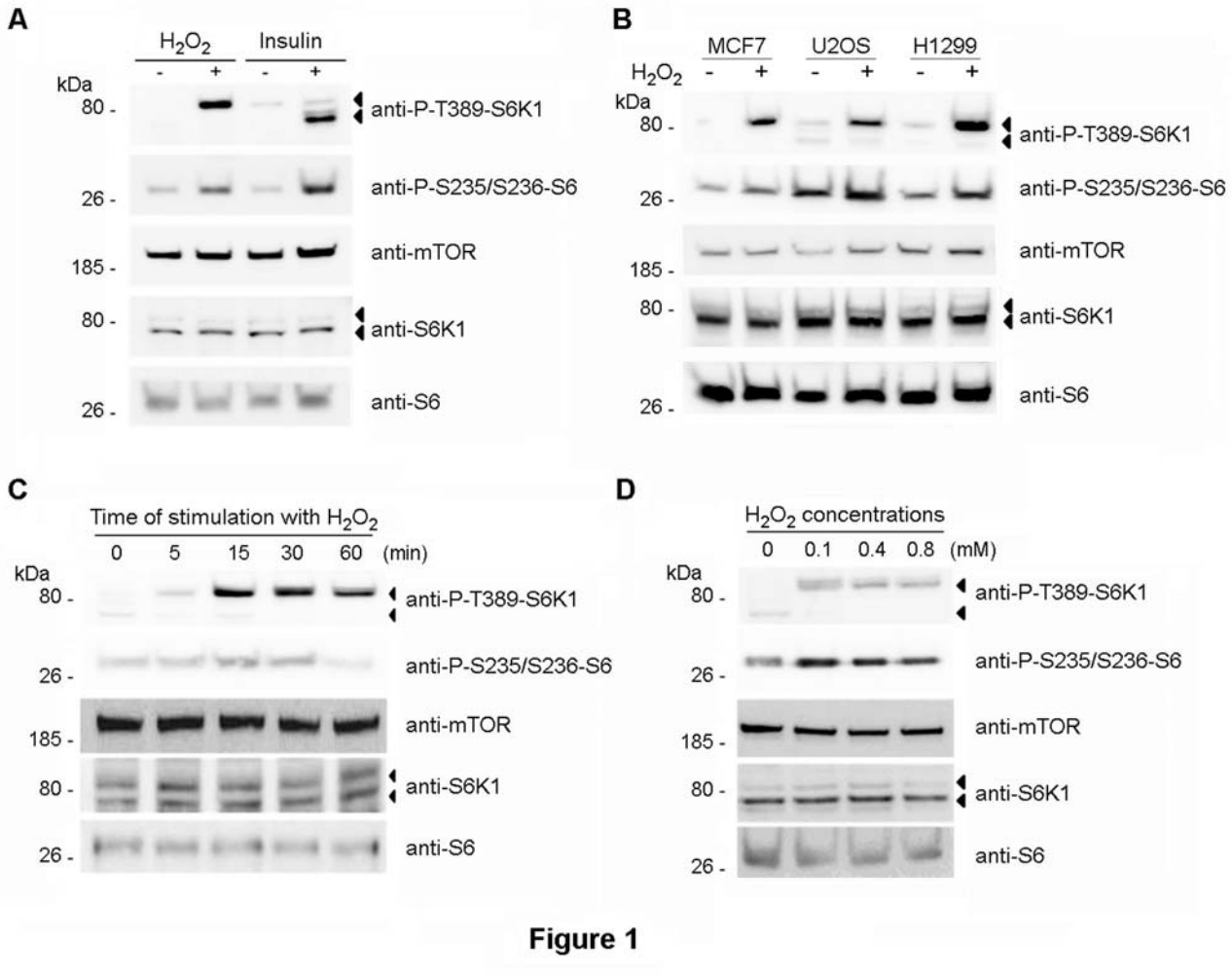

Figure 1

Figure 1. Phosphorylation of p85 and S6 ribosomal proteins in response to H_2O_2. Human cells were treated with 0.4 mM H_2O_2 for 30 min (A,B) or deprived of serum overnight and then stimulated with 200 nM insulin for 30 min (A). Experiments of time and dose course were performed in MCF7 cells with 0.4 mM H_2O_2 (C) or for 30 min (D), respectively. Cell lysates were analyzed by Western blot with the indicated antibodies. Molecular weight markers are indicated on the left.

doi: 10.1371/journal.pone.0075523.g001

Activation of the MAPK signaling pathways in response to the oxidative stress produced by H_2O_2

The previous data indicated that the phosphorylation of a p85 protein detected with anti-P-T389-S6K1 antibody in response to the oxidative stress mediated by H_2O_2 was independent of the mTOR/S6K1 signaling pathway. Thus, other pathways and proteins must be involved in this response. The MAPK signaling pathways are activated by incubation with H_2O_2. This activation is mediated by ERK and p38 kinases [7,20]. We had previously reported that these kinases also regulate amino acid signaling [17]. Under these conditions, ERK and p38 phosphorylate and activate RSK and MSK proteins in response to amino acids. RSK and MSK proteins are members of the family of serine /threonine kinases named AGC. S6K1 is also a member of this family. RSK and MSK proteins have a high degree of homology with the hydrophobic motif of S6K1, where T389 is located [16,17]. These structural similarities, together with the electrophoretic mobility of RSK and MSK proteins around 85-90 kDa and the previously shown cross-reaction of anti-P-T389-S6K1 antibody with phosphorylated RSK and MSK proteins, led us to check whether these proteins were phosphorylated in response to oxidative stress by H_2O_2. We had used antibodies against phosphorylated residues of RSK and MSK equivalents to T389 in S6K1, concretely anti-P-S380-RSK and anti-P-S376-MSK antibodies. We observed that RSK and MSK proteins were phosphorylated after incubation with H_2O_2 (Figure 4A/4B). The time and dose course was similar to that found with the anti-P-T389-S6K1 antibody (Figure 1). These effects were also observed in other human cells such as H1299 and, in less extension, in U2OS cells (Figure 4C). As positive control of the response to H_2O_2, we analyzed the activation of ERK and p38.

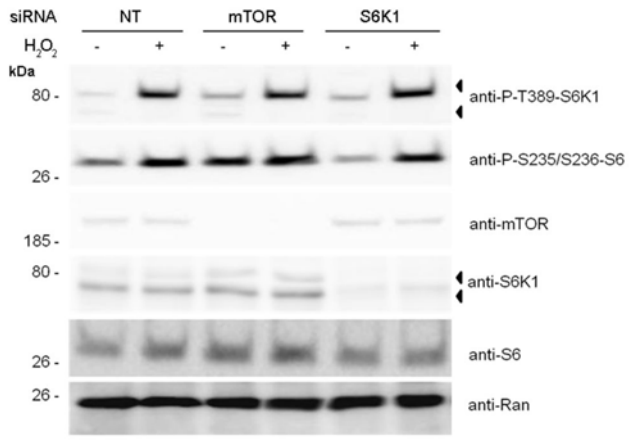

Figure 3

Figure 3. The mTOR/S6K1 signaling pathway is not activated in response to the oxidative stress produced by H_2O_2. MCF7 cells were transfected with the indicated siRNAs 72 h before treatment with 0.4 mM H_2O_2 for 30 min. Cell lysates were analyzed by Western blot with the indicated antibodies. Molecular weight markers are indicated on the left. NT means non-targeting control.

doi: 10.1371/journal.pone.0075523.g003

As shown in Figure 4, phosphorylation of ERK and p38 correlated with the phosphorylation of RSK and MSK proteins.

Functional activation of the MAPK signaling pathways included the translocation to the nucleus of phosphorylated p38 and ERK. We analyzed these translocations in response to H_2O_2. As shown in Figure 5, a rapid nuclear translocation of phosphorylated p38 and ERK was observed at 1-5 min of incubation. Phosphorylation and translocation of RSK was also detected at 1-5 min of incubation. Phosphorylation of H2AX (γH2AX) in response to DNA damage was used as a positive control of treatment with H_2O_2. After 30 min, foci of γH2AX were clearly detected.

Phosphorylation of p85 and S6 ribosomal proteins by H_2O_2 correlated with phosphorylation of RSK and MSK and were sensitive to inhibitors of the MAPK signaling pathways

The previous data suggested that the phosphorylation of p85 protein detected with anti-P-T389-S6K1 antibody was the phosphorylation of RSK and MSK. Thus, it is would be expected that inhibition of the MAPK signaling pathway must inhibit phosphorylation of p85 protein in a similar manner to RSK and MSK. We checked this possibility. We performed experiments with H_2O_2 in the presence of known inhibitors of the MAPK signaling pathways (Figure 6). We observed that the phosphorylation of p85 protein was dependent on U0126, a specific inhibitor of ERK phosphorylation, and SB203580, a specific inhibitor of p38 activity. Interestingly, when both inhibitors were simultaneously used, phosphorylation of p85 protein was almost completely inhibited, suggesting crosstalk between ERK and p38 signaling (Figure 6). Similar results

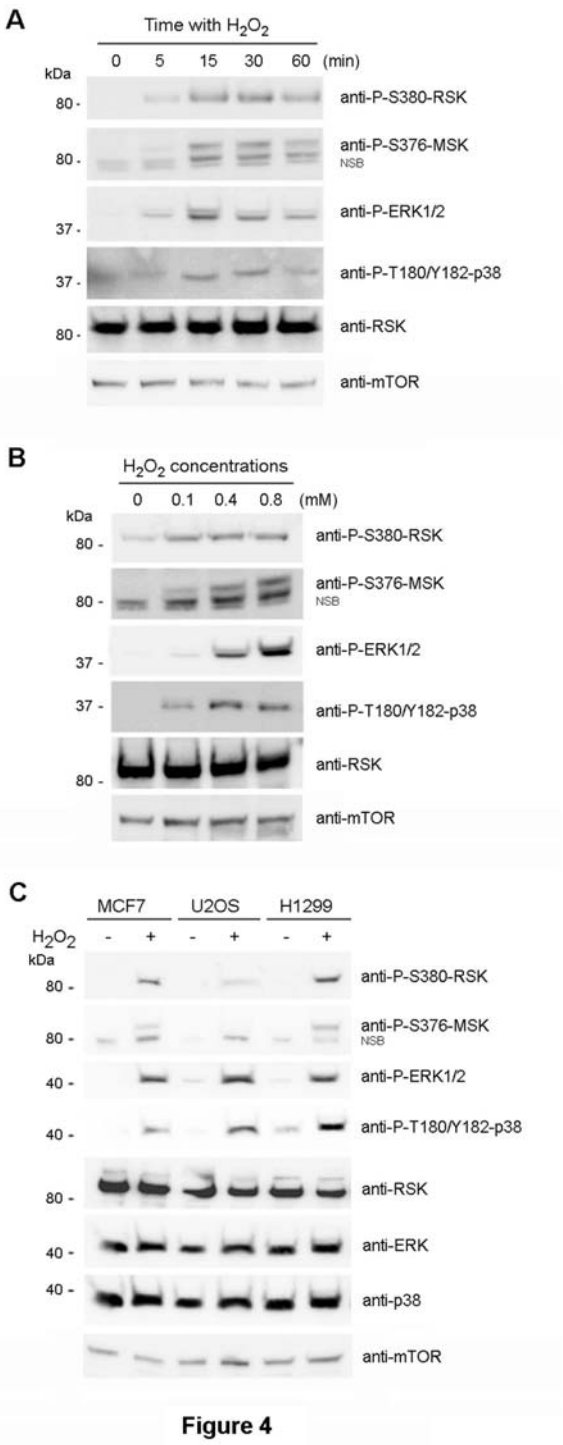

Figure 4

Figure 4. Activation of the MAPK signaling pathways in response to H_2O_2. Experiments of time and dose course were performed in MCF7 cells with 0.4 mM H_2O_2 (A) or for 30 min (B), respectively. Human cells were treated with 0.4 mM H_2O_2 for 30 min (C). Cell lysates were analyzed by Western blot with the indicated antibodies. NSB means non-specific band recognized by the antibody. Molecular weight markers are indicated on the left.

doi: 10.1371/journal.pone.0075523.g004

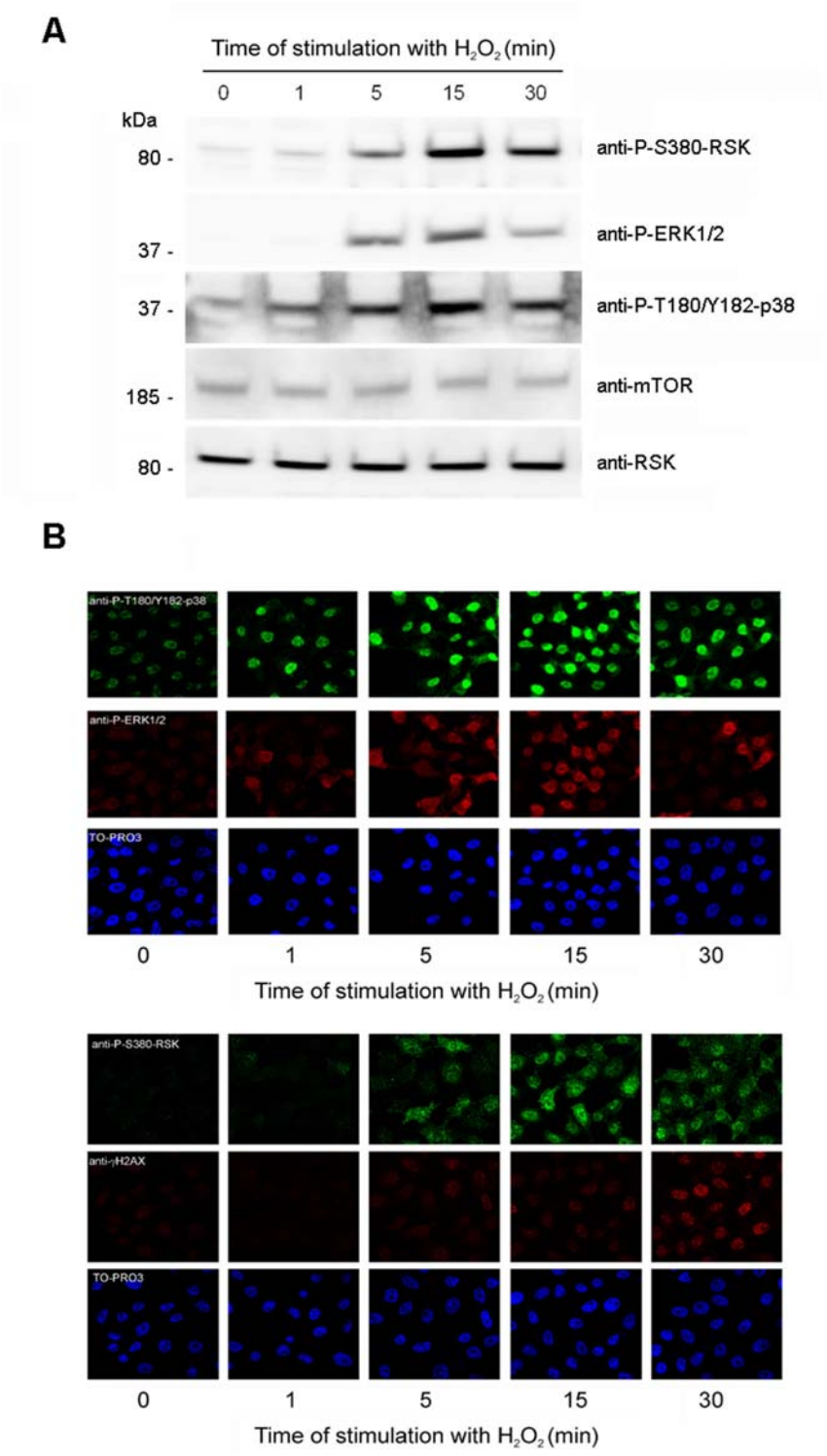

Figure 5

Figure 5. Nuclear translocation of phosphorylated ERK, p38 and RSK proteins. MCF7 cells were treated with 0.4 mM H_2O_2 for indicated times and analyzed by Western blot (A), as described in Figure 1, or by immunofluorescence (B) and using antibodies, as indicated in Experimental Procedures. Nuclear staining was detected with TO-PRO3.

doi: 10.1371/journal.pone.0075523.g005

were obtained with the phosphorylation of RSK and MSK. As a positive control, phosphorylation of ERK and p38 was analyzed. Phosphorylation of S6 ribosomal protein was specifically inhibited by the ERK inhibitor, suggesting a specific role of this kinase or of a downstream kinase in this regulation. Under these conditions, the presence of rapamycin or wortmannin did not significantly affect the phosphorylation of ERK, p38, RSK or MSK proteins. None of these treatments modified endogenous levels of S6K1, RSK, MSK or S6 proteins (Figure 6). Levels of other proteins such as mTOR were not altered (Figure 6).

To provide some evidence that p85 was likely RSK or MSK, knockdown experiments were performed. We used siRNA against the most abundant isoforms of RSK (RSK1 and RSK2) and MSK (MSK1/MSK2). The mix of siRNA against RSK or MSK isoforms decreased the p85 detection with anti-P-T389-S6K1 antibody (Figure 7). This decrease was more evident with simultaneous mix of siRNA against RSK and MSK isoforms. These results show that the anti-P-T389-S6K1 antibody was detecting RSK and MSK phosphorylated.

Activation of RSK and MSK by H_2O_2

The previous data suggest that the kinase activity of RSK and/or MSK is regulated by H_2O_2. To show this point, kinase assays were performed using purified kinases and GST-S6 fusion protein as substrate. As it is shown in Figure 8, the activities of RSK and MSK were stimulated by H_2O_2.

p38α did not regulate phosphorylation of p70 S6K1 in response to the oxidative stress produced by H_2O_2

It has been reported that loss of p38α impairs mTOR/p70 S6K1 activation in response to H_2O_2 through Akt-independent mechanisms [12]. These experiments were performed in wild-type (WT) and p38α-deficient mouse embryonic fibroblasts (MEFs). Bearing in mind the above data, we analyzed S6K1 and MAPK signaling pathways in WT and p38α-deficient MEFs. To analyze the phosphorylation of mouse S6K1 p70 isoform, we used the well-shown activation and phosphorylation of p70 S6K1 by insulin as positive control. We observed an increase in the phosphorylation of p70 S6K1 after 30 min treatment with insulin (Figure 9). No significant changes were observed in the phosphorylation of RSK, MSK and p38 proteins due to insulin treatment. In parallel experiments, we compared the response of WT and p38α-deficient MEFs to treatment with H_2O_2 (Figure 9). Under these conditions and in line with the above data in human cells, increased phosphorylation of mouse p85 protein was observed in WT MEFs. Phosphorylation of mouse p70 S6K1 was not regulated in WT and p38α-deficient MEFs. Incubation with H_2O_2 activated the MAPK signaling pathway. Thus, phosphorylation of RSK, MSK and p38 proteins was seen in WT MEFs. In p38α-deficient cells, we observed a marked reduction in phosphorylation of RSK and MSK proteins (Figure 9). Phosphorylation of p85 protein was also reduced in p38α-deficient cells, suggesting that the anti-P-T389-S6K1 antibody detected phosphorylated RSK and MSK in mouse cells. Altogether, these results confirm our previous observations of human cells in response to the oxidative stress produced by H_2O_2.

Discussion

The mTOR signaling pathway has an essential role in the regulation of mammalian growth and development. Hormones such as insulin and nutrients such as amino acids mediate their cellular effects through this pathway [21]. Several studies have analyzed the mTOR pathway in response to oxidative stress by H_2O_2. Most of these studies analyzed the activity of the mTOR complex 1 (mTORC1) through the analysis of S6K1 phosphorylation at T389 using anti-P-T389 antibodies. In some cases inhibition of mTORC1 activity was reported [11,14,15], whereas in others an increase was described [12,13,22]. These apparently contradictory results have been justified by the complexity of the mechanisms involved, cell type, H_2O_2 concentration and duration of the stress signal [12].

Stress conditions that produce DNA damage activate cell repair mechanisms where p53 activation is involved [1,23,24]. During p53 activation, inhibition of mTOR signaling has been observed [25]. Exposure of the cells to high H_2O_2 concentrations and/or during long time periods produces DNA damage and p53 activation. Thus, in these conditions, inhibition of the mTOR signaling pathway would be expected [11,14,15]. For low H_2O_2 concentrations or during shorter time periods, we showed that mTOR signaling was not involved and explained previous observations by the use of the anti-P-T389-S6K1 antibody from Cell Signaling. We showed that this antibody recognized a phosphorylated protein of 85 kDa in response to H_2O_2. Knockdown experiments together with the use of specific inhibitors let us show that this phosphorylated protein of 85 kDa was not regulated by mTOR and was not S6K1. A similar situation had been previously reported in signaling by amino acids, for which authors showed that the phosphorylated p85 protein recognized by the anti-P-T389-S6K1 antibody was phosphorylated RSK and MSK proteins [17]. To avoid misinterpretations in future experiments, we recommend that researchers using this anti-P-T389-S6K1 antibody check the correct size of the band detected and confirm their results with knockdown experiments. Simultaneous analysis with another well-known stimulus such as insulin also helps to detect the involvement of S6K1. We would also like to highlight that, since the S6 ribosomal protein may be a substrate of different kinases such as S6K1 or RSK [10,17], results using anti-P-S6 antibody to analyze mTOR/S6K1 signaling can be misinterpreted under conditions of activation of the MAPK signaling pathway.

Members of the MAPK family such as ERK, JNK or p38 are phosphorylated and activated in response to oxidative stress [1,7,20]. We confirmed the phosphorylation and activation (nuclear translocation) of ERK and p38 proteins by H_2O_2. Moreover, we reported the phosphorylation and activation of their substrates RSK and MSK. Interestingly, in human cells phosphorylation of both RSK and MSK proteins was sensitive to ERK and p38 activities, indicating that both kinases were necessary to phosphorylate RSK and MSK proteins completely in response to H_2O_2. In contrast, in mouse cells, phosphorylation of MSK by H_2O_2 seemed exclusively dependent on p38 since, in the absence of p38α, MSK phosphorylation was completely abolished. In this context,

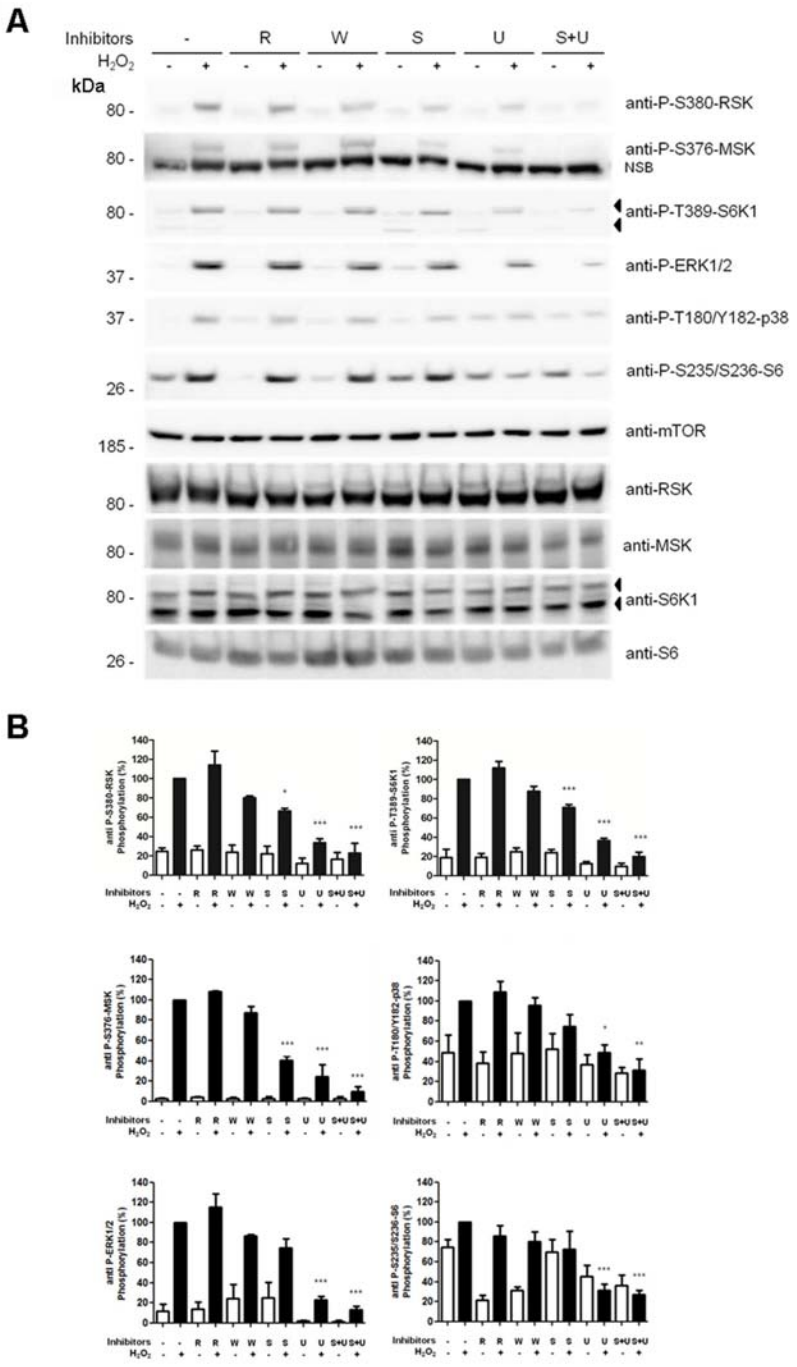

Figure 6

Figure 6. Phosphorylation of p85, RSK and MSK proteins was sensitive to inhibitors of the MAPK signaling pathways. (A) MCF7 cells were treated with 0.4 mM H_2O_2 for 30 min. Where indicated, cells were pre-incubated with 5 μM SB203580 (S), 5 μM U0126 (U), 100 nM wortmannin (W) or 20 nM rapamycin (R) for 60 min before treatment with H_2O_2. Cell lysates were analyzed by Western blot with the indicated antibodies. NSB means non-specific band recognized by the antibody. Molecular weight markers are indicated on the left. (B) Histograms represent the phosphorylation ratio of the indicated proteins. All bands were standardized with respect to mTOR levels. Values are the means ± SEM of the percentage of respective control for at least three independent experiments. Asterisks indicate values that are significantly different (*, $p<0.05$; **, $p<0.01$; ***, $p<0.001$) from the corresponding control value.

doi: 10.1371/journal.pone.0075523.g006

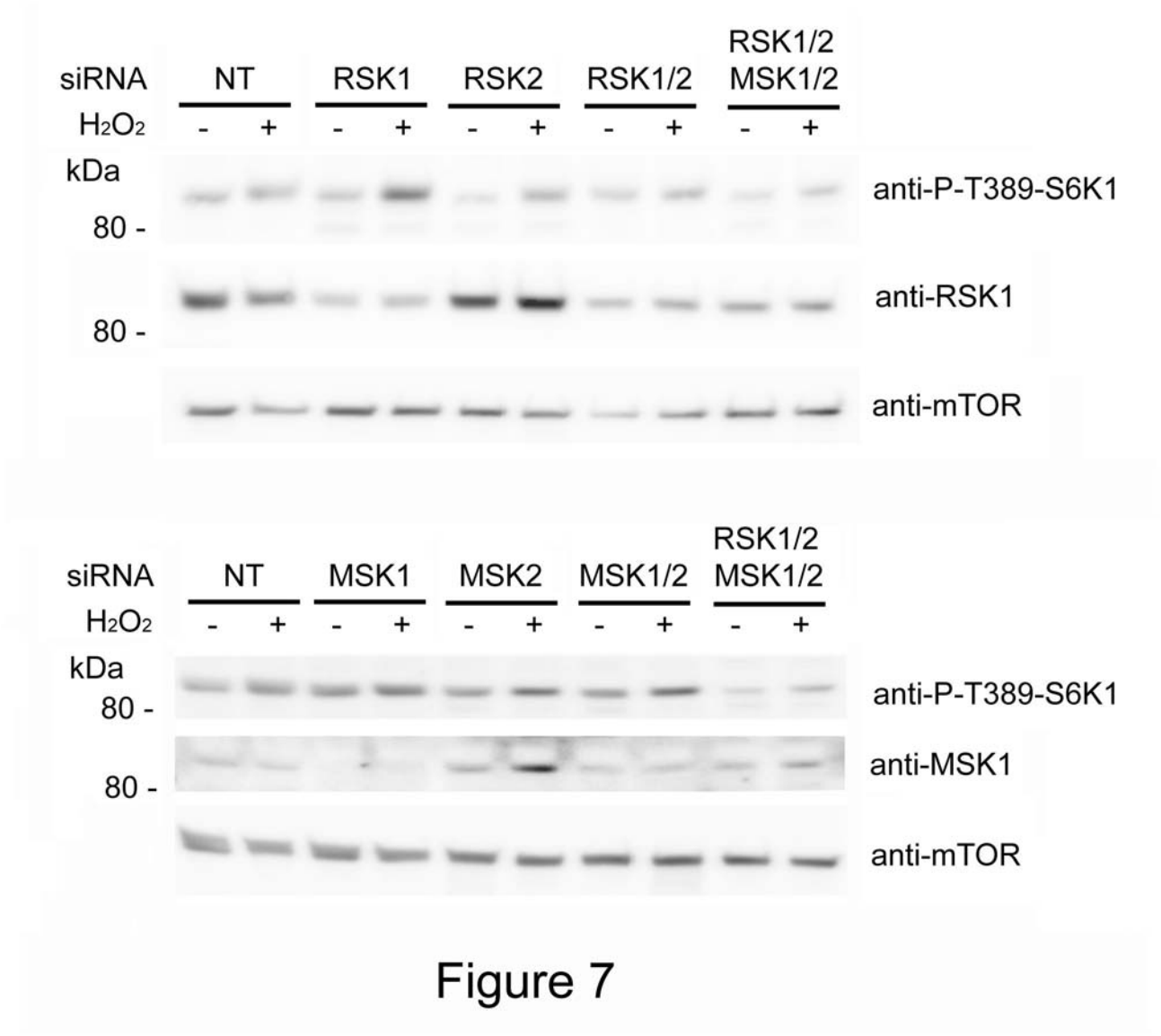

Figure 7

Figure 7. Anti-P-T389-S6K1 antibody detected RSK and MSK phosphorylated. MCF7 cells were transfected with the indicated siRNA 72 h before treatment with 0.4 mM H_2O_2 for 30 min. Cell lysates were analyzed by Western blot with the indicated antibodies. Molecular weight markers are indicated on the left. NT means non-targeting control.

doi: 10.1371/journal.pone.0075523.g007

regulation was reported of mTORC1/p70 S6K1 by p38 in *Drosophila melanogaster* cells [13] and in MEF knockdown for p38α [12]. Using this last model, we showed that p70 S6K1 phosphorylation was stimulated by insulin, but not by H_2O_2. As expected, insulin did not activate the MAPK signaling pathways. Instead, oxidative stress activated phosphorylation of p38/ ERK/MSK in WT MEFs and of RSK in p38α-deficient MEFs. Anti-P-T389-S6K1 antibody detected the phosphorylated p85 protein and its regulation correlated with phosphorylated RSK and MSK proteins. All these observations suggest that, at least in mouse and in human cells, the fast response to oxidative stress caused by low concentrations of H_2O_2 is mediated by MAPK signaling pathways and not by the mTORC1/p70 S6K1 signaling pathway. In summary, we believe that this report helps to explain previous controversial results and to clarify the cellular signaling activated in response to oxidative stress.

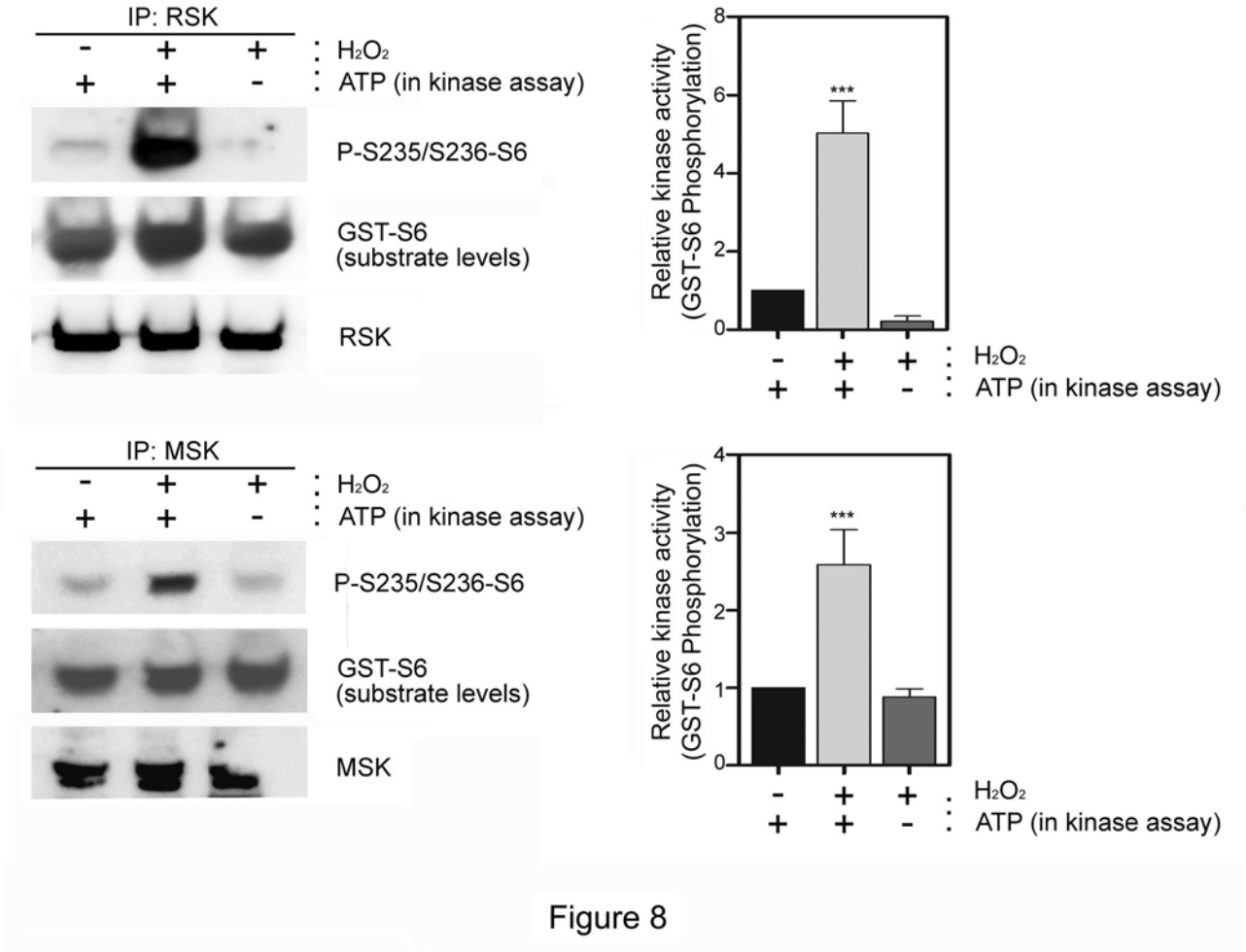

Figure 8

Figure 8. Activation of RSK and MSK by H_2O_2. *In vitro* kinase assay using RSK or MSK immunoprecipitates and purified GST-S6 as substrate. Lysates from MCF7 cells were immunoprecipitated with anti-RSK or anti-MSK antibodies (IP). Immunocomplexes were suspended in kinase buffer and incubated with purified GST-S6 in the presence or absence of ATP during 30 min at 30 °C. Reactions were stopped and the incorporation of phosphate was analyzed by immunoblotting using the anti-P-S235/S236-S6 antibody. Histograms: bands were normalized with respect to GST-S6 substrate levels detected with anti-GST antibody. Data represent the ratio of P-S235/S236-GST-S6 phosphorylation and are expressed as mean±SEM of percentage of respective control. Statistical analysis was carried out as indicated in Materials and methods.

doi: 10.1371/journal.pone.0075523.g008

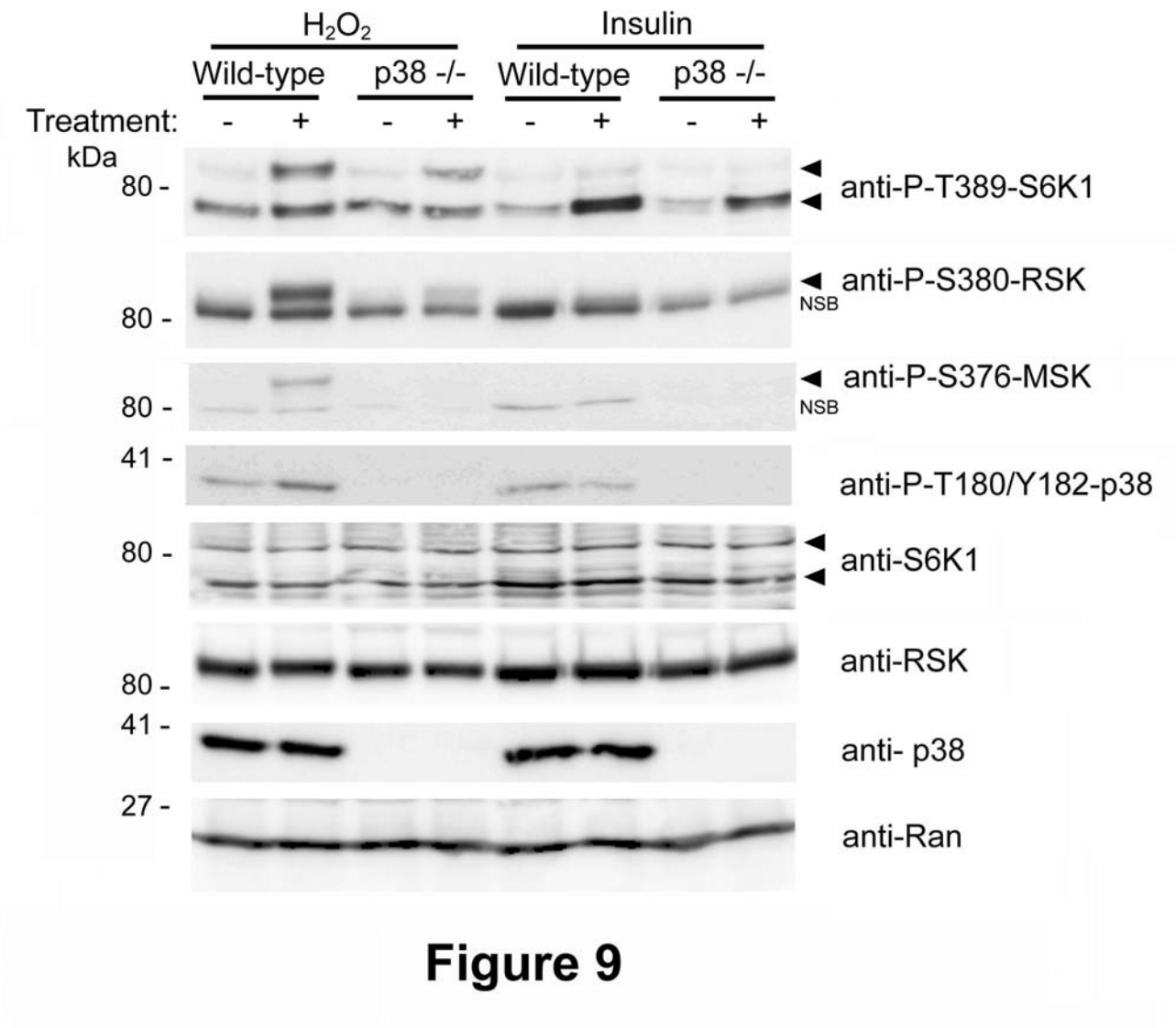

Figure 9

Figure 9. p38α did not regulate phosphorylation of p70 S6K1 in response to the oxidative stress caused by H_2O_2. WT and p38α-deficient MEFs were treated with 0.4 mM H_2O_2 for 30 min or deprived of serum overnight and then stimulated with 200 nM insulin for 30 min. Cell lysates were analyzed by Western blot with the indicated antibodies. NSB means non-specific band recognized by the antibody. Molecular weight markers are indicated on the left.

doi: 10.1371/journal.pone.0075523.g009

Acknowledgements

We thank Dr. A. Nebreda for p38α-deficient MEFs. We are also grateful to B. Torrejon, E. Castaño and E. Adanero for their technical assistance.

Author Contributions

Conceived and designed the experiments: AS CDB RB FV JRO JLR. Performed the experiments: AS MCR RCS TS. Analyzed the data: AS MCR RCS TS CDB RB FV JRO JLR. Contributed reagents/materials/analysis tools: RB FV JRO JLR. Wrote the manuscript: AS CDB RB FV JRO JLR.

References

1. Finkel T (2011) Signal transduction by reactive oxygen species. J Cell Biol 194: 7-15. doi:10.1083/jcb.201102095. PubMed: 21746850.
2. Block ML, Zecca L, Hong JS (2007) Microglia-mediated neurotoxicity: Uncovering the molecular mechanisms. Nat Rev Neurosci 8: 57-69. doi:10.1038/nrn2038. PubMed: 17180163.
3. Veal E, Day A (2011) Hydrogen peroxide as a signaling molecule. Antioxid Redox Signal 15: 147-151. doi:10.1089/ars.2011.3968. PubMed: 21375475.
4. Benhar M, Engelberg D, Levitzki A (2002) ROS, stress-activated kinases and stress signaling in cancer. EMBO Rep 3: 420-425. doi: 10.1093/embo-reports/kvf094. PubMed: 11991946.
5. Lu T, Finkel T (2008) Free radicals and senescence. Exp Cell Res 314: 1918-1922. doi:10.1016/j.yexcr.2008.01.011. PubMed: 18282568.
6. Gutteridge JM, Halliwell B (2010) Antioxidants: Molecules, medicines, and myths. Biochem Biophys Res Commun 393: 561-564. doi:10.1016/j.bbrc.2010.02.071. PubMed: 20171167.
7. Runchel C, Matsuzawa A, Ichijo H (2011) Mitogen-activated protein kinases in mammalian oxidative stress responses. Antioxid Redox Signal 15: 205-218. doi:10.1089/ars.2010.3733. PubMed: 21050144.
8. Dann SG, Selvaraj A, Thomas G (2007) mTOR Complex1-S6K1 signaling: At the crossroads of obesity, diabetes and cancer. Trends Mol Med 13: 252-259. doi:10.1016/j.molmed.2007.04.002. PubMed: 17452018.
9. Um SH, D'Alessio D, Thomas G (2006) Nutrient overload, insulin resistance, and ribosomal protein S6 kinase 1, S6K1. Cell Metab 3: 393-402. doi:10.1016/j.cmet.2006.05.003. PubMed: 16753575.
10. Magnuson B, Ekim B, Fingar DC (2012) Regulation and function of ribosomal protein S6 kinase (S6K) within mTOR signalling networks. Biochem J 441: 1-21. doi:10.1042/BJ20110892. PubMed: 22168436.
11. Chen L, Xu B, Liu L, Luo Y, Yin J et al. (2010) Hydrogen peroxide inhibits mTOR signaling by activation of AMPKalpha leading to apoptosis of neuronal cells. Lab Invest 90: 762-773. doi:10.1038/labinvest.2010.36. PubMed: 20142804.
12. Gutiérrez-Uzquiza Á, Arechederra M, Bragado P, Aguirre-Ghiso JA, Porras A (2012) p38α mediates cell survival in response to oxidative stress via induction of antioxidant genes: Effect on the p70S6K pathway. J Biol Chem 287: 2632-2642. doi:10.1074/jbc.M111.323709. PubMed: 22139847.
13. Cully M, Genevet A, Warne P, Treins C, Liu T et al. (2010) A role for p38 stress-activated protein kinase in regulation of cell growth via TORC1. Mol Cell Biol 30: 481-495. doi:10.1128/MCB.00688-09. PubMed: 19917724.
14. Alexander A, Cai SL, Kim J, Nanez A, Sahin M et al. (2010) ATM signals to TSC2 in the cytoplasm to regulate mTORC1 in response to ROS. Proc Natl Acad Sci U S A 107: 4153-4158. doi:10.1073/pnas.0913860107. PubMed: 20160076.
15. Jin HO, Seo SK, Woo SH, Kim ES, Lee HC et al. (2009) Activating transcription factor 4 and CCAAT/enhancer-binding protein-beta negatively regulate the mammalian target of rapamycin via Redd1 expression in response to oxidative and endoplasmic reticulum stress. Free Radic Biol Med 46: 1158-1167. doi:10.1016/j.freeradbiomed.2009.01.015. PubMed: 19439225.
16. Hauge C, Frödin M (2006) RSK and MSK in MAP kinase signalling. J Cell Sci 119: 3021-3023. doi:10.1242/jcs.02950. PubMed: 16868029.
17. Casas-Terradellas E, Tato I, Bartrons R, Ventura F, Rosa JL (2008) ERK and p38 pathways regulate amino acid signalling. Biochim Biophys Acta 1783: 2241-2254. doi:10.1016/j.bbamcr.2008.08.011. PubMed: 18809440.
18. Porras A, Zuluaga S, Black E, Valladares A, Alvarez AM et al. (2004) P38 alpha mitogen-activated protein kinase sensitizes cells to apoptosis induced by different stimuli. Mol Biol Cell 15: 922-933. PubMed: 14617800.
19. Cubillos-Rojas M, Amair-Pinedo F, Tato I, Bartrons R, Ventura F et al. (2010) Simultaneous electrophoretic analysis of proteins of very high and low molecular mass using tris-acetate polyacrylamide gels. Electrophoresis 31: 1318-1321. doi:10.1002/elps.200900657. PubMed: 20309890.
20. Trempolec N, Dave-Coll N, Nebreda AR (2013) SnapShot: P38 MAPK signaling. Cell 152: 656-656. doi:10.1016/j.cell.2013.01.029. PubMed: 23374355.
21. Laplante M, Sabatini DM (2012) mTOR signaling in growth control and disease. Cell 149: 274-293. doi:10.1016/j.cell.2012.03.017. PubMed: 22500797.
22. Wu XN, Wang XK, Wu SQ, Lu J, Zheng M et al. (2011) Phosphorylation of raptor by p38beta participates in arsenite-induced mammalian target of rapamycin complex 1 (mTORC1) activation. J Biol Chem 286: 31501-31511. doi:10.1074/jbc.M111.233122. PubMed: 21757713.
23. Reinhardt HC, Schumacher B (2012) The p53 network: Cellular and systemic DNA damage responses in aging and cancer. Trends Genet 28: 128-136. doi:10.1016/j.tig.2011.12.002. PubMed: 22265392.
24. Lanni C, Racchi M, Memo M, Govoni S, Uberti D (2012) P53 at the crossroads between cancer and neurodegeneration. Free Radic Biol Med 52: 1727-1733. doi:10.1016/j.freeradbiomed.2012.02.034. PubMed: 22387179.
25. Feng Z, Zhang H, Levine AJ, Jin S (2005) The coordinate regulation of the p53 and mTOR pathways in cells. Proc Natl Acad Sci U S A 102: 8204-8209. doi:10.1073/pnas.0502857102. PubMed: 15928081.

Cell Biology:

The E3 Ubiquitin Protein Ligase HERC2 Modulates the Activity of Tumor Protein p53 by Regulating Its Oligomerization

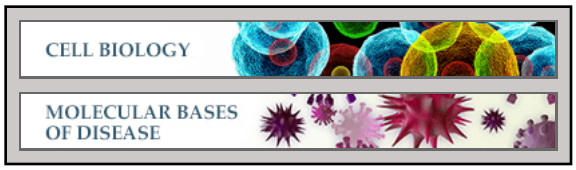

Monica Cubillos-Rojas, Fabiola Amair-Pinedo, Roser Peiró-Jordán, Ramon Bartrons, Francesc Ventura and Jose Luis Rosa

J. Biol. Chem. 2014, 289:14782-14795.
doi: 10.1074/jbc.M113.527978 originally published online April 9, 2014

THE JOURNAL OF BIOLOGICAL CHEMISTRY VOL. 289, NO. 21, pp. 14782–14795, May 23, 2014

The E3 Ubiquitin Protein Ligase HERC2 Modulates the Activity of Tumor Protein p53 by Regulating Its Oligomerization*

Received for publication, October 17, 2013, and in revised form, April 9, 2014 Published, JBC Papers in Press, April 9, 2014, DOI 10.1074/jbc.M113.527978

Monica Cubillos-Rojas, Fabiola Amair-Pinedo, Roser Peiró-Jordán, Ramon Bartrons, Francesc Ventura, and Jose Luis Rosa[1]

From the Departament de Ciències Fisiològiques II, Campus de Bellvitge, Institut d'Investigació Biomèdica de Bellvitge (IDIBELL), Universitat de Barcelona, L'Hospitalet de Llobregat, Barcelona 08907, Spain

Background: HERC2 has been implicated in DNA repair mechanisms and neurological disorders.
Results: HERC2 binds p53 and regulates its transcriptional activity, affecting cellular processes modulated by p53 such as cell growth or DNA damage response.
Conclusion: HERC2 modulates p53 activity by regulating its oligomerization.
Significance: HERC2 is a novel regulator of p53 signaling.

The tumor suppressor p53 is a transcription factor that coordinates the cellular response to several kinds of stress. p53 inactivation is an important step in tumor progression. Oligomerization of p53 is critical for its posttranslational modification and its ability to regulate the transcription of target genes necessary to inhibit tumor growth. Here we report that the HECT E3 ubiquitin ligase HERC2 interacts with p53. This interaction involves the CPH domain of HERC2 (a conserved domain within Cul7, PARC, and HERC2 proteins) and the last 43 amino acid residues of p53. Through this interaction, HERC2 regulates p53 activity. RNA interference experiments showed how HERC2 depletion reduces the transcriptional activity of p53 without affecting its stability. This regulation of p53 activity by HERC2 is independent of proteasome or MDM2 activity. Under these conditions, up-regulation of cell growth and increased focus formation were observed, showing the functional relevance of the HERC2-p53 interaction. This interaction was maintained after DNA damage caused by the chemotherapeutic drug bleomycin. In these stressed cells, p53 phosphorylation was not impaired by HERC2 knockdown. Interestingly, p53 mutations that affect its tetramerization domain disrupted the HERC2-p53 interaction, suggesting a role for HERC2 in p53 oligomerization. This regulatory role was shown using cross-linking assays. Thus, the inhibition of p53 activity after HERC2 depletion can be attributed to a reduction in p53 oligomerization. Ectopic expression of HERC2 (residues 2292–2923) confirmed these observations. Together, these results identify HERC2 as a novel regulator of p53 signaling.

p53 plays a central role in coordinating cellular responses to stress by determining whether cells respond to various types and levels of stress with apoptosis, cell cycle arrest, senescence, DNA repair, cell metabolism, or autophagy. p53 functions as a transcription factor that activates and represses a wide range of genes. Although some effects of p53 may be independent of transcription, the p53-controlled transactivation of target genes is an essential feature of each stress response pathway. p53 is normally kept at low levels through ubiquitination and proteasomal degradation mediated by several E3 ubiquitin ligases. Activation of p53 in response to stress classically consists of three sequential steps: p53 stabilization, sequence-specific DNA binding, and recruitment of the general transcriptional machinery to activate the transcription of p53 target genes. During these steps, p53 activation is controlled by several posttranslational modifications, such as ubiquitination, phosphorylation, and acetylation, and by interactions with other proteins. Genetic studies suggest that p53 activation *in vivo* is even more complex, and an antirepression step involving the release of p53 from repression factors such as MDM2 and MDMX has been proposed to reconcile these models (1–5).

p53-interacting proteins may regulate p53 activation at different levels, and, thus, the identification of new p53 interactors and analysis of their biological relevance is likely to shed more light on p53-dependent cellular processes. The proteins Cullin 7 (CUL7), Parkin-like cytoplasmic (PARC), and HECT- and RCC1-like domains 2 (HERC2) contain a common domain named CPH (a conserved domain within Cul7, PARC, and HERC2 proteins) (6, 7). Both CUL7 and PARC are known to bind cytoplasmic p53 through their CPH domains, and both promote cell growth by antagonizing p53 function (6–8). Consistent with this, *in vivo* studies clearly implicate CUL7 in growth regulation, and CUL7 germ line mutations were found in patients with autosomal recessive 3-M and Yakuts short stature syndromes, which are characterized by profound growth retardation (9).

HERC family proteins contain two characteristic domains: HECT and RCC1-like. Proteins with HECT domains have been reported to function as E3 ubiquitin ligases, and those containing RCC1-like domains have been reported to function as GTPase regulators. These two activities are essential in a number of important cellular processes, such as the cell cycle, cell signaling, and membrane trafficking (10–14). HERC proteins can be classified into two subgroups: large (HERC1–2) and

* This work was supported by Spanish Ministerio de Ciencia e Innovación Grants BFU2011-22498 and BFU2009-07380) and by Instituto de Salud Carlos III Grant RETIC, RD06/0020.
[1] To whom correspondence should be addressed: Dept. de Ciències Fisiològiques II, Campus de Bellvitge, Universitat de Barcelona, L'Hospitalet de Llobregat, Barcelona 08907, Spain. E-mail: joseluisrosa@ub.edu.

small (HERC3–6 in humans and HERC3–5 in mice). Structurally, small HERC proteins contain little more than the two characteristic domains, whereas, functionally, they have been related to ubiquitination and ISGylation processes associated with membrane traffic and the immune response (15–19). Large HERC proteins contain additional domains, including several RCC1-like domains. HERC1 has been implicated in membrane trafficking and cell proliferation/growth through its interactions with the ARF, Rab, clathrin, M2-pyruvate kinase, and TSC2 proteins (20–23). *HERC2* is one of two major genes responsible for eye color in humans (24). Several radiation and ethylnitrosourea-induced mutations at the mouse *Herc2* locus cause neuromuscular tremor, runting, juvenile lethality, and sperm defects (25–27). In humans, a single-base mutation in the *HERC2* gene has also been implicated in a syndrome similar to Angelman syndrome that causes neurodevelopmental delay (28, 29). Other mutations affecting members of the HERC family have been associated with sterility, growth retardation, and neurodegeneration (30, 31). More recently, HERC2 has also been implicated in cell cycle and DNA damage responses. Thus, it has been reported that HERC2 may function as an assembly factor for the RNF8-Ubc13 complex, which promotes Lys-63-linked polyubiquitination at sites of DNA damage in response to DNA double strand breaks (32). Furthermore, HERC2 interacts with claspin, a protein essential for G_2/M checkpoint activation and replication fork stability, suggesting that HERC2 regulates the progression of DNA replication (33).

HERC2 may also function as an E3 ubiquitin ligase for degradation of the xeroderma pigmentosum A protein during circadian control of nucleotide excision repair and of the breast cancer suppressor BRCA1 during the cell cycle, respectively (34, 35). More recently, it has been reported that NEURL4 is also a substrate of HERC2, participating in the ubiquitin-dependent regulation of centrosome architecture (36). Additionally, HERC2 can stimulate the ubiquitin-protein ligase activity of other E3 ligases such as E6AP (37). All of these observations suggest a multifunctional role of HERC2 in cell biology.

In this study, we report a new function for HERC2. We show that HERC2 binds to p53 and that the silencing of HERC2 alters p53 activity as a transcriptional factor, affecting the expression of genes regulated by p53 such as *p21*, *p53R2*, and *p53AIPI*. Under these conditions, we observed increased cellular growth and focus formation in clonogenic assays. The HERC2-p53 interaction is disrupted by p53 mutations in the tetramerization domain. Additionally, cross-linking experiments with glutaraldehyde indicated that HERC2 regulates the oligomerization of p53. These findings demonstrate that HERC2 is a key component in p53 regulation.

EXPERIMENTAL PROCEDURES

Reagents—The following reagents were used: anti-HERC2 monoclonal, anti-clathrin heavy chain (BD Biosciences); anti-mTOR, anti-TSC1, anti-phospho-Ser-15-p53, and anti-Lamin A/C (4C11, Cell Signaling Technology); anti-TSC2 (C-20), anti-p21 (C-19), and anti-p53 (FL-393) (Santa Cruz Biotechnology, Inc.); anti-p53 Ab-5 (DO-7) (Neo Markers); anti-MDM2 (2A10) (Abcam); anti-GST monoclonal (GenScript); anti-Ran and anti-HERC1 (22); anti α-tubulin (Ab-1), bleomycin sulfate and nutlin-3a (Calbiochem); Z-Leu-Leu-Leu-al (MG132) (Sigma-Aldrich); horseradish peroxidase-conjugated secondary antibodies (Invitrogen); protein A-Sepharose, protein G-Sepharose, and glutathione-Sepharose (GE Healthcare); Talon metal affinity resin (BD Bioscience); Immobilon-P PVDF transfer membrane (Millipore Corp.); cycloheximide (Applichem); luciferase assay system (Promega); and luminescent β-galactosidase detection kit II (Clontech Laboratories).

Plasmids, Antibodies, and siRNAs—pEGB-p53 constructs (WT, ΔN200, ΔN300, and ΔN300ΔC43), p53 constructs (WT, NLS, NES, R337C, and L344P), His-p53 constructs (1–360 and 1–320), luciferase reporters (p21WAF1, p53AIPI, and p53R2), and the Myc-HERC2 F3 construct (residues 2292–2923) were provided by Dr. Y. Xiong (6), Dr. Y. Zhang (38), Dr. C. H. Arrowsmith (39), Dr. Y. Taya (40), and Dr. T. Ohta (35), respectively. The Gateway system (Invitrogen) was used to generate HERC2 and HERC1 plasmids. cDNAs encoding the amino terminus (residues 1–199), the CPH domain (residues 2547–2640), and the carboxyl terminus (residues 4785–4834) of the human HERC2 protein and the amino terminus (residues 1–155) of the human HERC1 were amplified by PCR from human fetal brain or HeLa cDNA libraries using specific oligonucleotides. Amplified fragments were used to generate entry clones with pDONR221 and expression vectors with pDEST15 (GST fusion) or pDEST17 (His fusion) following standard Gateway protocols. The plasmids were sequenced. Fusion proteins were expressed in bacteria, purified, and used for pull-down experiments and to generate anti-HERC2 (named bvg3 and bvg4 antibodies against residues 1–199 and bvg1 and bvg2 antibodies against residues 4785–4834) and anti-HERC1 (bvg5 and bvg6 antibodies against residues 1–155) polyclonal antibodies, as described previously (15). Two siRNAs targeting the human sequence of HERC2 (H2.2, GACUGUAGCCAGAUUGAAA and H2.4, GGAAAGCACUGGAUUCGUU) were purchased from Ecogen or GenePharma. Similar results were obtained with both. siRNAs for HERC1 (Q1, CGGCAUGGAUGAACAAAUU), p53 (p53, GACUCCAGUGGUAAUCUAC) and a non-targeting siRNA (NT,[2] UAGCGACUAAACACAUCAA) were purchased from Ecogen or GenePharma.

Cell Culture and Transfections—HeLa, HEK-293, U2OS, and H1299 cells were cultured at 37 °C in DMEM (Invitrogen) with 10% fetal bovine serum. Transfection of cells (plasmids and siRNAs) was carried out using calcium phosphate. Briefly, the day before transfection, the cells were seeded into 6-well plates at 30% confluence. On the day of transfection, cells were at 60% confluence. For a final volume of 100 μl, 50 μl of CaBES solution (500 mM $CaCl_2$ and 100 mM BES (pH 6.95)) was mixed with 50 μl of MilliQ water containing 4 μg of plasmid DNA or siRNA to reach a final concentration of 100 nM. Then, 100 μl of BES solution (280 mM NaCl, 0.75 mM Na_2HPO_4, 0.75 mM NaH_2P0_4, and 50 mM BES) at the appropriate pH was slowly added while aerating the mix. The final mix was incubated for 15 min at room temperature and then added to the cells. Bleomycin or cycloheximide was added to a final concentration of 10 μg/ml or 15 μg/ml, respectively, at the indicated times. MG132 was

[2] The abbreviations used are: NT, non-targeting; BES, 2-[bis(2-hydroxyethyl)-amino]ethanesulfonic acid; IP, immunoprecipitation.

added to the cells for 6 h to a final concentration of 10 μM. For the treatment with nutlin, the cells were incubated for 16 h to a final concentration of 10 μM.

Cell Lysate and Immunoblotting—Cells were lysed and processed as described previously (41). Giant and small proteins were analyzed simultaneously using the LAG (42) or the Tris acetate PAGE systems (43, 44). Band intensities were analyzed using a gel documentation system (LAS-3000, Fujifilm). Protein levels were normalized and expressed as a percentage of controls.

Immunoprecipitations and Pulldowns—Cells lysed with CHAPS buffer (10 mM Tris-HCl (pH 7.5), 100 mM NaCl, 50 mM NaF, and 0.3% CHAPS) containing 50 mM β-glycerophosphate, 1 mM sodium vanadate, 1 mM phenylmethylsulfonyl fluoride, 5 μg/ml leupeptin, 5 μg/ml aprotinin, 1 μg/ml pepstatin A, and 100 μg/ml benzamidine were centrifuged for 10 min at 13,000 × *g*. Animal tissues were processed and analyzed as described previously (30). For immunoprecipitation (IP), supernatants (input) were incubated with preimmune serum or with anti-HERC2 (bvg3 or bvg4), anti-HERC1 (410 or bvg6), or anti-p53 antibodies for 2 h at 4 °C and immunoprecipitated with protein A-Sepharose or protein G-Sepharose for 1 h at 4 °C. In these experiments, HERC2 was detected with anti-HERC2 monoclonal antibody. For pulldowns, supernatants (input) were incubated with 5 μg of purified GST fusion proteins bound to a glutathione resin for 1 h at 4 °C. Pellets were washed three times with CHAPS buffer and analyzed by PAGE and immunoblot analysis. For direct interaction, His-p53 (wild-type, amino acids 1–393), deleted His-p53 (amino acids 1–320), and GST-CPH fusion proteins were expressed in bacteria and purified using Talon or glutathione resins, similarly as described previously (15). 4 μg of purified His-p53 (1–393) or deleted His-p53 (1–320) bound to a resin was incubated with 2 μg of purified GST-CPH protein in 0.2 ml of binding buffer (50 mM Tris-HCl (pH 7.5), 150 mM NaCl, 2.5 mM $MgCl_2$, 5 mM imidazole, 0.5% Nonidet P-40, 2 mM DTT, and 1 mg/ml BSA) for 1 h at 4 °C. Pellets were washed four times with binding buffer and analyzed by PAGE and immunoblot analysis.

Subcellular Fractionation—Cells were resuspended in buffer A (10 mM Hepes (pH 7.9), 10 mM KCl, 1.5 mM $MgCl_2$, 0.34 M sucrose, 10% glycerol, 1 mM DTT, and 0.1% Triton X-100) containing 50 mM NaF, 20 mM β-glycerophosphate, 1 mM sodium vanadate, 1 mM phenylmethylsulfonyl fluoride, 5 μg/ml leupeptin, 5 μg/ml aprotinin, 1 μg/ml pepstatin A, and 100 μg/ml benzamidine and incubated on ice for 5 min for permeabilization. Total cell lysates were prepared by resuspending the lysate directly in sample buffer. After permeabilization, the cells were centrifuged at 4500 rpm for 5 min at 4 °C. Supernatants were collected and considered cytoplasmic fraction. Pellets were washed with buffer A and centrifuged at 4500 rpm for 5 min at 4 °C. This step was repeated three times. The final pellet (nuclear fraction) was resuspended in the initial volume half of buffer A. All fractions were sonicated before analysis by PAGE.

Luciferase Assay—U2OS or H1299 cells were transfected with the corresponding reporter. Luciferase activity was quantified using a luciferase assay system (Promega). Luciferase values were normalized using β-galactosidase activity measured using the Luminescent β-Galactosidase Detection Kit II (Clontech Laboratories). Luminescence levels are expressed as a percentage of controls.

RT Quantitative PCR Analysis—Total RNA was isolated from transfected cells using the Ultraspec RNA isolation system (Biotecx) according to the protocol of the manufacturer. 2 μg of total RNA was reverse-transcribed using the high-capacity cDNA reverse transcription kit (Applied Biosystems). Quantitative PCR was carried out using the ABI Prism 7900 HT fast real-time PCR system, and commercially available human TaqMan assays (Applied Biosystems) were used to quantify gene expression of *CDKN1A* (p21) (Hs00355782_m1). The housekeeping gene *GAPDH* (HS99999905_m1) was used for normalization. PCR data were captured and analyzed using the Sequence Detector software (SDS version 2.3, Applied Biosystems).

Proliferation and Clonogenic Assays—For proliferation assays, 24 h after siRNA transfection, cells were reseeded at 3000 cells/well in triplicate in 6-well dishes for 7 days in DMEM (Invitrogen) with 5% calf serum. The cells were stained with crystal violet (containing 2% ethanol) after dissolving the dye in 1% SDS. The absorbance at 550 nm was quantified and plotted proportional to cell number. For clonogenic assays, 500 cells were reseeded and grown until cells formed sufficiently large colonies (~15 days). The colonies were stained with crystal violet and quantified using ImageJ software.

Protein Cross-linking Assay—Cells were transfected with the indicated plasmids and siRNAs and lysed in CHAPS buffer 72 h after transfection. After lysis, the cells were centrifuged, and the supernatant was recovered. Glutaraldehyde was added to the supernatant at the indicated concentrations and incubated on ice for 30 min, as described previously (38). The reaction was stopped with sample buffer 4×, and the samples were analyzed by Western blot analysis.

Statistical Analysis—Results are expressed as mean ± S.E. Data for multiple variable comparisons were analyzed by one-way analysis of variance. For comparison of significance, Dunnett's test or Tukey's test were used according to the statistical program GraphPad Prism.

RESULTS

The Ubiquitin Ligase HERC2 Interacts with p53—To detect endogenous HERC2 protein, we generated polyclonal antibodies against the carboxyl terminus (named bvg1 and bvg2) and the amino terminus (named bvg3 and bvg4) of the human HERC2 protein (Fig. 1*A*). Immunopurified antibodies specifically detected purified HERC2 fragments (Fig. 1*A*) and endogenous HERC2 protein (Fig. 1*B*, electrophoretic mobility of around 500 kDa) by immunoblotting. A commercial monoclonal anti-HERC2 antibody confirmed the band detected by polyclonal antibodies. Polyclonal antibodies were also able to immunoprecipitate endogenous HERC2 protein (Fig. 1*C*). The HERC2 homolog HERC1 has a similar electrophoretic mobility. To show the specificity of the above antibodies against HERC2, we performed knockdown experiments. Thus, in the presence of HERC2 siRNA, anti-HERC2 antibodies did not recognize HERC1 (Fig. 1*D*). Likewise, in the presence of HERC1 siRNA, anti-HERC1 antibodies did not recognize HERC2 pro-

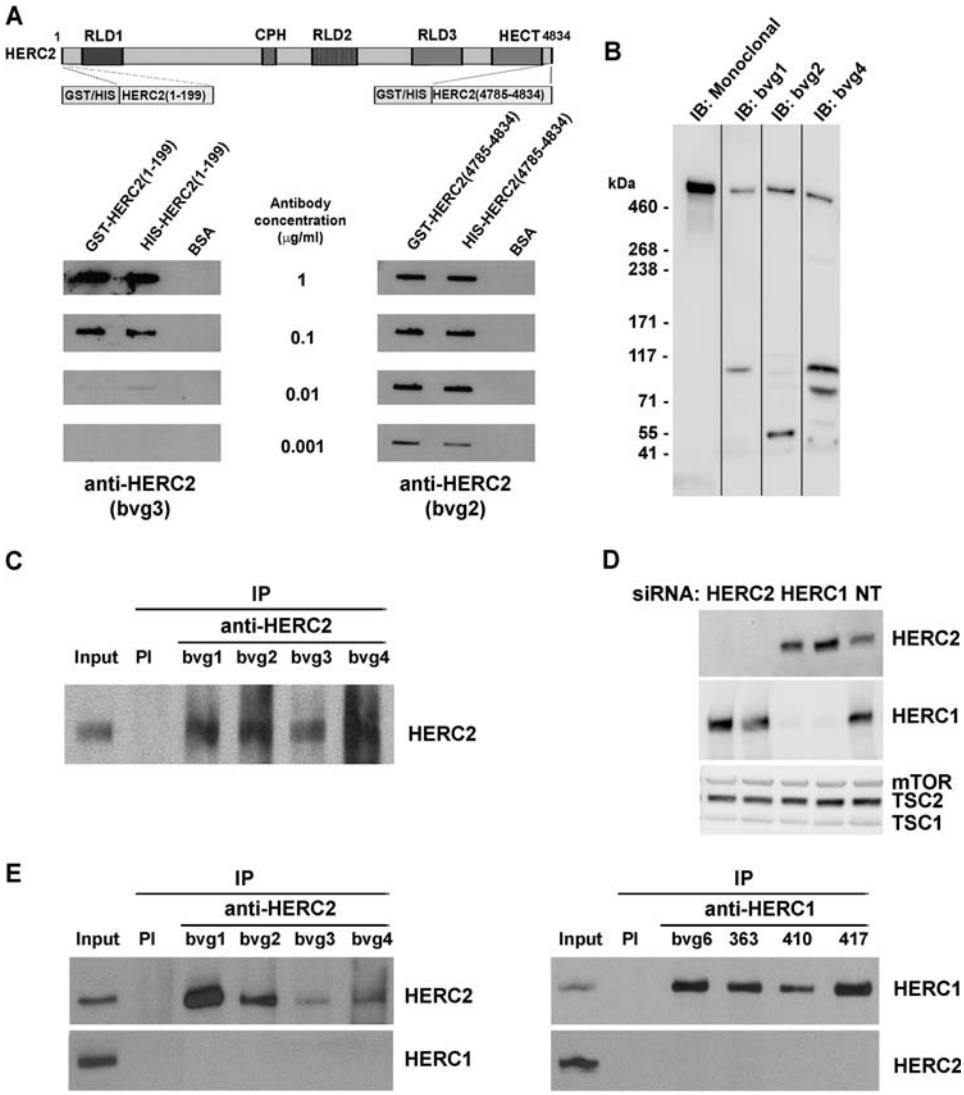

FIGURE 1. **Characterization of the HERC2 protein.** *A*, structure of the HERC2 protein. The RCC1-like domains 1–3 (*RLD1–3*) and the CPH and HECT domains are indicated. Fusion proteins against the indicated amino acid residues were purified and used to generate anti-HERC2 antibodies. Regarding the sensitivity of antibodies, different concentrations of affinity-purified antibodies were tested on slot blots containing 100 ng of fusion proteins or BSA as a negative control. *B*, specificity of anti-HERC2 antibodies. Lysates of HEK-293 were analyzed by immunoblotting (*IB*) with the indicated antibodies. *C*, anti-HERC2 polyclonal antibodies (bvg1–4) were tested in IP assays with lysates (*Input*) of HEK-293 cells, followed by immunoblotting with anti-HERC2 monoclonal antibody. *PI*, preimmune serum. *D*, lysates from transfected HEK-293 cells with the indicated siRNAs were analyzed by immunoblotting with antibodies against the indicated proteins. *mTOR*, mammalian target of rapamycin. *E*, HEK-293 cell lysates (*Input*) were immunoprecipitated with the indicated antibodies and analyzed by immunoblotting with antibodies against the indicated proteins. Input represents 5% of the extract used.

tein. It has been shown previously that small HERC proteins can form heteromeric complexes (17). To determine whether the giant proteins HERC2 and HERC1 can also form heteromeric complexes, we performed coimmunoprecipitation experiments. Fig. 1*E* shows that HERC2 and HERC1 did not form such complexes.

Following identification of the endogenous HERC2 protein, we used anti-HERC2 antibodies to check the interaction between HERC2 and p53. Immunoprecipitation experiments with two different antibodies against HERC2 (bvg3 and bvg4) showed the coimmunoprecipitation of endogenous p53 with HERC2 in U2OS cells, a human osteosarcoma cell line expressing wild-type p53 (Fig. 2*A*). Reverse immunoprecipitation using anti-p53 antibodies also showed, although in a lesser amount, the coimmunoprecipitation of HERC2 in U2OS cells but not in H1299 human cells, which do not express p53 (Fig. 2*B*). To discard the theory that anti-HERC2 antibodies cross-react with p53, immunoprecipitations were performed in U2OS cells transfected with HERC2 siRNA. NT siRNA was used as negative control. As shown in Fig. 2*C*, the amount of p53 in the immunoprecipitates decreased when HERC2 was knocked down, indicating that there is no cross-reactivity. In addition, the HERC2-p53 interaction was also confirmed with pulldown experiments using glutathione beads in lysates from H1299 cells transfected with plasmids expressing GST or GST-p53. As shown in Fig. 2*D*, GST-p53 specifically interacts with HERC2. This interaction was also observed in other human cell lines expressing wild-type p53, such as HEK-293 and HeLa (Fig. 2*E*). As expected, this interaction was not observed in H1299 cells (Fig. 2*E*). In mouse tissues such as brain or kidney we also observed the coimmunoprecipitation of p53 with HERC2 (Fig. 2*F* and results not shown). Anti-HERC1 antibodies could not

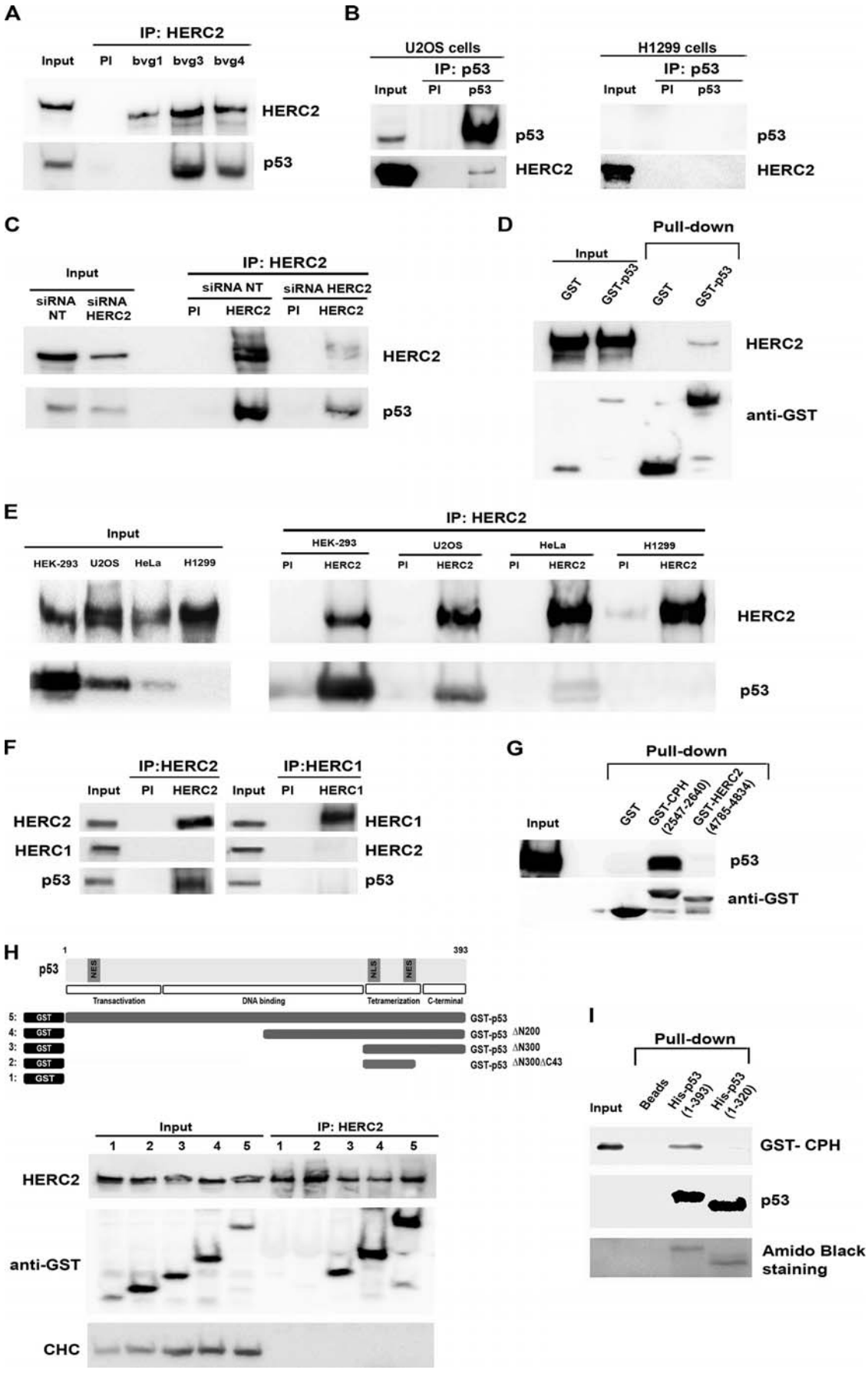

coimmunoprecipitate p53, indicating the specificity of the HERC2-p53 interaction (Fig. 2*F*).

CUL7, PARC, and HERC2 share a CPH domain (6, 7). Because the CPH domain of CUL7 and PARC is sufficient for p53 binding (6–8), we tested whether the CPH domain of HERC2 was also sufficient to mediate the interaction with p53. We performed pulldown assays with GST or GST fusion constructs of HERC2 purified from bacteria (GST-CPH (residues 2547–2640) and GST-HERC2 (carboxyl-terminal residues 4785–4834)) and lysates from HEK-293 cells. Fig. 2*G* shows that the CPH domain of HERC2 was sufficient for this interaction. No interaction was observed with GST-HERC2 (residues 4785–4834) nor with the negative control GST.

To map the HERC2-binding domain of p53, we expressed a series of GST-p53 deletion mutants in H1299 cells (6). Anti-HERC2 antibodies coimmunoprecipitated all the GST-p53 fusion proteins expressed except the GST-p53$^{\Delta N300\Delta C43}$ fusion protein (Fig. 2*H*), indicating that the last 43 amino acid residues of p53 are essential for the interaction with HERC2. Similar results were obtained using HEK-293 cells.

To analyze whether HERC2 can directly interact with p53, we purified His-p53 (wild-type, residues 1–393), deleted His-p53 (residues 1–320), and the GST-CPH fusion protein from bacteria. With these purified protein, we observed a direct and specific interaction between His-p53 (wild-type) and GST-CPH (Fig. 2*I*).

HERC2 Regulates the Transcriptional Activity of p53—HERC2 belongs to the E3 ubiquitin ligase family (12). To determine whether HERC2 regulates p53 levels in a similar manner to other E3 ubiquitin ligases such as MDM2, we depleted U2OS cells of HERC2 using interference RNA experiments. Cells were transfected independently with two different specific siRNAs of HERC2 (H2.2 or H2.4) or with NT siRNA as a negative control. HERC2 knockdown did not significantly modify p53 protein levels (Fig. 3*A*). The content of other proteins, such as Ras-related nuclear protein (Ran), was not altered either.

p53 functions as a transcriptional factor regulating gene expression. One of the genes most studied is the cell cycle inhibitor *p21* (3). In this context, we analyzed p21 levels by immunoblotting, observing a great decrease after HERC2 depletion (Fig. 3*B*). To rule out the possibility that a posttranslational mechanism could be involved in the regulation of p21 levels by HERC2, experiments were performed using the translational inhibitor cycloheximide. Time course experiments with cycloheximide after siRNA transfection showed that the half-life of p21 was not modified significantly by HERC2 depletion (Fig. 3*C*), suggesting that HERC2 could be involved in the transcriptional regulation of p21 by p53. To show that a transcriptional mechanism could be involved in the regulation of p21 by HERC2, luciferase reporter assays were performed in U2OS cells transfected with the *p21* promoter. We observed a great decrease in *p21* promoter activity after HERC2 depletion in U2OS cells (Fig. 3*D*). Endogenous p21 mRNA levels were also decreased by HERC2 knockdown (Fig. 3*E*). Similar decreases were observed using p53 siRNA in U2OS cells (Fig. 3, *D* and *E*). No variations were observed in p53-null H1299 cells (Fig. 3, *D* and *E*). These results were also confirmed with other genes regulated by p53, such as *p53R2* or *p53AIPI*. Thus, the promoter activity of *p53R2* or *p53AIPI* was reduced significantly after HERC2 depletion (Fig. 3*F*).

Cellular processes such as growth arrest, apoptosis, and DNA damage responses are regulated by p53. The above results demonstrate that HERC2 regulates the transcriptional activity of p53. We wondered whether HERC2 could also regulate cellular processes. To address this question, we analyzed the growth of U2OS cells. We observed a significant increase in growth after HERC2 depletion (Fig. 4*A*). These results were confirmed via a clonogenicity assay. Thus, after 15 days, the HERC2 knockdown tripled the colony number (Fig. 4*B*). Similar increases were observed using p53 siRNA in U2OS cells (Fig. 4, *A* and *B*). No variations were observed in H1299 cells (Fig. 4, *A* and *B*).

HERC2 Regulates p53 Activity in a Proteasome- and MDM2-independent Manner—p53 levels are controlled by E3 ubiquitin ligases that target p53 for proteasomal degradation. It is well known that the inhibition of proteasome activity increases p53 levels. We wondered whether the regulation of p53 activity by HERC2 was dependent on the proteasome. To this end, we first confirmed the increase in p53 levels in the presence of the proteasome inhibitor MG132 in U2OS cells transfected with control siRNA (Fig. 5*A*, *first* and *fourth lanes*). This increase correlated with the increase in p21. Knockdown of HERC2 did not affect p53 levels in the presence of MG132 (Fig. 5*A*). However, p21 levels were reduced to a similar extent in the absence of MG132, suggesting that the inhibition of p53 activity by HERC2 was independent of proteasome activity.

It has been reported that inhibition of MDM2 activity with inhibitors such as nutlin increases p53 signaling (45). We wondered whether MDM2 activity could be involved in the regulation of p53 activity by HERC2. Immunoblotting experiments in U2OS cells showed that the inhibition of MDM2 activity in the presence of nutlin increased MDM2 levels (Fig. 5*B*, *first* and *fourth lanes*). Under these conditions, the levels of p53 were barely affected. In contrast, p21 levels were increased greatly in the presence of nutlin, suggesting an increase in the transcrip-

FIGURE 2. **HERC2 binds to p53.** Lysates from U2OS (*A–C* and *E*), H1299 (*B* and *H*), HEK-293 (*E* and *G*), and HeLa (*E*) cells or from mouse brain (*F*) were subjected to IP with preimmune serum (*PI*) or with the indicated antibodies and analyzed by immunoblotting with antibodies against the indicated proteins. *C*, lysates from transfected U2OS cells with the indicated siRNAs were subjected to immunoprecipitation and analyzed by immunoblotting as above. *D*, pulldown experiments with H1299 cells transfected with GST or GST-p53 constructs. 48h post-transfection, lysates from these cells were incubated with glutathione-Sepharose, and proteins retained on Sepharose were analyzed by immunoblotting. *F*, lysates from mouse brain were immunoprecipitated with antibodies against HERC2 (bvg3) or HERC1 (410) and analyzed by immunoblotting with antibodies against the indicated proteins. *G*, pulldown experiments with purified GST and GST fusion proteins coupled to glutathione-Sepharose in lysates from HEK-293 cells. Proteins retained on Sepharose were analyzed by immunoblotting with antibodies against the indicated proteins. *H*, H1299 cells transfected with the indicated constructs were immunoprecipitated with anti-HERC2 polyclonal antibody and analyzed by immunoblotting with antibodies against the indicated proteins. *CHC*, clathrin heavy chain. *I*, direct interaction. Beads with purified proteins (His-p53 (wild-type, residues 1–393) or deleted His-p53 (residues 1–320)) were incubated with purified GST-CPH (residues 2547–2640). Interacting proteins were pulled down and analyzed by immunoblotting or staining with Amido Black. In all experiments, input represents 5% of the extract used.

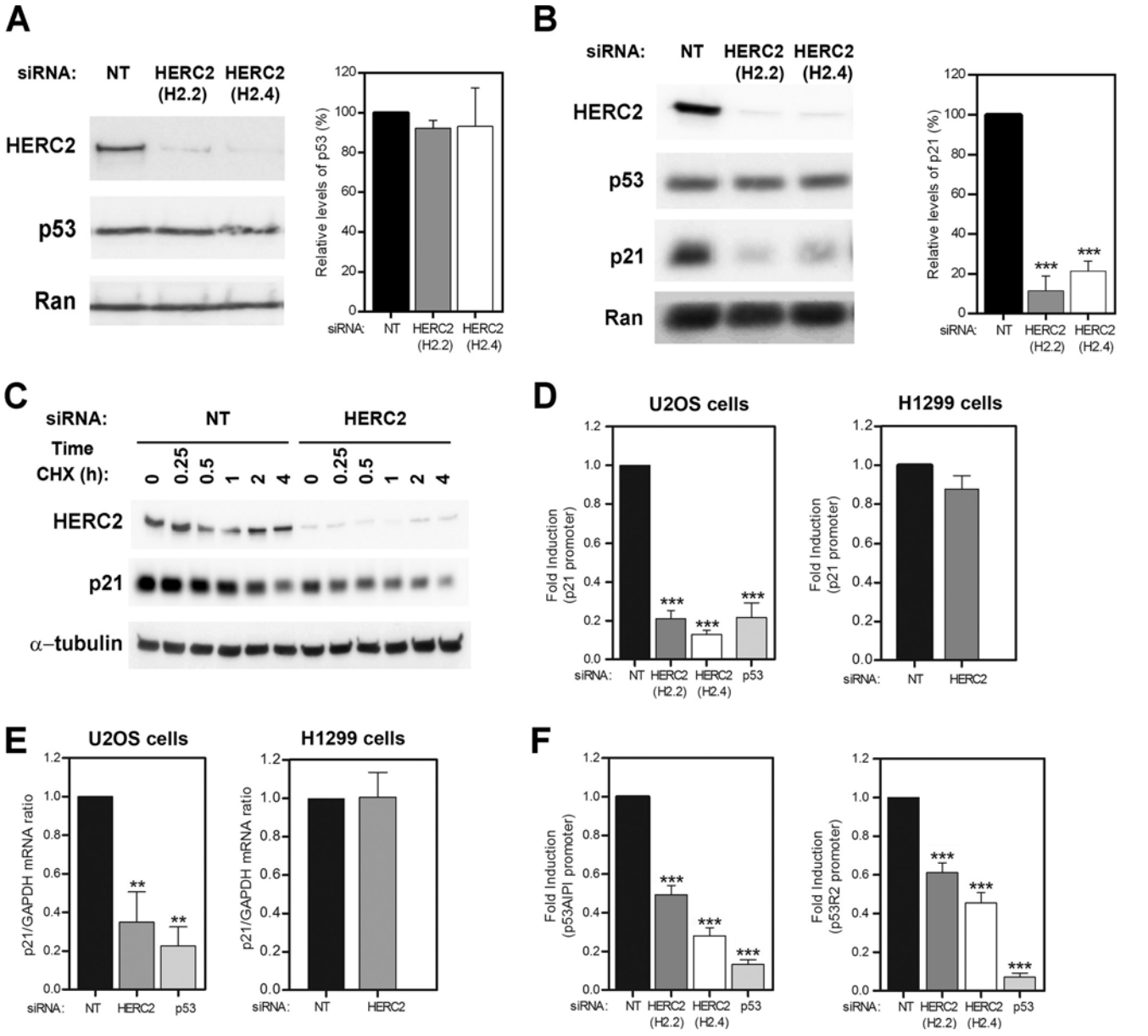

FIGURE 3. **HERC2 is required for transcriptional activity of p53.** *A* and *B*, lysates from transfected U2OS cells with NT or HERC2 siRNAs were analyzed by immunoblotting with antibodies against the indicated proteins. Levels of p53 or p21 were quantified and normalized with respect to Ran levels. *C*, similar to the above, but cells were treated with cycloheximide (*CHX*) for the indicated times. *D*, U2OS or H1299 cells were transfected with the *p21* promoter (*p21WAF1*) and the indicated siRNAs. The luciferase activity was quantified as indicated under "Experimental Procedures." (E) RT quantitative PCR analysis was performed in U2OS or H1299 cells to quantify gene expression of *p21*. The levels of expression were normalized with respect to *GAPDH* gene expression. (F) U2OS cells were transfected with the promoter of *p53R2* or *p53AIPI* and the indicated siRNAs. The luciferase activity was quantified as indicated under "Experimental Procedures." Data are expressed as mean ± S.E. Statistical analysis was carried out as described under "Experimental Procedures." The differences are shown with respect to NT siRNA. **, $p < 0.01$; ***, $p < 0.001$.

tional activity of p53. In these conditions, knockdown of HERC2 decreased p21 levels to a similar extent as in the absence of nutlin (Fig. 5*B*), suggesting that the inhibition of p53 activity by HERC2 was independent of MDM2 activity. This suggestion was confirmed by knockdown experiments of MDM2. Depletion of MDM2 slightly increased p53 and p21 levels (Fig. 5*C*, *first* and *third lanes*). Under these conditions, HERC2 depletion decreased p21 levels independently of MDM2 (Fig. 5*C*, *second* and *fourth lanes*). Because endogenous levels of MDM2 were very low in U2OS cells, we repeated all of these experiments in the presence of the proteasome inhibitor MG132. Under these conditions, we obtained similar results for p53 signaling, and higher levels of MDM2 were detected (Fig. 5*C*, *fifth* through *eighth lanes*).

HERC2 Interacts with p53 in Cytoplasmic and Nuclear Fractions—In stressed cells, p53 activation generally consists of three sequential activating steps: stress-induced stabilization mediated by phosphorylation, DNA binding, and recruitment of the general transcriptional machinery (2–4). We wondered whether HERC2 could be involved in the regulation of these steps. To this end, we investigated whether the phosphorylation of p53 could be affected by HERC2 depletion. To activate p53 phosphorylation, we used bleomycin, a radiomimetic chemical used as a chemotherapeutic agent in cancer treat-

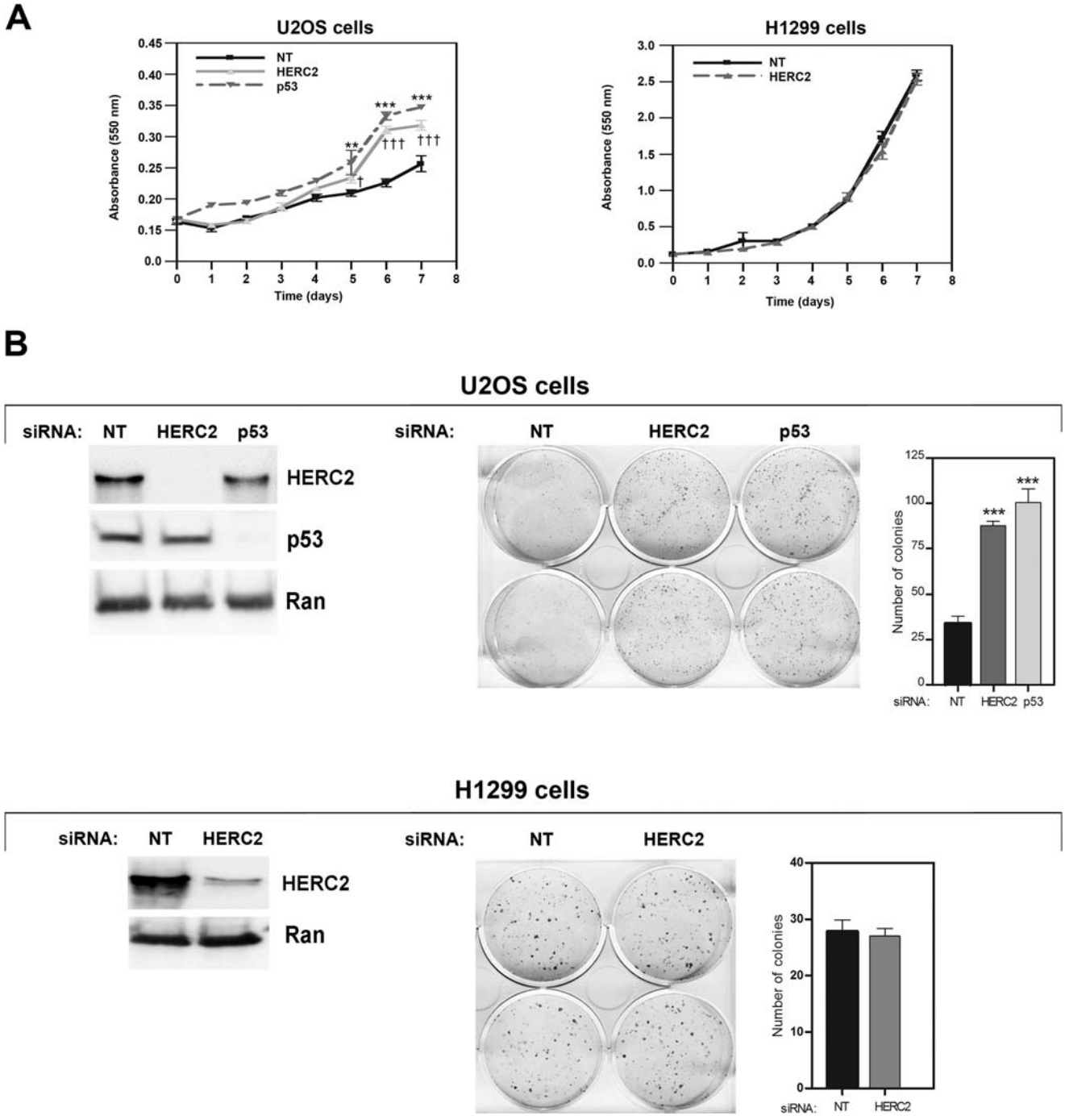

FIGURE 4. **HERC2 regulates cellular growth.** *A*, U2OS or H1299 cells were transfected with the indicated siRNAs, and cell proliferation was analyzed as indicated under "Experimental Procedures." *B*, colony formation assays were performed in U2OS or H1299 cells as indicated under "Experimental Procedures." The protein levels at 72 h post-transfection are shown in the *left panel*, and the quantification of the number of colonies is shown in the *right panel*. Data are expressed as mean ± S.E. Statistical analysis was carried out as described under "Experimental Procedures." The differences are shown with respect to NT siRNA. **, $p < 0.01$; ***, $p < 0.001$; *T*, $p < 0.05$; *TTT*, $p < 0.001$.

ment. Bleomycin interacts with DNA to directly produce double strand breaks (46, 47). As expected, bleomycin activated p53 phosphorylation on serine 15 (*P-S15-p53*) in U2OS cells transfected with non-targeting siRNA (Fig. 6*A*). This phosphorylation was clearly detected after 1 h of treatment and increased for at least the next 6 h (Fig. 6*A*). During this time, the p53 level also increased (stabilization), but not that of other proteins tested, such as Ran (negative control). Under these conditions, down-regulation of HERC2 did not prevent the phosphorylation and stabilization of p53 (Fig. 6*A*). Thus, the phospho-Ser-15-p53/p53 ratio was similar in cells transfected with NT or HERC2 siRNAs, suggesting that HERC2 does not regulate this step.

To bind DNA and activate the transcriptional machinery, p53 is translocated from the cytoplasm to the nucleus. Because proteins such as PARC and CUL7 have been reported to be involved in this process (6–8), we tested whether HERC2 also regulates the subcellular localization of p53. Cytoplasmic and

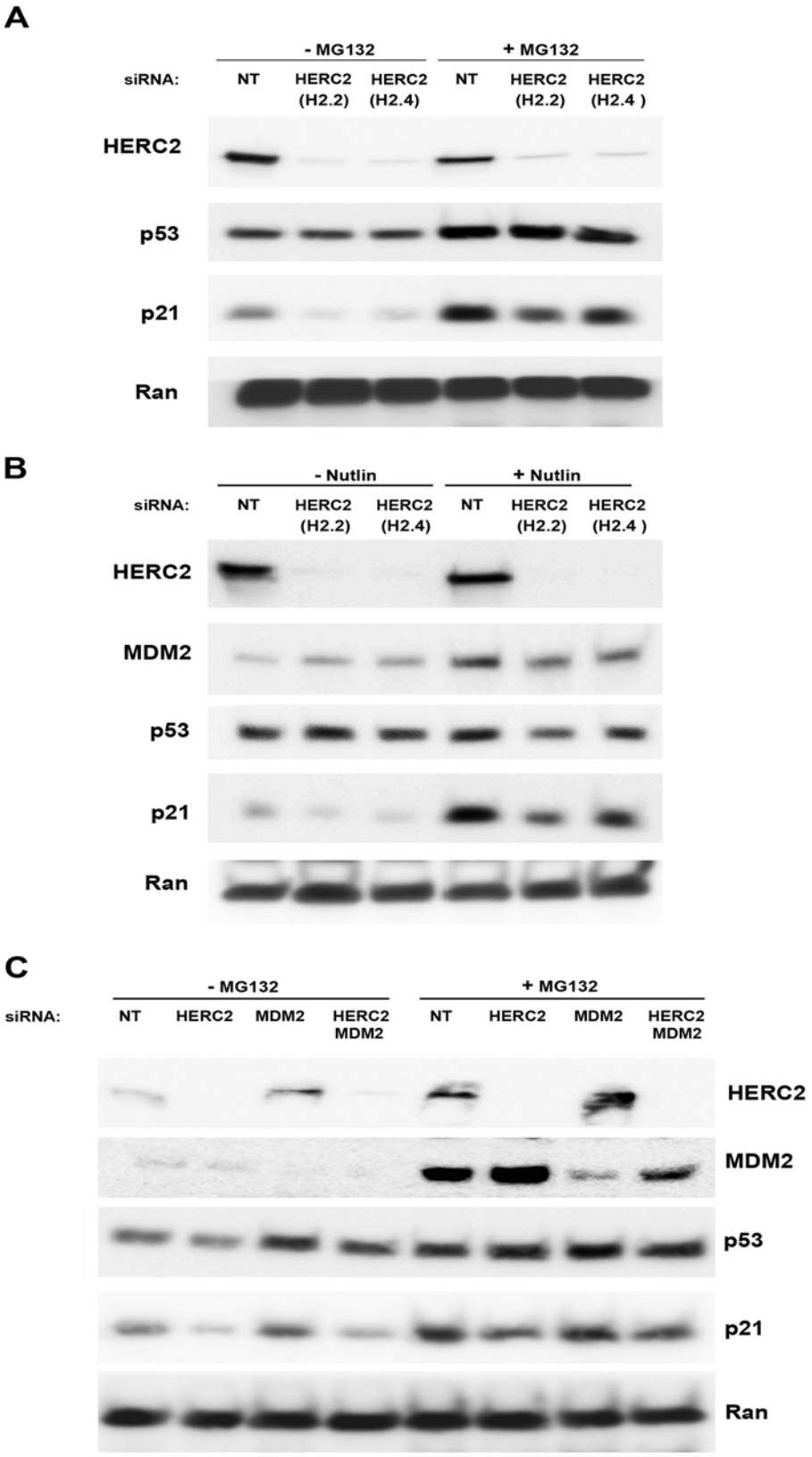

FIGURE 5. **HERC2 regulates p53 activity in a proteasome- and MDM2-independent manner.** Lysates from transfected U2OS cells with NT or HERC2 siRNAs were analyzed by immunoblotting with antibodies against the indicated proteins. Before lysis, cells were treated with the proteasome inhibitor MG132 (*A* and *C*) or with the MDM2 inhibitor Nutlin 3a (*B*) for 6 and 16 h, respectively. Data are representative of at least three independent experiments.

nuclear fractions were separated and analyzed in the presence or absence of bleomycin. Interestingly, HERC2 was present in both fractions, whereas the homolog HERC1 was restricted to the cytoplasmic fraction (Fig. 6*B*). Phosphorylation and stabilization of p53 and its nuclear translocation were observed after treatment with bleomycin (Fig. 6*B*). p53 translocation was not

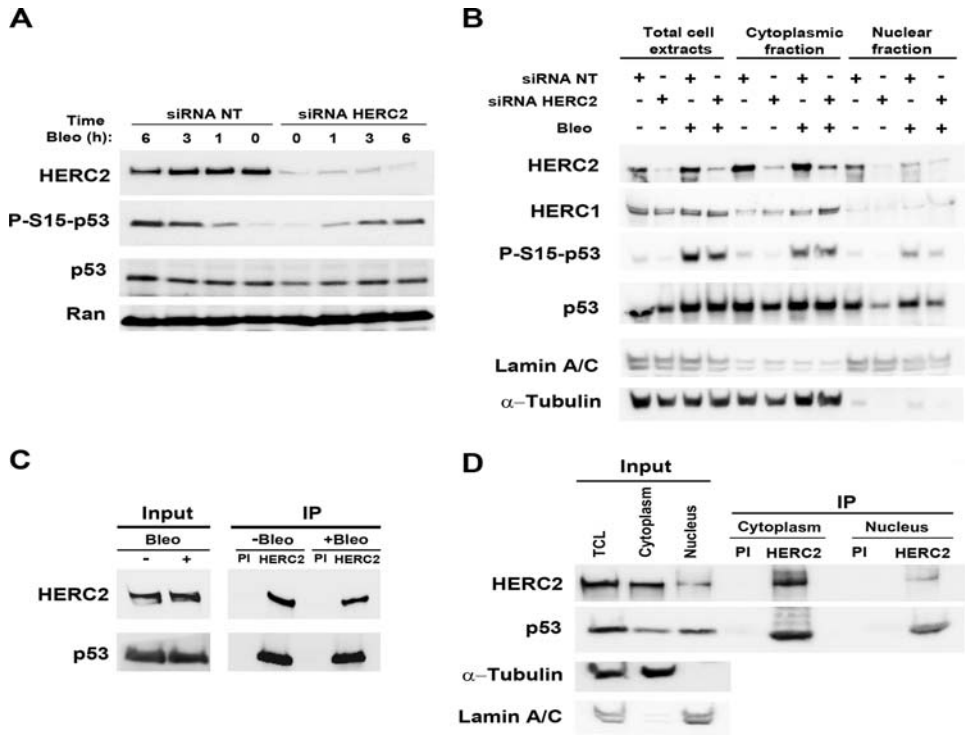

FIGURE 6. **HERC2 interacts with p53 in cytoplasmic and nuclear fractions.** *A* and *B*, U2OS cells transfected for 72 h with NT or HERC2 siRNA were treated with bleomycin (*Bleo*) for the indicated times. Lysates were analyzed by immunoblotting with antibodies against the indicated proteins. *B*, transfected U2OS cells were treated with bleomycin for 3 h. Lysates were subjected to subcellular fractionation as indicated under "Experimental Procedures" and analyzed by immunoblotting with antibodies against the indicated proteins. *C*, U2OS cells were treated with bleomycin for 3 h, and lysates were immunoprecipitated (*IP*) with preimmune serum (*PI*) or with anti-HERC2 polyclonal antibodies and analyzed by immunoblotting with antibodies against the indicated proteins. Lysates from non-treated cells were used as a control. *D*, lysates from U2OS cells were fractionated as indicated under "Experimental Procedures." The fractions corresponding to the cytoplasm and nucleus were subjected to immunoprecipitation as in *C*. α-Tubulin and Lamin A/C were used as controls of subcellular fractionation. Input represents 5% of the extract used. *TCL*, total cell lysates.

impaired by HERC2 depletion. Lamin A/C and α-tubulin are shown as controls of the nuclear and cytoplasmic fractions, respectively (Fig. 6*B*). Furthermore, HERC2-p53 interaction was maintained after treatment with bleomycin (Fig. 6*C*).

Because HERC2 and p53 are present in the cytoplasmic and nuclear fractions, we investigated whether their interaction was maintained in both fractions. Coimmunoprecipitation studies with HERC antibodies showed that the HERC2-p53 interaction occurs in both fractions (Fig. 6*D*).

Mutations That Affect the Tetramerization Domain of p53 Disrupt the Interaction with HERC2—We observed that the deletion of the last 43 amino acid residues of p53 (residues 350–393) impaired its interaction with HERC2 (Fig. 2*H*). Because this domain contains part of the tetramerization domain of p53 (3), we wondered whether this p53 domain was required for the HERC2-p53 interaction. To this end, we performed coimmunoprecipitation experiments with anti-HERC2 antibodies in p53-null human H1299 lung cancer cells. H1299 cells were transfected with different mutants of p53. Cells transfected with wild-type p53 were used as controls. First, we expressed the $p53^{NLS}$ and $p53^{NES}$ mutants, which fail in nuclear import or nuclear export activities, respectively (38). The $p53^{NLS}$ mutant confined to the cytoplasm is comparable with the wild-type p53 because it maintains its capacity for oligomerization and can be acetylated. In contrast, the $p53^{NES}$ mutant confined to the nucleus fails to oligomerize because the C-terminal NES overlaps with the tetramerization domain (38). As shown in Fig. 7*A*, we observed that the HERC2-p53 interaction is disrupted when the mutant $p53^{NES}$ is expressed, suggesting that an intact tetramerization domain of p53 is required for its interaction with HERC2.

To confirm this observation, we used two p53 mutants in which the tetramerization domain was affected. These mutants were $p53^{R337C}$ and $p53^{L344P}$. Individuals with these mutations suffer from Li-Fraumeni syndrome (38). Plasmids containing these mutations were transfected into H1299 cells, and the p53 mutants that were expressed were analyzed. We found that neither mutant was able to associate with HERC2 (Fig. 7*B*), confirming the previous observation that an intact oligomerization domain of p53 is required for its interaction with HERC2. As expected, p21 levels were induced by wild-type p53 expression but not by the expression of p53 mutants (Fig. 7).

HERC2 Regulates p53 Oligomerization—Our data show that HERC2 interacts with p53 and regulates its transcriptional activity. Because this interaction is mediated by an intact oligomerization domain in p53 and because p53 oligomerization has been reported as an essential step for its transcriptional activity (48), we wondered whether HERC2 could regulate p53 oligomerization. To answer this question, we studied p53 oligomerization using a protein cross-linking assay (38). H1299 cells were transfected with wild-type p53 together with siRNAs and analyzed 72 h later. Cell lysates were isolated, treated with increasing amounts of glutaraldehyde, and analyzed by SDS-PAGE and immunoblotting. As shown in Fig. 8*A* (*left panel*),

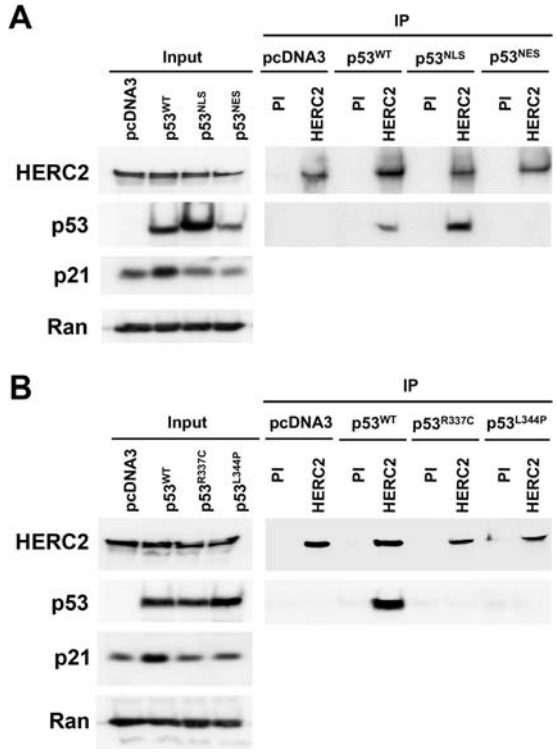

FIGURE 7. **The tetramerization domain of p53 is required for the HERC2-p53 interaction.** H1299 cells were transfected with the indicated plasmids for 48 h. Lysates were then subjected to immunoprecipitation with anti-HERC2 polyclonal antibody and analyzed by immunoblotting with antibodies against the indicated proteins. *A*, p53 mutants that fail in nuclear import ($p53^{NLS}$) or nuclear export ($p53^{NES}$). *PI*, preimmune serum. *B*, p53 mutants ($p53^{R337C}$ and $p53^{L344P}$) associated with Li-Fraumeni syndrome. *pcDNA3*, negative control of transfection; $p53^{WT}$, p53 wild-type. Data are representative of at least three independent experiments. Input represents 5% of the extract used.

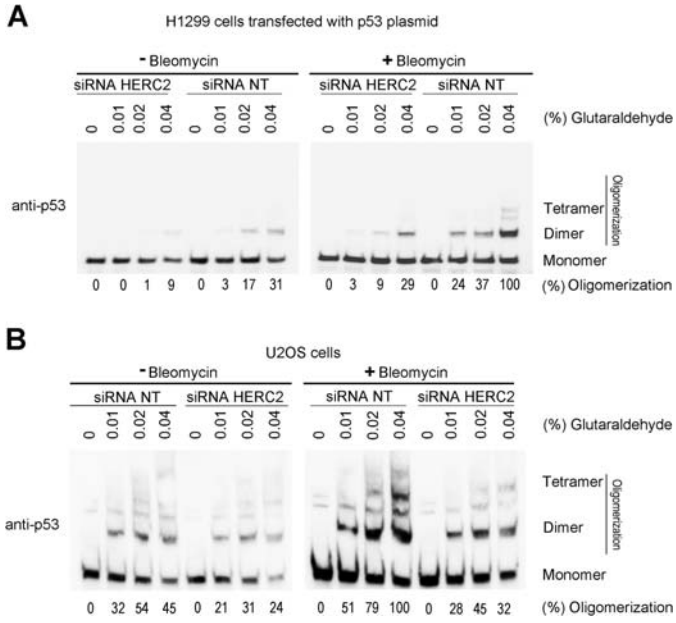

FIGURE 8. **HERC2 regulates p53 oligomerization.** *A*, H1299 cells transfected with the wild-type p53 plasmid and the indicated siRNAs for 72 h were treated with bleomycin for 3 h. Lysates were incubated on ice with glutaraldehyde at the indicated concentrations (percent) for 30 min. Samples were analyzed by immunoblotting with anti-p53 antibody. Monomers, dimers, and tetramers of p53 are indicated. The percentage of oligomerization was calculated with dimers and tetramers. The condition with the higher levels of oligomers was considered as 100%. *B*, oligomerization of endogenous p53. U2OS cells were analyzed as in *A*. Data are representative of at least three independent experiments.

monomers, dimers, and tetramers of p53 were detected with anti-p53 antibody. Under these conditions, HERC2 depletion inhibited p53 oligomerization.

Next, we hypothesized that this inhibition would be more obvious in cells with activated p53. Given that in the previous experiments we showed that bleomycin stimulated p53 activity, we used the same drug. Thus, in H1299 cells transfected with wild-type p53, we observed the stimulation of p53 oligomerization by bleomycin and its inhibition by the knockdown of HERC2 (Fig. 8*A*, *right panel*). All of these results were confirmed in another human cell line with endogenous p53. In U2OS cells, HERC2 depletion inhibited p53 oligomerization (Fig. 8*B*). These results could indicate that HERC2 is necessary to maintain p53 oligomerization. We wondered whether HERC2 could also promote p53 oligomerization. To this end, H1299 cells were transfected with wild-type p53 and with a HERC2 construct (Myc-HERC2 F3) expressing residues 2292–2923, which include the CPH domain (39). We observed a great stimulation of p53 oligomerization by the expression of Myc-HERC2 F3 (Fig. 9, *A* and *B*). Luciferase reporter assays showed that this stimulation correlated with a significant increase of its transcriptional activity (Fig. 9*C*).

DISCUSSION

This study identified HERC2 as a protein that binds p53, thus regulating cellular events mediated by p53. HERC2 interacts with p53 through its CPH domain. Consistent with this, HERC1, a structural homolog of HERC2 that does not contain a CPH domain, did not interact with p53. Moreover, and in contrast to what has been described for smaller members of the HERC family (17), the largest members, HERC1 and HERC2, did not form heteromers. The HERC2-binding domain of p53 was located in its carboxyl terminus, similar to other p53-binding proteins with CPH domains, such as PARC and CUL7 (6–8). Structural studies of the CPH domain of PARC and CUL7 indicated that this domain interacts with the tetramerization domain of p53 (residues 310–360) (49). In agreement with these data, deletion of the last 43 amino acid residues of p53 (residues 350–393) impaired the interaction with HERC2 (Fig. 2*H*), suggesting that an intact tetramerization domain in p53 is required for this interaction. These results led us to check whether HERC2 could interact with oligomerized p53. Using p53 mutants, we found that HERC2 does not interact with p53 mutants defective in oligomerization (Fig. 7). These observations could explain the large amount of p53 in HERC2 immunoprecipitates (Fig. 2). Interestingly, we demonstrated that HERC2 regulates the transcriptional activity of p53 (Figs. 3 and 9). Thus, we show that, in the absence of HERC2, the transcriptional activity of p53 decreases in unstressed cells. These observations were also confirmed in stressed cells. Interestingly, after genotoxic stress induced with bleomycin, the interaction between HERC2 and p53 was maintained.

To shed light on the molecular mechanism involved in the regulation of transcriptional activity of p53 by HERC2, we showed that, in the absence of HERC2, phosphorylation and

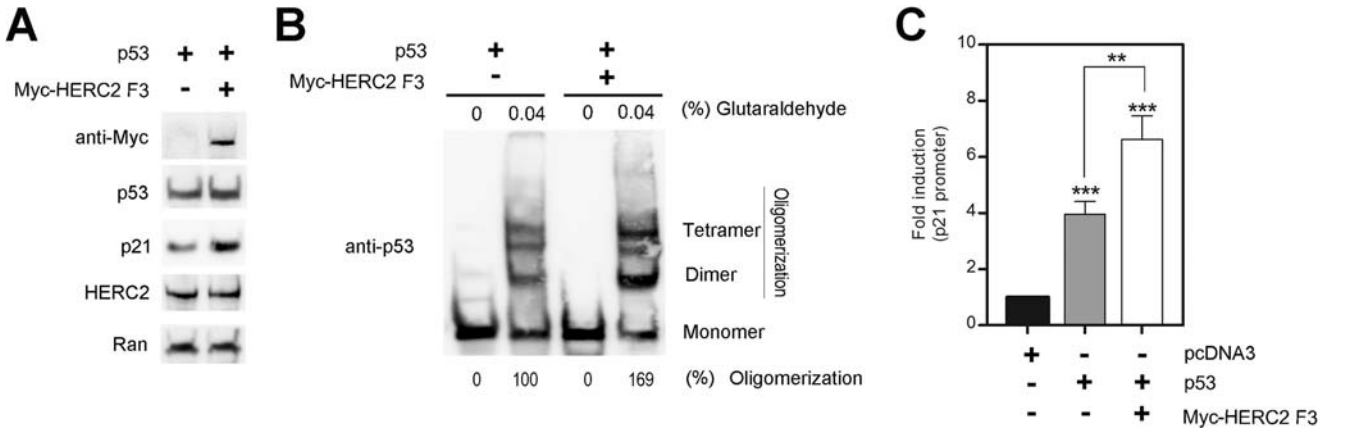

FIGURE 9. **HERC2 promotes p53 oligomerization.** H1299 cells were transfected with wild-type p53 and Myc-HERC2 F3 (residues 2292–2923) constructs and analyzed by immunoblotting with antibodies against the indicated proteins (*A*) or treated with glutaraldehyde at the indicated concentrations (percent) for 30 min to analyze p53 oligomerization as in Fig. 8 (*B*). *C*, H1299 cells were transfected with the *p21* promoter (*p21WAF1*) and the indicated plasmids. The luciferase activity was quantified as indicated under "Experimental Procedures." Data are expressed as mean ± S.E. Statistical analysis was carried out as described under "Experimental Procedures." **, $p < 0.01$; ***, $p < 0.001$.

nuclear translocation of p53 were not impaired. Bearing the above data in mind, and also bearing in mind that p53 acetylation is essential for p53 activation (50) and that p53 oligomerization is essential for the carboxyl terminal lysine acetylation of p53 (38), we were finally able to show that HERC2 regulates p53 oligomerization. All these results led us to propose the next working model. HERC2 interacts with oligomerized p53 and regulates its oligomerization. In response to cellular stress, such as DNA damage produced by bleomycin, p53 oligomerization is stimulated, and p53 is phosphorylated and translocated to the nucleus to activate transcription of its specific gene targets, such as *p21*. Under these conditions, p53 oligomerization is regulated by HERC2. This model is consistent with published data showing that p53 oligomerization is sufficient to activate p53 transcriptional targets (51), but it does not explain why bleomycin does not increase HERC2-p53 interaction (Fig. 6*C*). Although a possible explanation could be that initially all HERC2 is bound to oligomerized p53, more studies will be necessary to shed light on these steps.

HERC2 belongs to the E3 ubiquitin ligase family. E3 ubiquitin ligases have been classified into two main types: HECT and RING (12, 13, 52). HERC2 belongs to the HECT family and PARC and CUL7 to the RING family. p53 levels are regulated by ubiquitin-dependent proteasomal degradation. E6AP and MDM2 are E3 ubiquitin ligases of the HECT and RING families, respectively, which bind and ubiquitinate p53, thus regulating its levels (12, 53). However, this does not seem to be the case for CPH domain-containing E3 ubiquitin ligases. Knockdown of PARC, CUL7, or HERC2 proteins did not increase p53 levels (Refs. 7, 8) and our data). In fact, substrates other than p53 have been reported for these proteins. For example, Cyclin D1 and insulin receptor substrate 1 (IRS-1) are targeted by CUL7 E3 ubiquitin ligase complex for ubiquitin-dependent degradation (9, 54). For HERC2, several substrates have been identified in recent years. Thus, it has been reported that HERC2 ubiquitinates xeroderma pigmentosum A protein, thus promoting its proteasomal degradation (34). Xeroderma pigmentosum A is a limiting factor in the mechanism of DNA repair known as nucleotide excision repair. HERC2 had been implicated previously in the machinery of DNA repair in response to ionizing radiation (32). Interestingly, BRCA1, a protein that also participates in this repair mechanism, has also been reported to be a substrate of HERC2 (35). In this context, down-regulation of HERC2 improved the activation of the nucleotide excision repair mechanism by the chemotherapeutic drug cisplatin (34). Cisplatin produces intra- and interstrand DNA diadducts that are repaired by nucleotide excision repair (55). Bleomycin and ionizing radiation induce double strand DNA breaks that are mainly repaired by homologous recombination and non-homologous end joining machineries (47). Cisplatin and bleomycin are potent anticancer agents used in the chemotherapy of various types of cancer. For example, cisplatin is the drug of choice in testicular and ovarian cancers and a main component of combination therapy regimens for many other cancers, including head and neck, lung, gastric, and colorectal cancers (55). Bleomycin is given in testicular cancer, lymphoma, and cancers of the head and neck (56–58). Knowing the molecular mechanism involved in the action of these drugs will lead to a better understanding of their effects on tumor cells, which will, in turn, allow the design of more efficient trials (combination therapy) as well as the development of specific inhibitors against regulatory proteins that increase the efficiency of these drugs. Because HERC2 regulates both DNA repair mechanisms (32, 34), it seems plausible that specific inhibitors of this protein might increase the cytotoxic action of cisplatin or bleomycin. However, one must bear in mind that HERC2 could also function as a tumor suppressor protein and that inhibition of its activity would cause a decrease in p53 activity.

p53 mutations that affect its oligomerization have been associated with Li-Fraumeni syndrome and Li-Fraumeni-like syndromes (38, 59, 60). In these cases, a decrease in p53 activity has been observed. This study shows the regulation of p53 oligomerization by HERC2 and suggests that HERC2 mutations that affect p53 oligomerization could also be associated with these syndromes. In addition to this putative role in cancer, HERC2 has also been associated with neurological disorders. Thus, a HERC2 mutation associated with a neurodevelopmental delay

similar to Angelman syndrome has been reported (28, 29). In this case, the HERC2 mutation was associated with a decrease in E6AP (UBE3A) activity (28, 37). In summary, although more remains to be learned about HERC2 biology and its role in human diseases, our results establish HERC2 protein as an important regulator of p53 signaling.

Acknowledgments—We thank Y. Xiong, Y. Zhang, C. H. Arrowsmith, Y. Taya, T. M. Thomson, and Taiane Schneider for reagents and/or comments and A. Gimeno, I. Tato, E. Adanero, E. Castaño, and B. Torrejon for technical assistance.

REFERENCES

1. Bode, A. M., and Dong, Z. (2004) Post-translational modification of p53 in tumorigenesis. *Nat. Rev. Cancer* **4,** 793–805
2. Brady, C. A., and Attardi, L. D. (2010) p53 at a glance. *J. Cell Sci.* **123,** 2527–2532
3. Kruse, J. P., and Gu, W. (2009) Modes of p53 regulation. *Cell* **137,** 609–622
4. Meek, D. W. (2009) Tumour suppression by p53: a role for the DNA damage response? *Nat. Rev. Cancer* **9,** 714–723
5. Vousden, K. H., and Prives, C. (2009) Blinded by the light: The growing complexity of p53. *Cell* **137,** 413–431
6. Andrews, P., He, Y. J., and Xiong, Y. (2006) Cytoplasmic localized ubiquitin ligase Cullin 7 binds to p53 and promotes cell growth by antagonizing p53 function. *Oncogene* **25,** 4534–4548
7. Kasper, J. S., Arai, T., and DeCaprio, J. A. (2006) A novel p53-binding domain in CUL7. *Biochem. Biophys. Res. Commun.* **348,** 132–138
8. Nikolaev, A. Y., Li, M., Puskas, N., Qin, J., and Gu, W. (2003) PARC: a cytoplasmic anchor for p53. *Cell* **112,** 29–40
9. Sarikas, A., Xu, X., Field, L. J., and Pan, Z. Q. (2008) The Cullin7 E3 ubiquitin ligase: a novel player in growth control. *Cell Cycle* **7,** 3154–3161
10. Garcia-Gonzalo, F. R., and Rosa, J. L. (2005) The HERC proteins: functional and evolutionary insights. *Cell Mol. Life Sci.* **62,** 1826–1838
11. Hadjebi, O., Casas-Terradellas, E., Garcia-Gonzalo, F. R., and Rosa, J. L. (2008) The RCC1 superfamily: from genes, to function, to disease. *Biochim. Biophys. Acta* **1783,** 1467–1479
12. Rotin, D., and Kumar, S. (2009) Physiological functions of the HECT family of ubiquitin ligases. *Nat. Rev. Mol. Cell Biol.* **10,** 398–409
13. Scheffner, M., and Kumar, S. (2014) Mammalian HECT ubiquitin-protein ligases: biological and pathophysiological aspects. *Biochim. Biophys. Acta* **1843,** 61–74
14. Hochrainer, K., Mayer, H., Baranyi, U., Binder, B., Lipp, J., and Kroismayr, R. (2005) The human HERC family of ubiquitin ligases: novel members, genomic organization, expression profiling, and evolutionary aspects. *Genomics* **85,** 153–164
15. Cruz, C., Ventura, F., Bartrons, R., and Rosa, J. L. (2001) HERC3 binding to and regulation by ubiquitin. *FEBS Lett.* **488,** 74–80
16. Dastur, A., Beaudenon, S., Kelley, M., Krug, R. M., and Huibregtse, J. M. (2006) Herc5, an interferon-induced HECT E3 enzyme, is required for conjugation of ISG15 in human cells. *J. Biol. Chem.* **281,** 4334–4338
17. Hochrainer, K., Kroismayr, R., Baranyi, U., Binder, B. R., and Lipp, J. (2008) Highly homologous HERC proteins localize to endosomes and exhibit specific interactions with hPLIC and Nm23B. *Cell Mol. Life Sci.* **65,** 2105–2117
18. Kroismayr, R., Baranyi, U., Stehlik, C., Dorfleutner, A., Binder, B. R., and Lipp, J. (2004) HERC5, a HECT E3 ubiquitin ligase tightly regulated in LPS activated endothelial cells. *J. Cell Sci.* **117,** 4749–4756
19. Wong, J. J., Pung, Y. F., Sze, N. S., and Chin, K. C. (2006) HERC5 is an IFN-induced HECT-type E3 protein ligase that mediates type I IFN-induced ISGylation of protein targets. *Proc. Natl. Acad. Sci. U.S.A.* **103,** 10735–10740
20. Chong-Kopera, H., Inoki, K., Li, Y., Zhu, T., Garcia-Gonzalo, F. R., Rosa, J. L., and Guan, K. L. (2006) TSC1 stabilizes TSC2 by inhibiting the interaction between TSC2 and the HERC1 ubiquitin ligase. *J. Biol. Chem.* **281,** 8313–8316
21. Garcia-Gonzalo, F. R., Cruz, C., Muñoz, P., Mazurek, S., Eigenbrodt, E., Ventura, F., Bartrons, R., and Rosa, J. L. (2003) Interaction between HERC1 and M2-type pyruvate kinase. *FEBS Lett.* **539,** 78–84
22. Rosa, J. L., Casaroli-Marano, R. P., Buckler, A. J., Vilaró, S., and Barbacid, M. (1996) p619, a giant protein related to the chromosome condensation regulator RCC1, stimulates guanine nucleotide exchange on ARF1 and Rab proteins. *EMBO J.* **15,** 4262–4273
23. Rosa, J. L., and Barbacid, M. (1997) A giant protein that stimulates guanine nucleotide exchange on ARF1 and Rab proteins forms a cytosolic ternary complex with clathrin and Hsp70. *Oncogene* **15,** 1–6
24. White, D., and Rabago-Smith, M. (2011) Genotype-phenotype associations and human eye color. *J. Hum. Genet.* **56,** 5–7
25. Ji, Y., Walkowicz, M. J., Buiting, K., Johnson, D. K., Tarvin, R. E., Rinchik, E. M., Horsthemke, B., Stubbs, L., and Nicholls, R. D. (1999) The ancestral gene for transcribed, low-copy repeats in the Prader-Willi/Angelman region encodes a large protein implicated in protein trafficking, which is deficient in mice with neuromuscular and spermiogenic abnormalities. *Hum. Mol. Genet.* **8,** 533–542
26. Lehman, A. L., Nakatsu, Y., Ching, A., Bronson, R. T., Oakey, R. J., Keiper-Hrynko, N., Finger, J. N., Durham-Pierre, D., Horton, D. B., Newton, J. M., Lyon, M. F., and Brilliant, M. H. (1998) A very large protein with diverse functional motifs is deficient in rjs (runty, jerky, sterile) mice. *Proc. Natl. Acad. Sci. U.S.A.* **95,** 9436–9441
27. Walkowicz, M., Ji, Y., Ren, X., Horsthemke, B., Russell, L. B., Johnson, D., Rinchik, E. M., Nicholls, R. D., and Stubbs, L. (1999) Molecular characterization of radiation- and chemically induced mutations associated with neuromuscular tremors, runting, juvenile lethality, and sperm defects in jdf2 mice. *Mamm. Genome* **10,** 870–878
28. Harlalka, G. V., Baple, E. L., Cross, H., Kühnle, S., Cubillos-Rojas, M., Matentzoglu, K., Patton, M. A., Wagner, K., Coblentz, R., Ford, D. L., Mackay, D. J., Chioza, B. A., Scheffner, M., Rosa, J. L., and Crosby, A. H. (2013) Mutation of HERC2 causes developmental delay with Angelman-like features. *J. Med. Genet.* **50,** 65–73
29. Puffenberger, E. G., Jinks, R. N., Wang, H., Xin, B., Fiorentini, C., Sherman, E. A., Degrazio, D., Shaw, C., Sougnez, C., Cibulskis, K., Gabriel, S., Kelley, R. I., Morton, D. H., and Strauss, K. A. (2012) A homozygous missense mutation in HERC2 associated with global developmental delay and autism spectrum disorder. *Hum. Mutat.* **33,** 1639–1646
30. Mashimo, T., Hadjebi, O., Amair-Pinedo, F., Tsurumi, T., Langa, F., Serikawa, T., Sotelo, C., Guénet, J. L., and Rosa, J. L. (2009) Progressive Purkinje cell degeneration in tambaleante mutant mice is a consequence of a missense mutation in HERC1 E3 ubiquitin ligase. *PLoS Genet.* **5,** e1000784
31. Rodriguez, C. I., and Stewart, C. L. (2007) Disruption of the ubiquitin ligase HERC4 causes defects in spermatozoon maturation and impaired fertility. *Dev. Biol.* **312,** 501–508
32. Bekker-Jensen, S., Rendtlew Danielsen, J., Fugger, K., Gromova, I., Nerstedt, A., Lukas, C., Bartek, J., Lukas, J., and Mailand, N. (2010) HERC2 coordinates ubiquitin-dependent assembly of DNA repair factors on damaged chromosomes. *Nat. Cell Biol.* **12,** 80–86
33. Izawa, N., Wu, W., Sato, K., Nishikawa, H., Kato, A., Boku, N., Itoh, F., and Ohta, T. (2011) HERC2 Interacts with Claspin and regulates DNA origin firing and replication fork progression. *Cancer Res.* **71,** 5621–5625
34. Kang, T. H., Lindsey-Boltz, L. A., Reardon, J. T., and Sancar, A. (2010) Circadian control of XPA and excision repair of cisplatin-DNA damage by cryptochrome and HERC2 ubiquitin ligase. *Proc. Natl. Acad. Sci. U.S.A.* **107,** 4890–4895
35. Wu, W., Sato, K., Koike, A., Nishikawa, H., Koizumi, H., Venkitaraman, A. R., and Ohta, T. (2010) HERC2 is an E3 ligase that targets BRCA1 for degradation. *Cancer Res.* **70,** 6384–6392
36. Al-Hakim, A. K., Bashkurov, M., Gingras, A. C., Durocher, D., and Pelletier, L. (2012) Interaction proteomics identify NEURL4 and the HECT E3 ligase HERC2 as novel modulators of centrosome architecture. *Mol. Cell Proteomics.* **11,** 1–14
37. Kühnle, S., Kogel, U., Glockzin, S., Marquardt, A., Ciechanover, A., Matentzoglu, K., and Scheffner, M. (2011) Physical and functional interaction of the HECT ubiquitin-protein ligases E6AP and HERC2. *J. Biol. Chem.* **286,** 19410–19416

38. Itahana, Y., Ke, H., and Zhang, Y. (2009) p53 Oligomerization is essential for its C-terminal lysine acetylation. *J. Biol. Chem.* **284,** 5158–5164
39. Sheng, Y., Laister, R. C., Lemak, A., Wu, B., Tai, E., Duan, S., Lukin, J., Sunnerhagen, M., Srisailam, S., Karra, M., Benchimol, S., and Arrowsmith, C. H. (2008) Molecular basis of Pirh2-mediated p53 ubiquitylation. *Nat. Struct. Mol. Biol.* **15,** 1334–1342
40. Enari, M., Ohmori, K., Kitabayashi, I., and Taya, Y. (2006) Requirement of clathrin heavy chain for p53-mediated transcription. *Genes Dev.* **20,** 1087–1099
41. Casas-Terradellas, E., Tato, I., Bartrons, R., Ventura, F., and Rosa, J. L. (2008) ERK and p38 pathways regulate amino acid signalling. *Biochim. Biophys. Acta* **1783,** 2241–2254
42. Casas-Terradellas, E., Garcia-Gonzalo, F. R., Hadjebi, O., Bartrons, R., Ventura, F., and Rosa, J. L. (2006) Simultaneous electrophoretic analysis of proteins of very high and low molecular weights using low-percentage acrylamide gel and a gradient SDS-PAGE gel. *Electrophoresis* **27,** 3935–3938
43. Cubillos-Rojas, M., Amair-Pinedo, F., Tato, I., Bartrons, R., Ventura, F., and Rosa, J. L. (2010) Simultaneous electrophoretic analysis of proteins of very high and low molecular mass using Tris-acetate polyacrylamide gels. *Electrophoresis* **31,** 1318–1321
44. Cubillos-Rojas, M., Amair-Pinedo, F., Tato, I., Bartrons, R., Ventura, F., and Rosa, J. L. (2012) Tris-acetate polyacrylamide gradient gels for the simultaneous electrophoretic analysis of proteins of very high and low molecular mass. *Methods Mol. Biol.* **869,** 205–213
45. Carvajal, D., Tovar, C., Yang, H., Vu, B. T., Heimbrook, D. C., and Vassilev, L. T. (2005) Activation of p53 by MDM2 antagonists can protect proliferating cells from mitotic inhibitors. *Cancer Res.* **65,** 1918–1924
46. Bonner, W. M., Redon, C. E., Dickey, J. S., Nakamura, A. J., Sedelnikova, O. A., Solier, S., and Pommier, Y. (2008) γH2AX and cancer. *Nat. Rev. Cancer* **8,** 957–967
47. Helleday, T., Petermann, E., Lundin, C., Hodgson, B., and Sharma, R. A. (2008) DNA repair pathways as targets for cancer therapy. *Nat. Rev. Cancer* **8,** 193–204
48. Chène, P. (2001) The role of tetramerization in p53 function. *Oncogene* **20,** 2611–2617
49. Kaustov, L., Lukin, J., Lemak, A., Duan, S., Ho, M., Doherty, R., Penn, L. Z., and Arrowsmith, C. H. (2007) The conserved CPH domains of Cul7 and PARC are protein-protein interaction modules that bind the tetramerization domain of p53. *J. Biol. Chem.* **282,** 11300–11307
50. Tang, Y., Zhao, W., Chen, Y., Zhao, Y., and Gu, W. (2008) Acetylation is indispensable for p53 activation. *Cell* **133,** 612–626
51. Gaglia, G., Guan, Y., Shah, J. V., and Lahav, G. (2013) Activation and control of p53 tetramerization in individual living cells. *Proc. Natl. Acad. Sci. U.S.A.* **110,** 15497–15501
52. Deshaies, R. J., and Joazeiro, C. A. (2009) RING domain E3 ubiquitin ligases. *Annu. Rev. Biochem.* **78,** 399–434
53. Bernassola, F., Karin, M., Ciechanover, A., and Melino, G. (2008) The HECT family of E3 ubiquitin ligases: multiple players in cancer development. *Cancer Cell* **14,** 10–21
54. Xu, X., Sarikas, A., Dias-Santagata, D. C., Dolios, G., Lafontant, P. J., Tsai, S. C., Zhu, W., Nakajima, H., Nakajima, H. O., Field, L. J., Wang, R., and Pan, Z. Q. (2008) The CUL7 E3 ubiquitin ligase targets insulin receptor substrate 1 for ubiquitin-dependent degradation. *Mol. Cell* **30,** 403–414
55. Jung, Y., and Lippard, S. J. (2007) Direct cellular responses to platinum-induced DNA damage. *Chem. Rev.* **107,** 1387–1407
56. Engert, A., Franklin, J., Eich, H. T., Brillant, C., Sehlen, S., Cartoni, C., Herrmann, R., Pfreundschuh, M., Sieber, M., Tesch, H., Franke, A., Koch, P., de Wit, M., Paulus, U., Hasenclever, D., Loeffler, M., Müller, R. P., Müller-Hermelink, H. K., Dühmke, E., and Diehl, V. (2007) Two cycles of doxorubicin, bleomycin, vinblastine, and dacarbazine plus extended-field radiotherapy is superior to radiotherapy alone in early favorable Hodgkin's lymphoma: final results of the GHSG HD7 trial. *J. Clin. Oncol.* **25,** 3495–3502
57. Linnert, M., and Gehl, J. (2009) Bleomycin treatment of brain tumors: an evaluation. *Anticancer Drugs* **20,** 157–164
58. Kawai, K., and Akaza, H. (2010) Current status of chemotherapy in risk-adapted management for metastatic testicular germ cell cancer. *Cancer Sci.* **101,** 22–28
59. Davison, T. S., Yin, P., Nie, E., Kay, C., and Arrowsmith, C. H. (1998) Characterization of the oligomerization defects of two p53 mutants found in families with Li-Fraumeni and Li-Fraumeni-like syndrome. *Oncogene* **17,** 651–656
60. Lomax, M. E., Barnes, D. M., Hupp, T. R., Picksley, S. M., and Camplejohn, R. S. (1998) Characterization of p53 oligomerization domain mutations isolated from Li-Fraumeni and Li-Fraumeni like family members. *Oncogene* **17,** 643–649